UNIVERSITY OF OSLO
Department of Chemistry

Comparative investigations of zeolite catalyst deactivation by coking in the conversion of methanol to hydrocarbons

Master thesis in Materials, energy and nanotechnology (MENA)

Kjetil Gurholt Evensen

January 2014

Acknowledgment

Abstract

With large countries as India and China in tremendous development accompanied by a growing worldwide population, questions arise in how energy demands can be met in the post-oil society. The methanol-to-hydrocarbon process, catalysed by Brønsted acidic zeolites, constitutes an alternative route for the production of gasoline and other valuable hydrocarbons from feedstocks such as natural gas and coal. Catalyst deactivation by coke formation is nevertheless a big concern, and a better understanding of this process is of utmost importance with respect to both economical and environmental concerns.

The deactivation by coke formation is studied over the medium and large pore zeolites H-ZSM-22, H-ZSM-5, H-Beta (two) and H-mordenite at a reaction temperature of 400 °C and WHSV = 2.00 h^{-1}. Gradually deactivated zeolites have been investigated with gas adsorption measurements, thermogravimetry and coke analysis by dissolution and extraction with subsequent chromatography. Large differences in catalyst lifetime was observed with rapid deactivation of H-mordenite and H-ZSM-22, compared to H-beta and the archetype H-ZSM-5. A broad distribution of polycyclic arenes was observed as retained coke species in gradually deactivated samples of both H-ZSM-22 and H-ZSM-5. This is in contrast to earlier observations done for H-ZSM-5, and might shed some light on the assumption of coking exclusively on the external surface of this catalyst at normal reaction temperatures.

GS-MS/FID analyses have been applied in a quantitative manner, but only H-ZSM-22 showed high relative amount of soluble coke, with a maximum of 60 % after 30 minutes time on stream. Only small amounts were detected for the large pore H-mordenite and beta zeolites and, it is believed that deactivation is caused by coking from larger graphitic species for these materials.

List of abbreviations

BET   Brunauer-Emmett-Teller

CBU   Composite building unit

DME   Dimethyl ether

EDS   Energy-dispersive spectroscopy

ESR   Electron spin resonance

FID   Flame ionization detector

GC   Gas chromatography

IR   Infrared

IS   Internal standard

IUPAC   International Union of Pure and Applied Chemistry

MFI   Mobil Five

MS   Mass spectrometry

MTG   Methanol-to-gasoline

MTH   Methanol-to-hydrocarbons

MTO   Methanol-to-olefins

MTP   Methanol-to-propylene

NMR   Nuclear magnetic resonance

RT   Room temperature

SBU   Secondary building unit

SEM	Scanning electron microscopy
TEM	Transmission electron microscopy
TGA	Thermogravimetric analysis
TOS	Time on stream
UV-VIS	Ultraviolet-visible
WHSV	Weight hourly space velocity
XRD	X-ray diffraction

Table of Contents

1. Introduction

1.1 Catalysis

Catalysis plays a major role in the industry today, and catalysts are in fact essential to humans and nearly all other forms of life. Approximately 85-90% of the products made in the chemical industry are formed through catalytic processes [1], and this share gives an indication of how things have advanced in the field since the very beginning in the early 19th century. At that time, several chemists for the first time observed and utilized catalytic phenomena and the term catalysis was originally coined in 1835 by the Swedish chemist Jöns Jacob Berzelius. He used the phrase *"catalysed process"* to describe what is now known as reactions where substances increase the rate at which chemical equilibrium is reached, without being changed or consumed themselves [2]. It is generally understood that catalysts add to the rate of a chemical reaction in one of the following ways:

- Increasing the number of collisions between reactant molecules
- Decreasing the energy barrier for a collision to result in a reaction
- Increasing the probability of a favourable orientation of the reactant molecules

In figure 1.1, both a catalysed- and a non-catalysed reaction are illustrated. The catalytic reaction starts with bonding of the reactants to the catalyst, which then offers an alternative and energetically more favourable path for the reaction. The figure also illustrates another fundamental principle in catalysis; the reaction enthalpy remains equal for both the catalysed and the non-catalysed reaction pathway. This implies that the presence of a catalyst does not change the thermodynamics of a reaction system, it only affects the rate of the reaction. For this reason, the equilibrium composition remains unchanged in both scenarios. The presence of a catalyst nevertheless allows a reaction to proceed more efficiently or under milder conditions than would otherwise be possible [3].
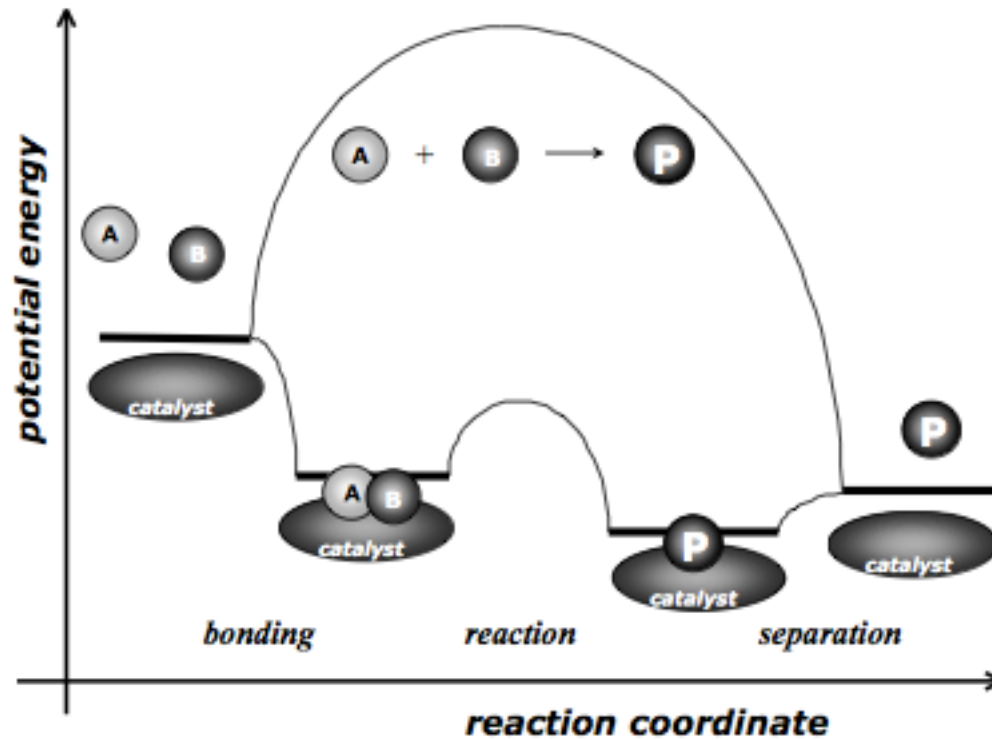
Figure 1.1: A potential energy diagram of a heterogeneous catalytic reaction showing the difference between a catalysed (bottom) and a non-catalysed (top) reaction [1].

It is customary to divide the field of catalysis into three different sub-disciplines: Heterogeneous, homogeneous and bio-catalysis. In heterogeneous catalysis, the catalyst and the reactants are in different phases. The catalyst is practically always a solid where the reactants adsorb to, either in the liquid or gaseous phase. Homogeneous catalysis on the other hand, refers to reaction systems where both the catalyst and the reactant molecules are in the same phase. The last discipline, bio-catalysis, involves the use of natural catalysts, such as enzymes.

Heterogeneous catalysis forms the background of this thesis, which deals with the conversion of methanol over a special type of solid catalysts belonging to a class of minerals called zeolites.

2. Zeolites – the catalysts

This chapter will serve as a brief introduction to zeolites with a special focus on their composition, general structure and properties in acid catalysis. The four zeolite structures relevant to this work are devoted a separate subchapter and will be explained a bit more in detail.

2.1 History, evolution and application – a brief review

In 1756, the Swedish mineralogist Axel Fredrik Cronstedt discovered a special type of minerals that released steam upon heating. He called them *zeolites,* from the Greek words *zein* (ζέω) and *lithos* (λίθος), meaning boiling stone [4].

After Cronstedts findings, the scientific interest in zeolites was sparse for over 200 years [5], but there were nevertheless made some interesting observations worth mentioning. Already from 1777 and into the 19th century, familiar characteristics such as adsorption properties, dehydration and reversible ion exchange were all described for the first time. Later, in 1896, Friedel proposed that zeolites consist of open spongy frameworks, an idea that was pursued and further developed when Weigel and Steinhoff in 1925 reported that dehydrated zeolite crystals would adsorb small organic molecules, but reject larger ones. This effect was seven years later established as "*molecular sieving"* by McBain. With these findings many characteristics of zeolites were known, and by the mid-1930s, the literature described ion exchange, adsorption, molecular sieving and structural properties of zeolite minerals [6], [7].

Especially the molecular sieving effect led scientists to become increasingly interested in the synthesis of zeolites, and Barrer in particular is acknowledged for his pioneering work in the field. He reported the first definitive synthesis of zeolites in 1948, a contribution that inspired others to initiate further studies in zeolite synthesis. From 1949 to 1954, Milton and co-worker Breck in the Linde Division of Union Carbide Corporation discovered a number of different commercially important zeolites, such as type A, X and Y. This made Union Carbide, now owned by Dow Chemical Company, commercialize synthetic zeolites as a new class of industrial

materials for separation and purification processes. Some years later, in 1959, the same company marketed a zeolite Y-based material as a catalyst for isomerization reactions. This was succeeded by Mobil Oil's introduction of zeolite X as a hydrocarbon cracking catalyst in 1962 [8].

From the 1980s to recent times, the discovery of new compositions and structures of zeolites have increased significantly. Zeolites have proven to be useful for several purposes, where the main applications are as adsorbents, catalysts and as ion exchange materials. Their use as catalysts constitute the largest value market with a share of approximately 55 % [6].

2.2 Composition, structure and properties

Zeolites are a class of microporous, crystalline, aluminosilicate minerals. The framework structure is based on primary building units of SiO_4 and AlO_4 tetrahedra linked through corner sharing of oxygen atoms (oxygen bridges). These building units are generally called TO_4 tetrahedra, where the T can refer to both silicon and aluminium atoms. Other types of atoms are also possible, but these materials are usually referred to as zeotypes and will not be covered in detail in this thesis. Of the zeotypes, SAPO-34 is the most well known. From the building units it is evident that the net formulae of the tetrahedra are SiO_2 and AlO_2^- respectively. Each aluminium atom incorporated in the framework will therefore carry a negative electric charge. This charge is balanced by extra-framework cations residing in the pores of the zeolite, resulting in a net neutral framework. As zeolites also contain adsorbed water molecules, an empirical formula of a hypothetical zeolite can be written

$$A_{y/m}^{m+}\left[(SiO_2)_x \cdot (AlO_2^-)_y\right] \cdot zH_2O, \tag{2.1}$$
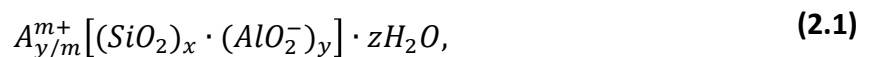
where A is a cation with charge m, x and y represents the number of silicon and aluminium atoms respectively and z is the number of water molecules adsorbed per unit cell. The extra-framework cations are mobile and exchangeable giving rise to the ion exchange property mentioned in section 2.1. The silicon to aluminium ratio, Si/Al, can not be higher than 1

according to Löwenstein's rule [9], which precludes linkages between two aluminium atoms in tetrahedral positions [10].

Although different frameworks can be fully explained by their primary building units, it is often convenient to describe them with secondary and composite building units. Secondary building units (SBUs) are finite units that contain up to 16 T-atoms, derived assuming that the entire framework is made up of one type of SBU only [11]. It should be noted however that more than one SBU can be used to describe a certain framework and that combinations often are employed. Composite building units (CBUs) are generally larger and more complex compared to the SBUs and cannot necessarily be used to build the entire framework. Together, these component units can give a better understanding of different zeolite frameworks and some examples are presented in figure 2.1 below. In the illustrations, the figure under each SBU (left panel) corresponds to the number of T-atoms making up the unit, while the designation under each CBU (right panel) is a tree letter code corresponding to one of the framework types containing the unit.
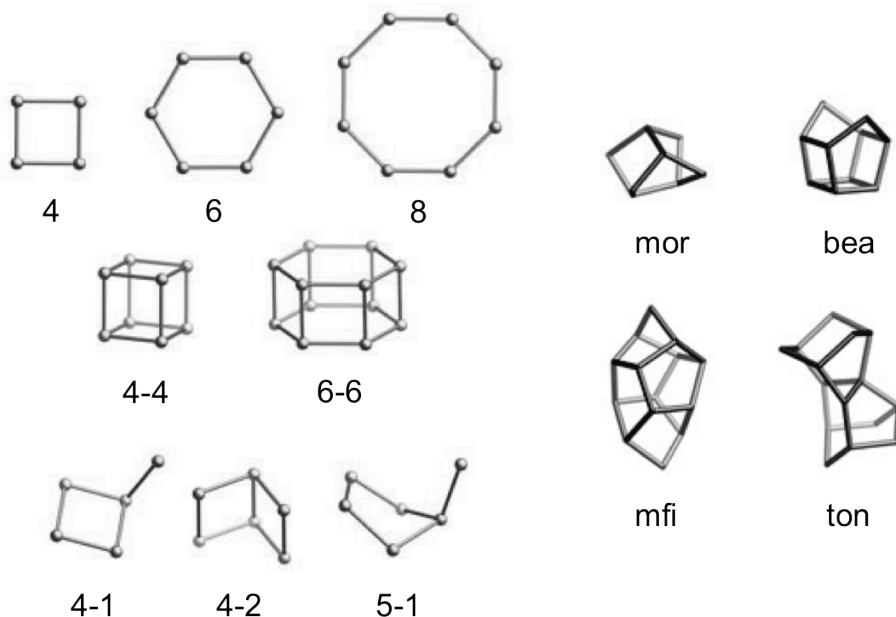
Figure 2.1: Examples of secondary building units (left panel) and composite building units (right panel). The number of T-atoms that constitute the SBU is given under each unit, while the tree letter code under the CBUs corresponds to one of the framework types containing the unit. Oxygen bridges have been omitted in the drawings [11].

When different building units are combined and put together, three-dimensional frameworks appear, and these may contain channels, channel intersections and cages, which individually and collectively are characteristics for the different framework types. The size, geometry and connectivity of these channel systems are defined by the frameworks and provide perhaps the easiest way to distinguish between the different. The pore openings, or windows, giving access to the intracrystalline surface area and channels are given in terms of the number of T-atoms forming the window. Zeolites with pore openings of 8-, 10- and 12 T-atoms are known as small, medium and large pore and have diameters of approximately 4.0, 5.5 and 7.5 Å respectively [12]. A special type of framework, Mobil Five (MFI), is illustrated in figure 2.2. The oxygen bridges are shown in red spheres while the T-atoms appear as yellow sticks.
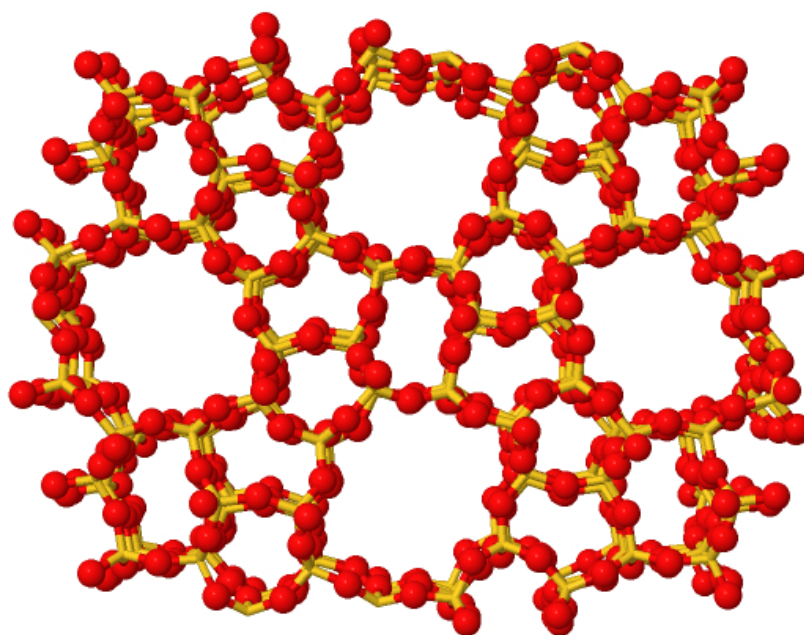
Figure 2.2: Illustration of the Mobil Five framework (MFI). Oxygen bridges and T-atoms are shown in red spheres and yellow sticks respectively [13].

Because the pore openings generally do not exceed 20 Å, zeolites fall within The International Union of Pure and Applied Chemistry's (IUPAC) classification as microporous materials [14]. The channels may be uniform, or non-uniform in cross section and may intersect with other channels to form two- and three-dimensional systems. This leads to highly porous materials,

and together with the pore openings, these features give rise to the previously mentioned molecular sieving effect in zeolites. As the porosity provides a large and accessible surface area, these phenomena also play a key role in heterogeneous catalysis.

2.3 Zeolite catalysis

It has been elucidated that extra-framework cations balance the net negative charge aluminium atoms introduce in the zeolite framework. If these extra-framework cations are protons, which can easily be obtained through ion exchange, Brønsted acid sites are formed and the zeolite can be used as a solid acid catalyst. Although this thesis only involves this kind of catalysis, zeolites and zeotypes can also be used as base, acid-base, redox and bifunctional catalysts [15]. The introduction of an acid site is illustrated in figure 2.3, where a proton compensates for the negative charge that arises when a silicon atom is substituted with an aluminium atom in a tetrahedral position. A zeolite on its protonated form is usually designated with an H in front of its name, e.g. H-ZSM-5, and this term will be used throughout this thesis.
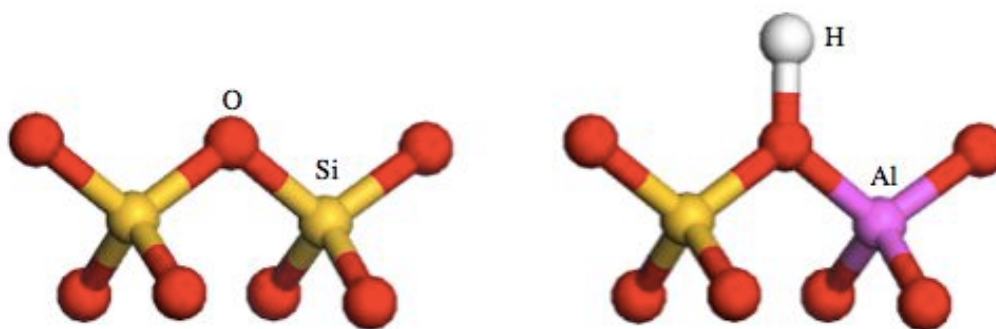
Figure 2.3: Illustration of oxygen corner sharing in two SiO$_4$ tetrahedra (left panel) and the formation of a Brønsted acid site when one SiO$_4$ tetrahedral is substituted with an AlO$_4$ tetrahedral (right panel) [16].

The maximum number of acid sites that can be introduced is in theory equal to the silicon to aluminium ratio in the framework, but the actual number is usually lower due to ion exchange, dehydroxylation and dealumination during activation at high temperatures (Lewis acid sites may also be formed [10]). The number of acid sites can therefore be adjusted either during synthesis

7

or during post synthesis treatments [15]. As many of the acid sites are localized in the channels and cavities of the zeolite, the accessibility and the spatial surroundings of these sites give rise to a property called shape selectivity. This phenomenon is further described in the following subchapter.

2.3.1 Shape selectivity in zeolite catalysis

An important topic in zeolite catalysis, and in catalysis in general, is the concept of selectivity. A selective catalyst or selective catalytic process refers to the situation where the desired product is produced in a satisfactory excess with respect to the relevant by-products [3]. A selective catalyst will thus be of interest with respect to both economical and environmental concerns. In zeolites, selectivity is to a large extent present because of their characteristic porous structure.

The pore openings and channel systems in zeolites are of molecular dimensions, which is of great importance when it comes to the diffusivity of molecules in the material. Small differences in molecular size and shape will determine if a molecule is able to diffuse in and/or out of the internal zeolite framework. This gives rise to properties known as reactant- and product shape selectivity.

Reactant shape selectivity applies to the size of the reactants. Molecules up to a certain size will be able to enter the framework through the pore openings, while others may be too large and therefore excluded. The latter will therefore not be converted into products.

Product shape selectivity is in a sense the opposite of reactant shape selectivity. Products formed in the channel intersections and cages may be too large to diffuse out and because of this, remain trapped inside the material. Unless further reactions occur and they are able to diffuse out, these products may eventually take part in the deactivation of the catalyst. The causes to and the process of deactivation will be discussed more in detail in section 3.3.

Another prominent example of shape selectivity in zeolites is the concept of transition state shape selectivity. As the name implies, this affects what type of transition states and intermediates a reaction may proceed through. This is simply a geometric effect, and occurs

because of steric hindrance of the intermediates caused by size limitations in the zeolite. The effect is independent of diffusion path length, i.e. crystal size, and differs with this respect somewhat from the two others mentioned.

There are several books and articles describing selectivity behaviour in zeolites [3, 15, 17], and Haag distinguishes between three underlying causes leading to shape selectivity – diffusion controlled, sorption controlled and transition state controlled [17]. Haag's description gives god explanations for the above-mentioned properties, with reactant and product shape selectivity being diffusion controlled, and transition state selectivity being a transition state controlled phenomenon.

The different types of shape selectivity described are illustrated in figure 2.4: **a** - reactant shape selectivity, **b** - transition state selectivity and **c** - product shape selectivity.
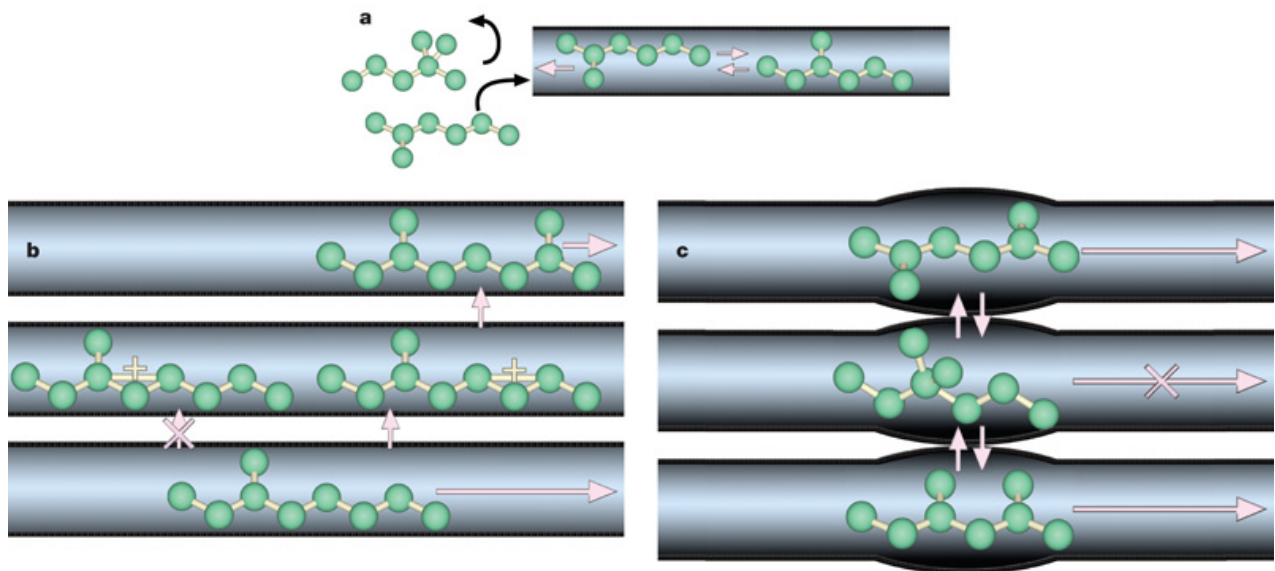
Figure 2.4: Illustration of shape selectivity in zeolites. a: reactant shape selectivity where one reactant is able to enter the zeolite channel, while a larger, more bulky is excluded. b: transition state shape selectivity illustrated with an allowed- and not allowed reaction pathway. c: product shape selectivity where one type of product is trapped inside the channel unable to diffuse out without further reactions [18].

2.4 Zeolites relevant to this work

The great diversity of zeolite frameworks is reflected by the fact that over 200 (206) different kinds have been confirmed [19]. In the following, the four zeolites relevant to this work will be presented. The name of the material is given first, with the three-letter code recognized by IUPAC as the framework type, in parenthesis. It is important to keep in mind that a framework can represent several materials – the data given here refers to the specific structure.

2.4.1 Zeolite ZSM-22 (TON)

ZSM-22 originates from Mobil Oils Research Department and the structure was reported by Kokotailo *et al.* in 1985 [20]. It belongs to the TON framework type, which can be constructed from 5-1 SBUs, and is composed of rings of 5-, 6- and 10 T-atoms [11]. ZSM-22 has a one-dimensional channel system running along [001] with dimensions of 5.5 × 4.5 Å, noted by Kokotailo *et al.* to be smaller compared to the 10-ring channels found in the ZSM-5 (see next page). The channel system is illustrated in Figure 2.5 below.

The zeolite has a framework density of 19.2 T-atoms per 1000 $Å^3$, orthorhombic symmetry and lattice constants a = 13.9 Å, b = 17.4 Å and c = 5.0 Å [11, 20].
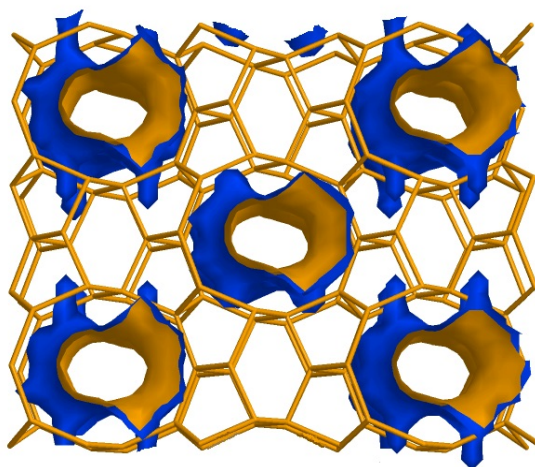
Figure 2.5: Illustration of the 10-ring one-dimensional channels along [001] in the TON framework [13].

2.4.2 Zeolite ZSM-5 (MFI)

The name ZSM-5 is an abbreviation for Zeolite Socony Mobil Five (as for ZSM-22) and this zeolite has found many applications in refinery and petrochemical processes [21].

ZSM-5 belongs to the MFI framework type, which can be described by pentasil (mfi) composite units, when linked together form a three-dimensional channel system with pore openings of 10 T-atoms. The zeolite is consequently a medium pore type with intersecting channels giving rise to voids in the framework. The channel system is illustrated in figure 2.6 and is constituted by straight channels running along [010] with dimensions of 5.3 × 5.6 Å and sinusoidal or zig-zag channels running along [100] with dimensions of 5.1 × 5.5 Å.

The crystal structure has orthorhombic symmetry and unit cell parameters a = 20.1 Å, b = 19.9 Å and c = 13.4 Å. The framework density is 17.9 T-atoms per 1000 Å^3 [11].
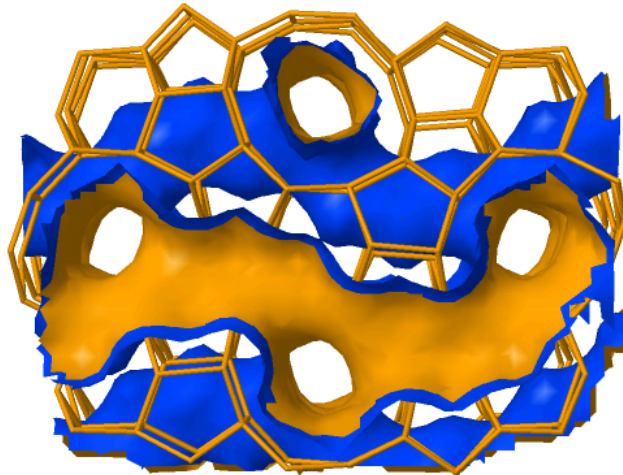
Figure 2.6: Illustration of the three-dimensional channel system in the MFI framework type along [010]. Notice the intersecting sinusoidal channels giving rise to voids in the material [13].

2.4.3 Beta Zeolite (*BEA)

The beta zeolite was first synthesized and patented by Wadlinger and co-workers during the 1960s [23] and is another material resulting from the work done at Mobil's laboratories. Its structure is complex with an intergrowth of three similar, but distinct structures denoted polymorph A, B and C [24]. These are stacked in a more or less random fashion, where any stacking sequence give rise to a three-dimensional 12-ring channel system as illustrated in figure 2.7 [5]. The channels running along [100] and [010] are straight, while the channels in the [001] direction are sinusoidal because of stacking disorders. In polymorph A, the straight channels have dimensions of 6.6 × 6.7 Å, while the sinusoidal channels have dimensions of 5.6 × 5.6 Å [11].

Beta polymorph A has a tetragonal crystal structure with lattice constants a = b = 12.7 Å and c = 26.4 Å. The framework has a density of 15.1 T-atoms per 1000 $Å^3$ [11].
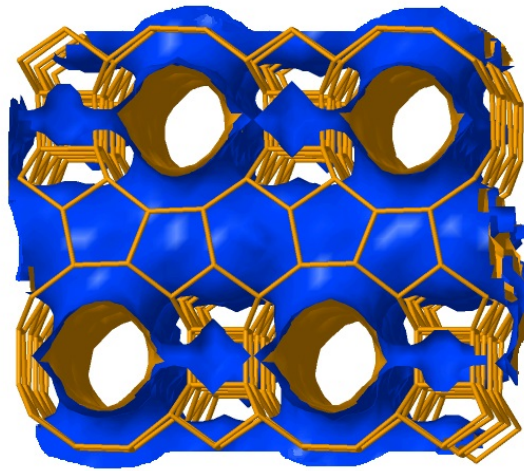
Figure 2.7: Illustration of the straight channels along [010] in the BEA* polymorph framework [13].

2.4.4 Mordenite (MOR)

Mordenite is a naturally occurring zeolite with sedimentary deposits present in several countries, especially in Bulgaria, Hungary, Japan and the United States. The zeolite was first synthesized by Sand in 1968 [25], and there has in fact been observed certain differences in the properties of the natural and the synthesized material [26].

In contrast to the MFI and TON frameworks, the MOR framework (illustrated in figure 2.8) has channels made up of up to 12 T-atoms and mordenite is thus referred to as a large pore zeolite. The lining of the 12-ring channels contains 8-rings, but the 8-ring openings of adjacent 12-ring channels are displaced with respect to one another and are therefore highly tortuous. This leads to side pockets, but still there is very limited access from one channel to the next. The channel system is as a consequence effectively one-dimensional in the [001] direction with 8- and 12-ring channels of dimensions 2.6 × 5.7 and 6.5 × 7.0 Å respectively [5, 11].

The crystal structure of mordenite is orthorhombic with lattice constants a = 18.1 Å, b = 20.5 Å and c = 7.5 Å. The zeolite has a framework density of 17.2 T-atoms per 1000 $Å^3$ [11].
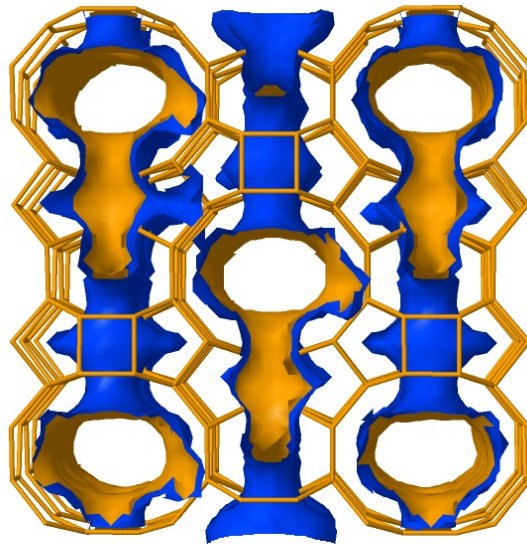
Figure 2.8: Illustration of the MOR framework with 12-ring channels running along [001] with accompanying side pockets [13].

3. The methanol to hydrocarbon process

With large countries as India and China in tremendous development accompanied by a growing worldwide population, questions arise in how energy demands can be met in the post-oil society. In this chapter, an alternative route for the production of gasoline and other hydrocarbons from natural gas and coal are presented. Zeolites play an important role in this process, and after an introduction, the focus will be put on chemistry related topics with respect to this remarkable material.

3.1 Introduction

The energy demand worldwide increases steadily [27] and with a world population exceeding 7 billion, this demand is unlikely to level off in the coming future. Fossil fuels are the main contributors to fulfil this need, and over 85 % of the energy consumption (year 2000) is derived from coal, oil and natural gas [28]. Besides the use within transportation, electricity production and heating, which of course amounts to greater parts, oil and natural gas are also important raw materials for the production of various chemicals and products that might be taken for granted in today's society. With current reserves and enormous demands, it is expected that oil reservoirs will be depleted before those of coal and natural gas [28]. Peak oil is a well-known term and the incentives of finding out how particularly coal and natural gas can be utilized best possible to replace the oil in years to come, are clear.

A process that may contribute in upgrading of coal and natural gas to gasoline or other higher value petrochemical products is the conversion of methanol to hydrocarbons (MTH) over acidic zeolite or zeotype catalysts. Figure 3.1 illustrates the process, starting with the conversion of coal or natural gas to synthesis gas by gasification or steam reforming. The synthesis gas is then reacted over a $Cu/ZnO/Al_2O_3$ catalyst to form methanol, which in the last step is transformed into gasoline and olefins. The selectivity is dependent on reaction conditions and type of zeolite used, and the process can therefore be tuned to achieve desired product distributions [29]. Due to this, the process is also termed methanol to gasoline (MTG), methanol to olefins (MTO) and

methanol to propylene (MTP) and more, depending on what type of hydrocarbons that constitutes the main products.
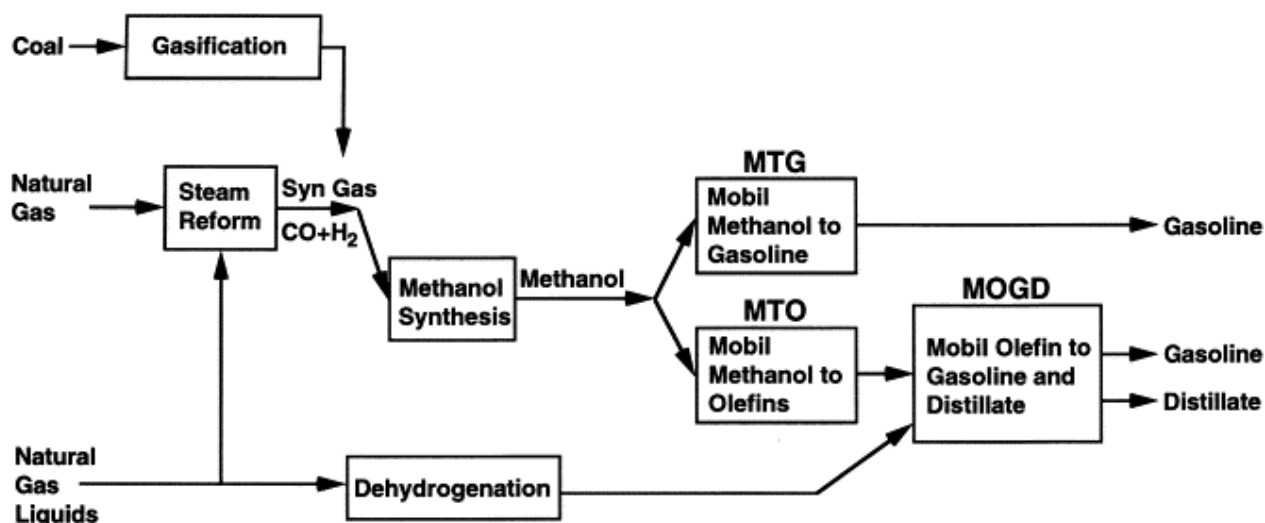
Figure 3.1: Sketch of coal and gas upgrading via synthesis gas and methanol. The final step is the conversion of methanol to hydrocarbon products over an acidic zeolite/zeotype catalyst [29].

The original MTG process was first conceived and developed as a response to the oil crisis during the 1970s, when researchers at Mobil discovered that methanol could be converted to gasoline over H-ZSM-5 catalysts. In a typical MTH reaction, methanol is dehydrated to an equilibrium mixture of dimethyl ether (DME), methanol and water. This mixture is then converted to light olefins, which can undergo further reactions into higher olefins. Due to the shape selectivity of H-ZSM-5 heavier hydrocarbons containing more than ten carbon atoms are practically not formed, a feature especially important in the MTG process, as C_{10} is the usual limit for conventional gasoline. A MTG plant was built in New Zealand in 1985 and supplied at a time one third of the country's gasoline needs. The plant was later shut down due to decreasing oil prices [28, 30].

In the MTO process, lighter olefins are the desired products and this is achieved over a H-SAPO-34 zeotype catalyst. H-SAPO-34 has narrower pore openings compared to H-ZSM-5, and restricts large and bulky molecules of diffusing out of the material, leading to a product range dominated by small, linear alkenes. An alternative to this process, made to maximize propene

15

yields, is the MTP process developed by Lurgi. This is based on a highly siliceous H-ZSM-5 catalyst, and as opposed to the H-SAPO-34 used in the MTO process, this catalyst has extremely low coking tendency (see section 3.3), beneficial with respect to simple regeneration of the catalyst [31].

3.2 Reaction mechanisms

The mechanisms of the MTH reaction has been of great interest from the origin of the process and various researchers and research groups have put efforts in understanding the underlying principles. Although many reaction mechanisms have been proposed over the years, this section will only cover the most recognized.

3.2.1 Introducing the hydrocarbon pool mechanism

Early, focus was put on the formation of the first C-C bond from methanol and/or DME, and more than 20 possible mechanisms were proposed [29]. The interest in these diminished with time and the origin of new and better propositions. A study from 2002 have in fact provided results contradictory to many of these early proposals [32]. Song *et al.* observed that when using highly purified reagents and careful tests, the initial rate of methanol conversion was drastically reduced, meaning that the earlier proposed mechanisms of direct C-C bond formation were not applicable.

A mechanism that in contrast has received considerable recognition with time, was proposed by Dahl and Kolboe during the 1990s. They introduced the hydrocarbon pool mechanism as a new alternative route to alkene formation [33-35]. The mechanism involves formation of alkenes via so-called hydrocarbon pool species adsorbed within the pores of the zeolite, and their suggestion was based on isotopic labeling studies with co-reaction of ^{13}C methanol, ethene (fed as ethanol) and propene (fed as isopropanol) over a H-SAPO-34 catalyst. Dahl and Kolboe observed that ethene and propene emerged almost unreacted in the effluent, while the labeled methanol was virtually completely converted to hydrocarbons. Hydrocarbons are in other words

not formed through methylations of co-reacted alkenes over this catalyst. The hydrocarbon pool mechanism is illustrated in figure 3.2.

$$nCH_3OH \xrightarrow{-nH_2O} (CH_2)_n$$

with equilibria to C_2H_4, C_3H_6, C_4H_8, and arrows to saturated and aromatic.
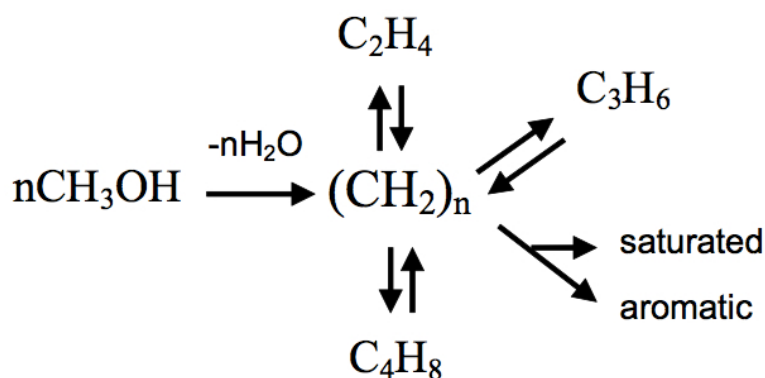
Figure 3.2: Schematic illustration of the hydrocarbon pool mechanism proposed by Dahl and Kolboe [34].

Dahl and Kolboe did not specifically elaborate what kind of chemical structures that actually dominate in the mechanism, but this is evidently an interesting topic. Various studies have been carried out in attempts to determine this and in fact prior to Dahl and Kolboe's introduction of the hydrocarbon pool mechanism, Mole and Whiteside [36] did some interesting observations related to this. They observed that the conversion of methanol to hydrocarbons increased by addition of aromatic hydrocarbons to the feed over a H-ZSM-5 catalyst, a phenomeon they called co-catalysis. Without drawing a direct conclusion from their observations, multiple studies by different research groups done over several zeolites and zeotypes (H-SAPO-34, H-ZSM-5, H-mordenite, H-beta) have indeed shown that different methylbenzenes are the main components taking part as intermediates in the hydrocarbon pool mechanism [37-41].

After further investigating the subject, Bjørgen *et al.* have also found that the heptamethylbenzenium cation, illustrated in figure 3.3, plays an analogous role in the process [42, 43].

Figure 3.3: Suggested role of the heptamethylbenzenium cation (top left) as a hydrocarbon pool species in zeolite H-beta [44]

The role of polymethylbenzenes as the major hydrocarbon pool species appears to be independent of the zeotype catalyst chosen [45], but there are clear differences in what types that dominate over the individual topologies. In a comparative study of H-beta and H-ZSM-5 by Svelle *et al.,* it was observed that the higher methylated benzenes (penta and hexamethylbenzene) are dominant intermediates for large-pore zeolite H-beta, while the lower methylbenzenes are dominant for the medium-pore H-ZSM-5 [46]. The observations were based on $^{12}C/^{13}C$ switching analysis, where unlabeled methanol was reacted over both catalysts to build up a hydrocarbon pool, before switching to ^{13}C-methanol after a certain amount of time to be able to follow the reactants. The background for the analysis was the observation of major differences in the relative ethene to propene yield for the two zeolites. It was found that H-ZSM-5 yields seven times more ethene relative to propene compared with H-beta and this was ascribed to the different intermediates dominating in the two materials.

The higher methylbenzenes have also been identified as important reaction intermediates for H-mordenite [47], which might indicate that these species require more spacious channels and intersections to dominate as participants in the hydrocarbon pool.

A question that arises is then how alkenes are formed from these hydrocarbon pool species. Olsbye *et al.* points out two distinct existing hypotheses for this, the paring and the side chain methylation schemes [30].

3.2.2 The paring and side chain methylation

The paring methylation scheme was originally proposed to explain how light paraffins were formed during hydrocracking of hexamethylbenzene [48]. Sullivan *et al.* explained it with *"peeling"* or *"paring"* of methyl groups from aromatic rings. The side chain methylation scheme on the other hand, originates from the previously mentioned work by Mole and Whiteside [36]. They pursued the aromatic co-catalysis concept previously observed and proposed the mechanism in a new publication just a few months later [49].

The two hypotheses are illustrated in figure 3.4 below.
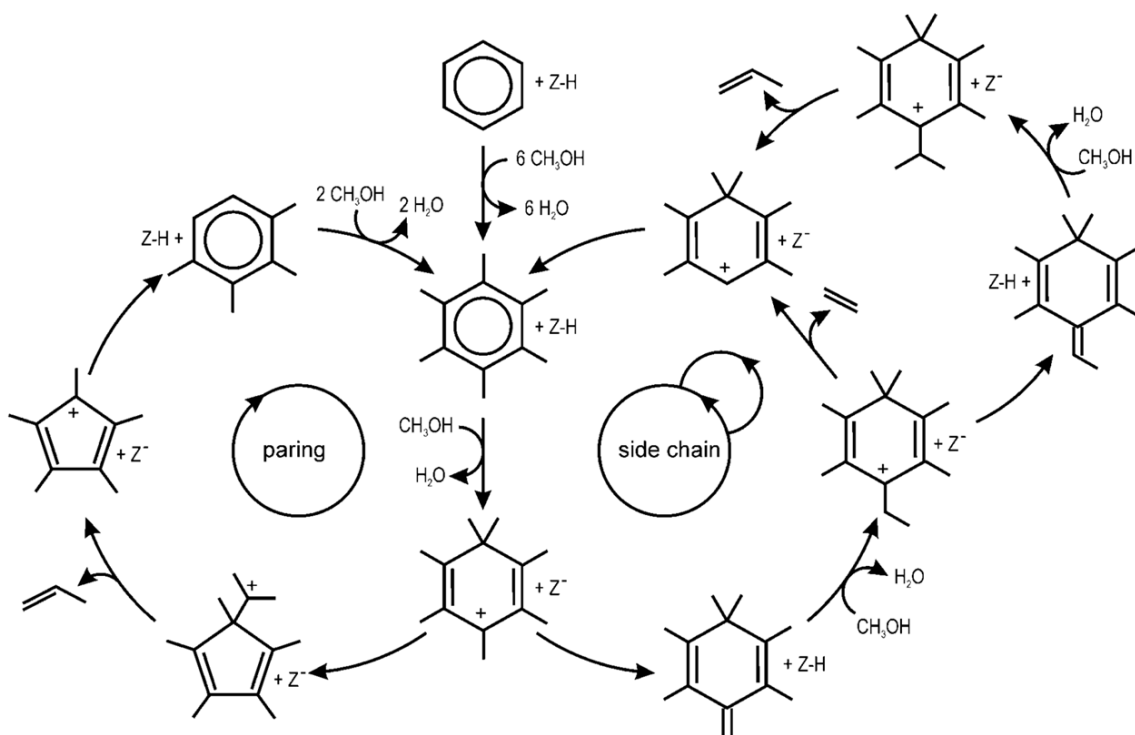
Figure 3.4: Schematic representation of the paring and side-chain reaction concepts in MTO-catalysis. The zeolite is represented by Z-H or Z⁻ in its protonated form, respectively [50].

19

3.2.3 Introducing the dual cycle concept

Although the hydrocarbon pool mechanism can be considered the most important reaction pathway in the MTH process, there has in recent times emerged a refinement of the original concept. In studies over a H-ZSM-5 catalyst, Svelle and Bjørgen *et al.* have found that the reaction proceeds through both the hydrocarbon pool mechanism and a cycle involving alkene methylations and interconversions, i.e. a methylation and cracking route [44, 51]. Based on isotopic labelling studies they concluded that the formation of ethene follows the hydrocarbon pool mechanism with lower methylbenzenes as dominant intermediates, while propene and higher alkenes are formed through the methylation/cracking cycle. A similar concept to the methylation/cracking cycle was proposed by Dessau and LaPierre already during the 1980s, but this was at the time suggested as a main reaction pathway also including ethene formation [52, 53].

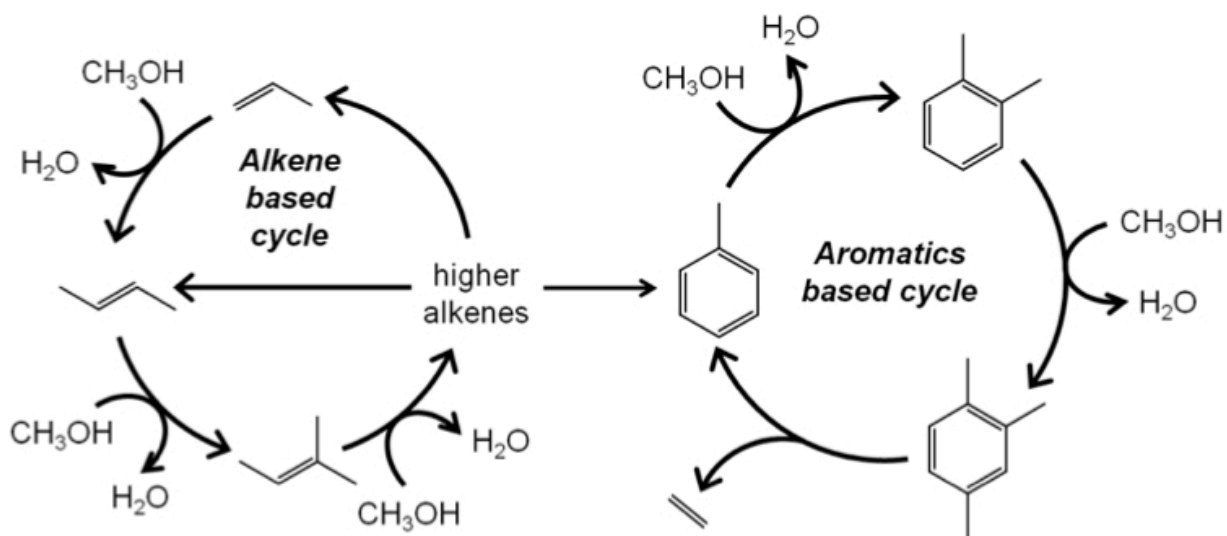The two cycles are illustrated in figure 3.5 and was by Svelle and Bjørgen referred to as the dual cycle concept.

Figure 3.5: The dual cycle concept for methanol conversion over H-ZSM-5, as suggested by Svelle and Bjørgen [30].

As a consequence of the introduction of the dual cycle concept, studies have been made on other zeolite topologies in the attempt to manipulate the cycles running. In a methanol conversion study on the H-ZSM-22 by Teketel *et al.*, very little ethene was observed compared to higher alkenes in the effluent [54]. This could indicate that the methylation/cracking cycle is dominant for this narrow one-directional topology, which was later confirmed in a following mechanistic study by the same group [55]. It was concluded that the aromatic based hydrocarbon pool mechanism is suppressed over H-ZSM-22 and the methanol conversion being controlled by the methylation/cracking pathway. This particular example illustrates how knowledge of reaction mechanisms over different zeolites provides a way to selectively control the product formation.

3.3 Catalyst deactivation

By definition, catalysts are not consumed during reactions, but catalyst deactivation is in a general sense nevertheless inevitable. Zeolites are no different than other catalysts, and the process of deactivation is an important topic in the MTH chemistry over this material.

3.3.1 Introduction and definition

During the conversion of methanol to hydrocarbons, zeolite catalysts generally lose activity with increasing time on stream (TOS). This type of deactivation can often be related to hydrocarbon deposits blocking access to the active acid sites in the zeolite. When such deposits are considered it is often referred to as coking of the catalyst, where coke can be defined as carbonaceous deposits deficient in hydrogen compared to the coke-forming reactant molecule(s) [56]. This definition can be somewhat inadequate when considering this type of deactivation as a whole, because in practice any molecule blocking access to the acid sites in zeolites can be regarded as deactivating species. The term coke will therefore in the following refer to any species leading to deactivation.

The formation of coke is in principle a *reversible* form of deactivation, and the coke can be removed by combustion in oxygen at high temperatures. By doing this, the catalyst is

regenerated and activity is regained. However, such regeneration procedures require high temperatures and will in industrial practice, increase the costs of investments. The regeneration process is also often incomplete and can because of the elevated temperatures lead to *irreversible* deactivation through chemical and structural alterations, damaging the catalyst [57]. For these reasons, catalyst deactivation is an intertwined issue, and ways to reduce the build up of coke are of great importance with respect to both economical and environmental concerns. Although catalyst damage (e.g. dealumination, framework collapse) also is a type of deactivation, the focus will be put on the actual coke – first, how it can be studied, and then, its formation in different topologies.

3.3.2 Techniques for studying coke deposition

Measurement of coke deposition and deactivation is essential for a better understanding of the mechanisms of deactivation by coke deposition [58]. Instead of focusing on actual results from recent research on the field, this section is meant as a brief overview to introduce the reader to different techniques used for studying the deposition of coke. The section is based on reviews from Karge [56] and Bibby *et al.* [59], as well as Guisnet and Ribeiro's book: *Deactivation and Regeneration of Zeolite Catalysts* [57]. Even though much of the literature originates from the early 90's and is not directed to MTH chemistry exclusively, the methods and techniques described are very much applicable also today.

In order to study the chemical identity of coke and its location, sophisticated techniques are required. The composition of the carbonaceous deposits can be quite complex, but different spectroscopic methods allow detailed investigation of the functionality and identity of the coke. Infrared (IR) spectroscopy was one of the first techniques employed to investigate the nature of coke deposits laid down on zeolite catalysts during hydrocarbon reactions, and is one of a number of suitable spectroscopic techniques that can be used for analysis. Others include Raman, ultraviolet-visible (UV-VIS), X-ray photoelectron (XPS), nuclear magnetic resonance (NMR) and electron spin resonance (ESR) spectroscopy to name a few. Several of these methods are also well suited for *in situ* investigations of zeolites and reactions catalysed by these

materials. Another advantage is the fact that most of the above-mentioned methods generally do not require destruction of the coke/zeolite system in order to liberate the coke-constituting species, and are therefore non-destructive.

Coke composition can also be analysed with gas chromatography (GC) combined with mass spectrometry (MS) and/or a flame ionization detector (FID). This can be accomplished by extracting the hydrocarbon residues with a suitable solvent (e.g. CH_2Cl_2), before analysing the solution. As coke can be formed on both the catalyst's inner (internal) and outer (external) surface (section 3.3.3), it may be necessary to first dissolve the coked zeolite catalysts in a mineral acid in order to liberate species trapped inside the zeolite channels. Venuto *et al.* were the first to do this and the method of dissolution and extraction through acid treatment was later on further developed and extensively used by Guisnet and co-workers. This kind of method has been widely used in this thesis and is described further in a devoted subchapter (see section 5.6). It should be mentioned that this technique has its limitations with respect to the fact that not all of the coke can be analysed. Insoluble coke might also be present, and because of this, the coke species are usually distinguished between a soluble and an insoluble part.

Adsorption measurements are another widely used technique in characterization of both fresh and spent (coked) zeolites. Comparison between the adsorption capacity of fresh and coked samples is frequently used to characterize the deposition of coke in the void volume of the zeolite structure. The measurements may illustrate a decrease in surface area and pore volume with increased coking, and serve to clarify whether the coke is predominantly deposited in the zeolite pores or on the external surface.

A method that is complementary to the already mentioned techniques is the thermogravimetric analysis (TGA). By measuring the weight loss with increasing temperatures, this is a suitable tool to acquire quantitative data. The method can also provide information to discriminate between different types of coke.

3.3.3 Coke formation

The formation and build up of coke in zeolites are complex and it can be difficult to distinguish between species functioning as reaction intermediates and species taking part in the deactivation of the catalyst. Coke formation is known to be dependent on factors such as acidic properties, reactant composition, reaction temperature and obviously the pore size and channel system in the zeolite used [59]. As mentioned, it can also be formed both on the catalyst's inner and outer surface, which further complicates the subject [60]. Rather than trying to generalize, it may therefore be appropriate to elucidate coke formation with respect to the distinct zeolite topologies.

The H-ZSM-5 is known for a unique resistance to deactivation, which obviously is a desired property for catalysts in the MTH process. Various studies [44, 60, 61], have reported deactivation by coke formation exclusively on the external surface of the H-ZSM-5 at normal reaction temperatures, and Bjørgen *et al.* mention this as a plausible reason for the superior lifetime properties of the catalyst [44]. In their study, a series of MTH reactions with increasing TOS were conducted at a reaction temperature of 370 °C, followed by dissolution/extraction experiments with subsequent analysis of the retained hydrocarbons from each experiment. After 14 days of reaction (the longest TOS), the catalyst suffered from severe deactivation, but still no aromatics larger than hexamethylbenzenes were found. Nor was there a correlation between the amount of hexamethylbenzenes and the degree of deactivation in any of the experiments. With that it was concluded that the deactivation was a result of formation of larger graphitic species on the external surface of the crystallites, species not detectable with the procedure used.

Despite of these convincing findings, a recent study has shed new light on the topic [62]. Barbera *et al.* made some interesting observations during an investigation of the regeneration property of NO_2 compared to O_2 in the removal of coke from H-ZSM-5 after methanol conversion at 350 °C. When NO_2 was used as an oxidizer, much of the coke could be removed with temperatures lower than usual, but there were still some residues inside the micropores of the catalyst. The species were mainly lower methylbenzenes and when the catalyst was

retested, it deactivated more rapidly. As mentioned, aromatics like the lower methylbenzenes act as active hydrocarbon pool species over the catalyst [44, 51], but might based on this also be seen as direct precursors for coke formation. It is difficult to draw any firm conclusions from Barbera *et al.*'s observations, but they nevertheless illustrate the complexity in distinguishing between species for product formation and species for coke formation in MTH reactions.

Another recent deactivation study [63] has also shown a bit contradictory results to Bjørgen *et al.*'s observations. After methanol conversions at 500 °C over a H-ZSM-5 catalyst with a Si/Al ratio of 40, larger polycyclic aromatics (up to four fused rings) were identified. The results are not directly comparable as the reaction temperature was higher and the Si/Al ratio of the catalysts employed differed, but still shows that there is controversy on the topic. It is worth mentioning that Bjørgen *et al.*'s study was conducted over a range of different Si/Al ratios without any serious discrepancies in the findings, which strongly suggests that the acid site density was of minor importance in this particular case. This connection, or rather lack of correlation between deactivation and acidity, is supported by a study from 2011 by Barbera *et al.* [64]. A large number of H-ZSM-5 based catalysts, with varying acidity (Brønsted acid site density), were tested in order to investigate how microstructural properties in such materials influence activity and deactivation in the conversion of methanol to hydrocarbons. Also here no correlation between deactivation and acid site density was observed. On the other hand, it was found that internal framework defects play a crucial role in the deactivation of H-ZSM-5 catalysts. Prior to the MTH tests, IR spectroscopy combined with adsorption of pyridine and 2,4,6-collidine was used to distinguish between external and internal silanol groups in the different catalysts. As a perfect zeolite crystal does not contain any silanol groups other than external, the internal silanol groups therefore represent defects in the zeolite. After plotting the IR intensity ratio of internal and external silanols, which can be interpreted as the amount of internal silanol groups per m^2 external surface area, against the measured deactivation rate, a clear linear correlation was found. From this result, the authors pinpointed that materials with a low internal silanol density and/or a large external surface area are expected to show a slow deactivation in the conversion of methanol to hydrocarbons, and vice versa. Although this effect is not fully understood, Barbera *et al.* discuss a possible scenario where the internal silanols

interact with coke precursors and other hydrocarbon products to result in a slower diffusion through the zeolite channels, hence a faster deactivation. Whatever the explanation, these findings clearly illustrate that in addition to coke formation at the external surface, internal coking also plays an important role in the deactivation of H-ZSM-5 materials.

The H-ZSM-5 is an archetype zeolite in the MTH process and has been subjected to many studies, but deactivation in the other zeolites relevant to this work must also be included.

Large pore zeolites such as H-beta and H-mordenite distinguish themselves a bit from the medium pore H-ZSM-5 when it comes to the phenomenon of coke formation. Their pores are big enough to accommodate species such as bicyclic arenes [65], which in a study by Bjørgen *et al.* [42] have been directly associated with the formation of coke and catalyst deactivation in zeolite H-beta. In Figure 3.6 their proposed scheme for the formation of these coke precursors from hexamethylbenzenes via multiple methylations and hydride transfers in this zeolite is presented. Later, the same group did a comparative study over three different large pore/cavity zeolites, including H-beta and H-mordenite, and after co-feeding of ^{13}C methanol and ^{12}C benzene, it was observed that the same hydrocarbons are built up and retained in the different topologies [47]. The reactions were thermally quenched after just 90 seconds and after dissolution/extraction of the coke/zeolite system, the largest compound observed was the heptamethylnaphthalene. In the related paper, also additional possible pathways for the formation of dihydro-trimethylnaphtalene (bottom right center in figure 3.6) were presented.

Deactivation and coke formation in the H-ZSM-22 zeolite is less investigated and needs further studies. The zeolite is actually quite new in terms of MTH reactions [54], which explains the few papers available on the material. However, H-ZSM-22's stability towards deactivation have been reported to be lower compared to other catalysts (H-ZSM-5 in particular) [66]. Two individual groups have also conducted studies where the retained hydrocarbons in the zeolite after conversion of methanol have been investigated [66, 67]. Aromatics as large as methylated anthracenes (three fused benzene rings) were reported and Teketel *et al.* argued for an increase towards even heavier compounds with extended reaction times [66]. In GC analyses of the

retained material after dissolution/extraction experiments, a reduction in the amount of soluble coke was observed after a certain TOS, yet the total amount of coke, determined by TGA, increased with reaction time. A similar effect was observed with increasing reaction temperatures; very little soluble coke could be detected with reaction temperatures above 450 °C, even at short reaction times. From this it was suggested that a shift in the relative importance of internal (soluble) to external (insoluble) coking as a function of reaction temperature (and time) could be likely.
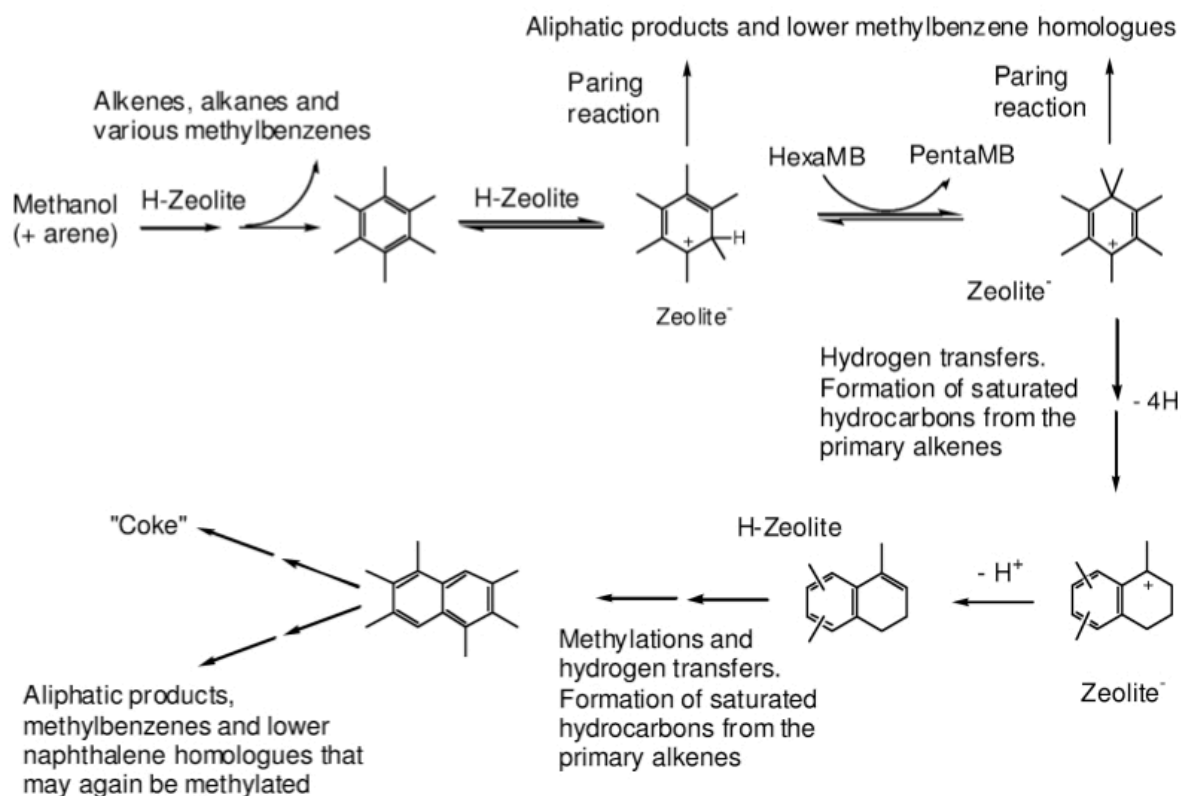
Figure 3.6: Bjørgen *et al.*'s proposed scheme for the formation of coke precursors from hexamethylbenzenes in H-beta [42].

4. Scope of this work

Whether reversibly by coke formation, or irreversibly by chemical damage of the catalyst, it is clear that zeolites in the conversion of methanol to hydrocarbons lose activity with time through deactivation. Although studies on reaction mechanisms have been the core of MTH research for more than 30 years, the interest in catalyst deactivation is growing and a large effort has been devoted to identify and locate coke-forming compounds in especially H-ZSM-5 and H-SAPO-34, but also in other zeolite topologies.

From the literature, it is evident that much of the insight on coke formation has been obtained through the technique of dissolving partially deactivated catalysts in a mineral acid, in order to extract and analyse the hydrocarbon residues with a GC-MS. This is a good technique for qualitative analysis, but still has its limitations. As previously discussed also insoluble coke might be present, and coke-species that fall into this category will not be detected. It is therefore of interest to investigate the relative amount of coke that can be analysed with this technique for different zeolite catalysts.

Although H-ZSM-5 is a widely used catalyst in the conversion of methanol to hydrocarbons, the benefits of applying other zeolites in MTH processes have previously been mentioned (e.g. to selectively control the product formation). A major challenge with other types of zeolites is the catalyst lifetime, as these tend to deactivate much more rapidly compared to the H-ZSM-5. To help increase the understanding of this, further investigations on other zeolite topologies are therefore desirable.

The purpose of this work is to investigate the deactivation behaviour of different zeolites in the conversion of methanol to hydrocarbons, with the primary objective to establish the dissolution/extraction technique in a quantitative manner. Partially deactivated zeolites are investigated with GC-MS combined with a FID, by TGA and by sorption measurements. The zeolites investigated include commercially available samples of H-ZSM-22, H-ZSM-5, H-beta and H-mordenite.

# 5. Methods used in this thesis

The five different zeolites employed in this work have been characterized by a number of techniques, some basic, and some more typical for porous, catalytic materials. The techniques used include X-ray powder diffraction (XRD), scanning electron microscopy (SEM) with energy-dispersive spectroscopy (EDS), sorption measurements based on Brunauer-Emmett-Teller (BET) theory, Fourier transform infrared (FTIR) spectroscopy and TGA. In the following chapter, the theory behind the respective methods will be explained. A special emphasis should be given to BET and TGA, as these techniques were used frequently in the course of work.

5.1 XRD

XRD is a technique used for phase identification and structure determination. As the name suggests, the technique is based on the phenomenon of diffraction, which occurs when waves encounter a solid.

The incident radiation, the X-rays, interacts with the regular arrays of atoms in the crystal lattice and give rise to a diffraction pattern. Although the diffracted radiation cancels each other out through destructive interference in most directions, some directions will lead to constructive interference and give rise to reflections. From this, a diffraction spectrum may be generated in which the intensities of the diffracted radiation are given as a function of the diffraction angles. The diffraction angles depend on the Bravais point lattice and the unit cell dimensions, while the diffracted intensities depend on the atomic numbers of the analysed material and their geometrical relation to the lattice points [68].

Figure 5.1 illustrates reflections of X-rays after interaction with the planes of atoms in a specimen. Incoming X-rays with a certain angle Θ are reflected in phase, which leads to wave fronts. The interplanar spacing between the (hkl) planes are termed d and half the so-called path difference, which is the travelling difference between the incident beam and the beams reflected in consecutive planes, is termed δ.
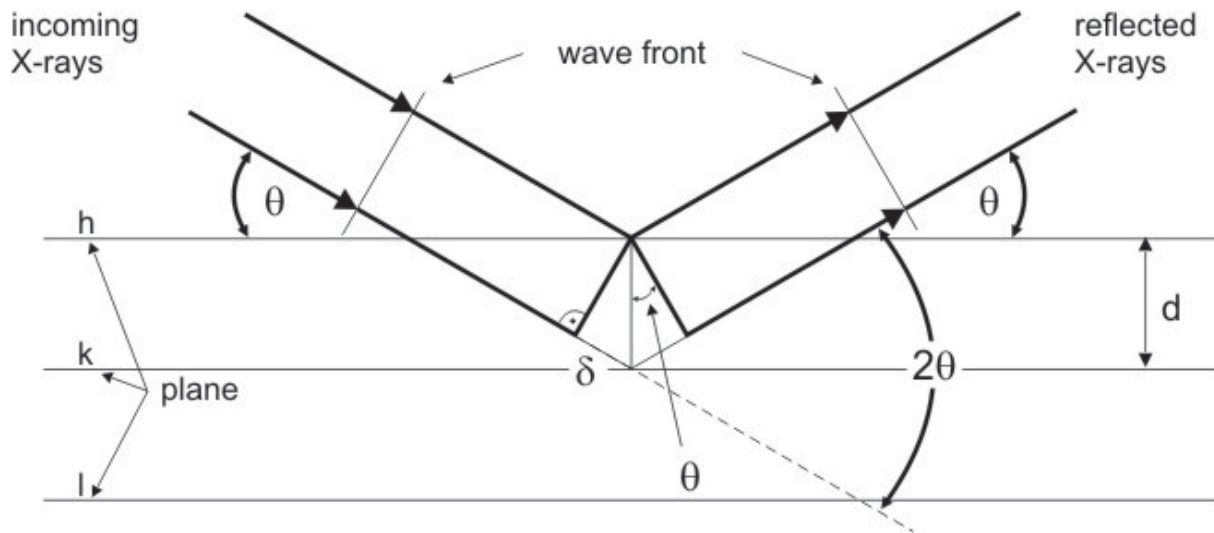
Figure 5.1: Illustration of diffraction of X-ray radiation in the periodic planes of a crystal lattice. The incident and reflected angles are marked Θ, half the path difference is termed δ, d is the interplanar spacing responsible for the given reflection and h, k and l are the lattice planes [69].

In order for constructive interference to happen, the path difference between the incident and diffracted radiation must equal an integer multiple of the wavelength. This makes a wave front, and in these cases, Bragg's equation is satisfied. Bragg's equation relates the wavelength of radiation to the interplanar spacing and the diffraction angle (see figure 5.1), and is given by:

$$n\lambda = 2dsin\Theta \tag{5.1}$$

where n is an integer, λ is the wavelength of radiation, d is the interplanar spacing between the crystal lattice planes and Θ is the angle of diffraction. 2dsinΘ is equal to the path difference 2δ in figure 5.1.

A diffraction spectrum is usually analysed by comparison to a library of diffraction standards. Because a crystalline material will generate a unique diffraction pattern with distinct diffraction angles and relative intensities, the diffraction spectrum may be treated as a fingerprint for a given structure. In this way, comparisons to a data library will help to determine the crystalline phases that are present.

5.2 SEM with EDS

The SEM is a powerful tool to observe and, when used with an EDS, analyse microscopic objects. Magnifications over several orders of magnitude can be obtained and the technique generally requires little preliminary work and sample preparation.

5.2.1 SEM

The image observed from a SEM is created when the surface of the specimen is irradiated with a finely focused electron beam. As the electron beam scans the specimen and penetrates the surface, both elastic and inelastic scattering occur, giving rise to different signals. These are then collected in respective detectors, converted into an electrical signal, amplified and then displayed as variations in brightness on a computer monitor [70]. Some of the signals generated that can be used for characterization are backscattered electrons, secondary electrons, X-rays, Auger electrons and cathodoluminescence.

Backscattered electrons are due to scattering of the incident electrons by angles larger than 180°. These electrons are decelerated by the electromagnetic field around atomic nuclei in the sample and scattered almost elastically [22]. The fraction of the incident beam backscattered are sensitive to the average atomic number of the specimen and increase with higher atomic numbers. This results in atomic number contrasts and offers the possibility of distinguishing between different phases [68].

Unlike backscattered electrons, secondary electrons are generated by inelastic scattering events with release of electrons from the sample surface. The incoming electrons, which can be both electrons originating from the incident beam and from backscattered electrons returning to the surface, can eject weakly bonded outer electrons from the sample if they have sufficiently high energy. The former will usually give an image with a better resolution, as this signal only is limited by the size of the beam prove diameter. There are four factors that directly affect the emission of secondary electrons: *the work function of the surface, the incident electron beam energy and (beam) current, the atomic number, and the local curvature of the surface [68].* The

last factor is perhaps the most important, because a region with a positive radius of curvature will increase the chances of secondary electrons escaping. This produces images with high resolution and good topographic depth as edges often will appear brighter compared to valleys or flat surfaces. The curvature effects are illustrated in figure 5.2.
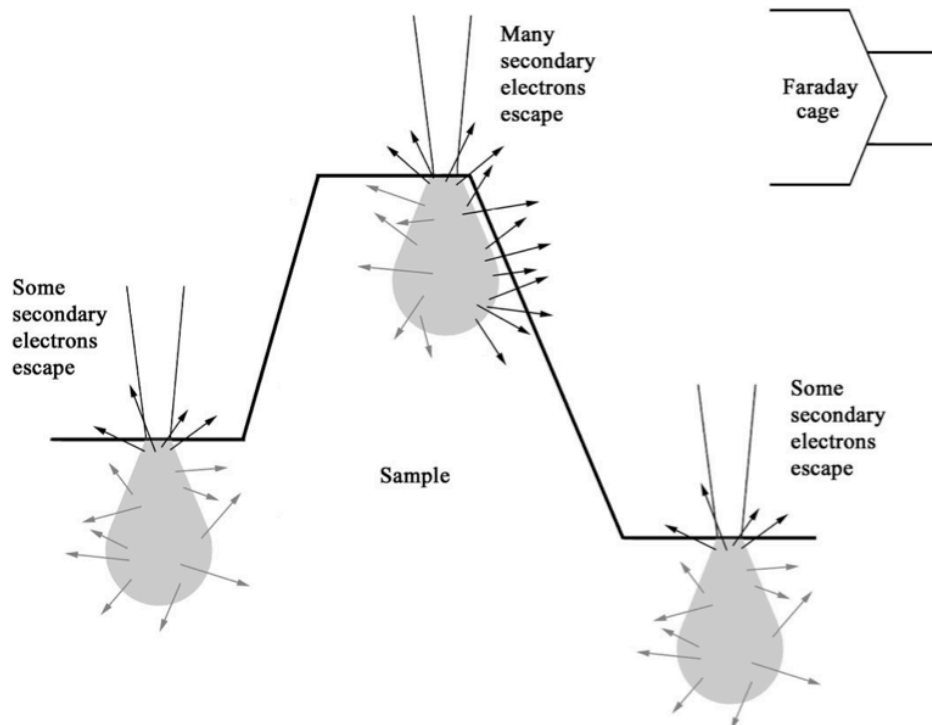
Figure 5.2: Illustration of curvature effects for secondary electron emissions. A positive radius of curvature increases the chance of secondary electrons escaping compared to flat areas of the sample [22].

5.2.2 EDS

When secondary electrons are ejected from the inner shells of an atom, decay by electronic transitions from higher to lower energy states occur. All such transitions lead to photon emissions and if there are transitions as described above, the emitted photons will have energies that correspond to X-rays [68]. These X-rays can then be detected in an energy-dispersive spectrometer and be used for qualitative and quantitative analysis of the sample composition.

5.3 Sorption measurements

Surface area and pore size distribution in solids are important attributes within heterogeneous catalysis. Sorption measurements are widely used for characterization of this and Brunauer, Emmett and Teller developed the theory that forms the background for the surface measurements done in this work. The t-plot method has been applied to estimate micro pore volume and the theory behind both will be described in the following subchapters.

5.3.1 BET theory

In a typical adsorption measurement, the amount of gas that is adsorbed on the surface of the sample is measured as a function of partial pressure at a fixed temperature. This is called an adsorption isotherm and provides the information necessary to calculate the surface area of the sample investigated. The calculation is based on the volume of gas needed to form a complete monomolecular layer at the surface, which can be extracted from the BET equation on its linear form [71]:

$$\frac{p}{v_{ads}(p_0 - p)} = \frac{1}{C \cdot v_{mono}} + \frac{C-1}{C \cdot v_{mono}} \cdot \frac{p}{p_0} \tag{5.2}$$

where p is the saturation vapour pressure, p_0 is the equilibrium pressure, v_{ads} is the volume of gas adsorbed, C is the BET constant and v_{mono} is the monomolecular volume capacity.

If $p/v_{ads}(p_0–p)$ is plotted versus p/p_0, a graph with slope $(C–1)/(C·v_{mono})$ and intercept $(1/C·v_{mono})$ is obtained, and from this the BET constant, C, and the monomolecular volume, v_{mono}, may be calculated. The monomolecular volume can then be converted to number of molecules through the ideal gas law:

$$pV = nRT \tag{5.3}$$

where p is the pressure of the gas, V is the volume of the gas, n is the amount of gas particles in moles, R is the universal gas constant and T is the temperature in kelvin. When equation (5.3) is rearranged and the Avogadro constant is included, the equation can now be written:

$$N = \frac{N_A p V}{RT} \tag{5.4}$$

where N is the total number of molecules needed for monomolecular coverage and N_A is Avogadro's constant. The surface area can be calculated as a product of the number of molecules and the molecular cross-sectional area (area occupied by one each molecule). For nitrogen, which is the adsorptive used in this work, this area is 0.162 nm^2 [71]. When this method is used, the surface area presented will be referred to as the BET surface area.

5.3.2 T-plot method

In t-plot analysis, the adsorbed amount, v_{ads}, is converted to the average thickness t, of adsorbed film by the relation

$$t = \frac{v_{ads}}{v_{mono}} d' \tag{5.5}$$

where d' is the effective thickness of the monolayer (N_2 = 0.354 nm) [71, 72].

The amount adsorbed is then plotted against t, and if the isotherm can be described by multilayer adsorption, the t-plot will be a straight line passing through origin. The slope is proportional to the surface area and any deviation in linearity gives information on sort of pores present, average pore size and pore volume [72].

5.4 FTIR

FTIR is a technique used to identify and quantify information on compounds and extended materials having covalent bonds. The technique is based on the fact that almost all such compounds absorb various frequencies of electromagnetic radiation in the infrared region, and an infrared absorption pattern, called an infrared spectrum, may therefore be used as a kind of fingerprint analysis for the substance of interest [73].

When incident photons interact with the specimen, absorption at certain frequencies occurs due to vibrational motions in the compound. A simplified, but yet well explanatory example is the assumption that a diatomic molecule can be considered as two vibrating masses connected to a spring. The spring, or the bond distance, continually changes and whenever the distance is stretched or compressed beyond its equilibrium, the potential energy of the system increases. The total amount of energy, both potential and kinetic, is proportional to the frequency of vibration, which for a harmonic oscillator is determined by the force constant, K, of the spring (bond strength) and the masses (m_1 and m_2) of the two atoms. With this in mind, the frequency of vibration of a bond (in cm^{-1}), derived from Hooke's Law, is given by:

$$\bar{v} = \frac{1}{2\pi c}\sqrt{\frac{K}{\mu}} \qquad\qquad (5.6)$$

where c is the velocity of light, K is the already introduced force constant of the spring and μ is the reduced mass given by:

$$\mu = \frac{m_1 m_2}{m_1 + m_2} \qquad\qquad (5.7)$$

Even though this is an approximation, it can with certainty be said that the force constant of the spring will vary from one bond to another. Looking at equation (5.6) it should be clear that two stronger bonds (larger force constant) vibrate at higher frequencies than weaker bonds and that

bonds between atoms of higher masses vibrate at lower frequencies than bonds between lighter atoms [73].

Absorption arises from excitations from the ground state to higher energy states and it is distinguished between fundamental absorptions and overtones. Fundamental absorptions are excitations to the lowest energy excited state only and are due to different stretching and bending modes of the bonds. Overtones are excitations to higher energy states corresponding to integer multiples of the fundamental absorptions, and can thus be observed as e.g. $2v$ in the spectrum.

The different groups in zeolites give rise to various absorption bands and can therefore be identified with this technique. Upon adsorption of a base in the zeolite, the individual bands will be shifted in the spectrum due to interactions with the guest species. The observed shifts for the v(OH) bands are directly proportional to the acidic strength [74], and FTIR combined with probe molecules, can therefore be used to investigate this.

5.5 TGA

In TGA, the change in weight is measured as a function of temperature. A microbalance is connected to a programmable furnace, where the temperature is either increased at a fixed rate or kept constant for a certain period of time. With this setup, changes such as water loss, removal of organic template and the oxidation of coke in the zeolite after reactions can be detected and measured.

A TGA plot for a zeolite sample is displayed in figure 5.3. There are two weight loss regions indicated. The first, A, can be attributed to loss of adsorbed water, while the second, B, is due to oxidation of coke accumulated during MTH reactions.
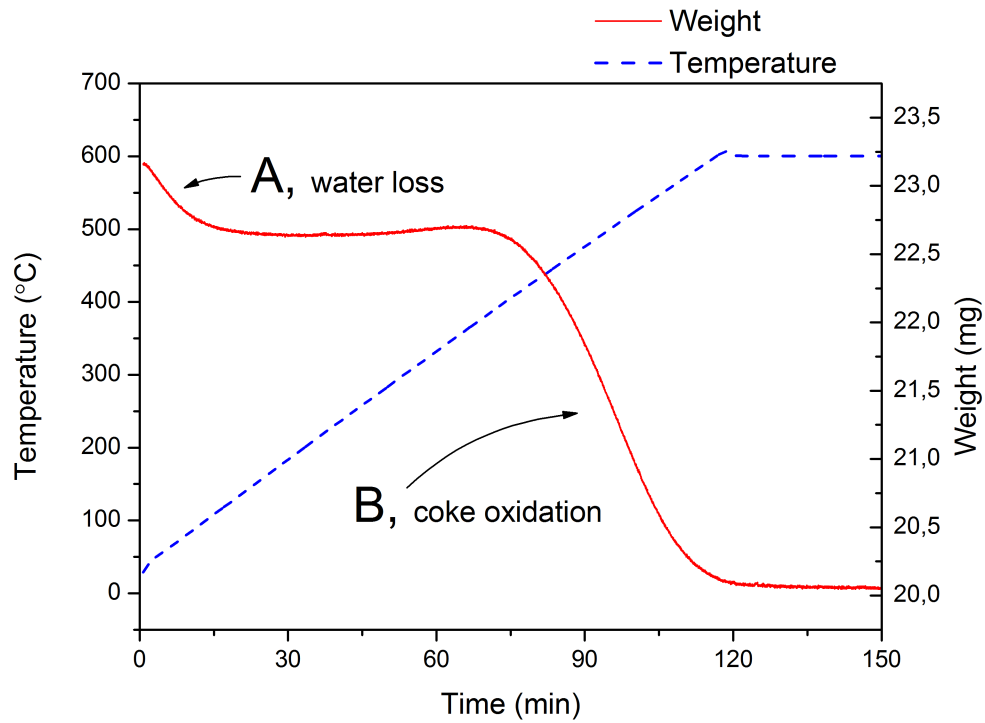
Figure 5.3: Hypothetical TGA plot from a zeolite after MTH conversion with A: loss of water and B: oxidation of coke.

6. Experimental

This chapter provides descriptions and explanations of how the practical work has been conducted. A brief presentation of the catalysts and catalyst treatment are followed by procedures for the different characterization techniques and a section on calibration. The experimental details concerning catalytic tests are left out and provided in a separate chapter (7. Catalytic tests).

6.1 Catalysts

Five commercially available zeolites, all presented in table 6.1, have been employed in this work. In order to distinguish between the two beta zeolites, they will in the following be referred to by their name given by the manufacturers, H-beta and H-BEA. The ZSM-5, the ZSM-22 and the beta zeolite (ref. H-beta) were all provided in undesired forms and therefore treated with calcination and/or ion exchange (see below). For the ZSM-5 only calcination was necessary as it was supplied with ammonium as compensating cations. Procedures for ion exchange and calcination are described in section 6.1.1.

Table 6.1: Catalysts used in this work.

Catalyst	Si/Al ratio	Manufacturer
H-ZSM-22	50	Zeolyst International
H-ZSM-5	13.5	Süd-Chemie
H-beta	27	PQ Corporation
H-BEA	12.5	Süd-Chemie
H-mordenite	10	Ventron

6.1.1 Ion exchange and calcination

The materials were calcined at 600 °C for 5 hours with a 3 hour heating ramp from room temperature (RT) to 600 °C. The ion exchange was done with 1M NH_3NO_3 for 3 x 2 hours in a 70 °C water bath. After ion exchange, the materials were left in a heating cabinet over night before calcination as described was repeated.

6.2 Characterization techniques

In this subchapter, the procedures for sample preparation and descriptions of setup and instruments used for each technique will be explained. For theoretical descriptions of the different methods, see chapter 5.

6.2.1 XRD

XRD characterisations were performed on a Siemens/Bruker D5000 diffractometer with Bragg-Brentano geometry and a position sensitive detector. The measurements were done with Cu K-alpha 1 radiation with wavelength of 1.5406 Å over a 2-theta scale from 2 – 60. The XRD data was analysed using EVA 8.0 software developed by SOCABIM and the diffraction patterns were compared to the Powder Diffraction File compiled and revised by the International Centre for Diffraction Data.

The materials were directly transferred to standard sample holders, finely chopped and evened out with a small piece of rectangular glass. The sample holders were turned upside down to remove remnants and ensure sample fixation.

6.2.2 SEM

The SEM investigations and elemental analysis were done with a FEI Quanta 200 FEG-ESEM with an EDAX EDS. Both pressed particles (250 – 420 µm) and powders were investigated, and the samples were sprinkled on carbon tape mounted to copper grids prior to investigation. Mostly

low vacuum mode and acceleration voltages from 10 - 20 kV were used due to problems with charge accumulation at the surface. The spot size was kept at 4.

6.2.3 Surface measurements

The surface areas of the fresh and spent catalysts were determined with a BELSORP II mini instrument. Nitrogen was used as adsorptive and the measurements were done at -196 °C with liquid nitrogen as coolant. About 50 mg of the fresh catalysts were used, while about 30 mg were used for the spent catalysts. The pre-treatment conditions were also different for the two types of samples:

- Fresh catalyst
    1 hour at 80 °C and 3 hours at 300 °C
- Spent catalyst
    1 hour at 80 °C and 4 hours at 200 °C

A lower temperature was used for the spent catalyst to avoid coke oxidation or other types of reactions of the retained hydrocarbons. Curve fittings to the data were done with the accompanying software, BelMaster.

6.2.4 FTIR

IR spectra were collected on a FTIR Bruker Vertex 80 with a mercury cadmium telluride (MCT) detector. CO was used as a probe molecule and its interaction with the different groups in the catalysts were followed by desorption at -196 °C by using liquid nitrogen as coolant. Thin wafers of the different samples were prepared and mounted to gold envelopes. Before the measurements, the pellets were pre-treated at 150, 300 and 450 °C for 1 hour at each temperature, a total of 3 hours. The spectra were collected with the software OPUS 8.0.

For H-ZSM-5, no measurement was conducted.

6.2.5 TGA

The measurements were done on a Rheometric Scientific SAT 1500 instrument and the data were collected with a RSI Orchestrator software.

Analyses were done in a flow of 20 ml/min of nitrogen (10 ml/min protection gas) and 10 ml/min of oxygen for both the fresh and spent catalysts. The temperature was for most samples increased from RT to 600 °C with a rate of 5 °C per minute. The temperature was kept at 600 °C for 2 hours. Approximately 50 mg were used for the fresh catalysts, while about 20 mg were used for the spent catalyst.

6.2.6 Catalyst dissolution and coke extraction

15 mg of the spent catalyst was transferred to a Teflon tube where 1 ml of 15 % HF was added to dissolve the zeolite framework. After 45 minutes, the zeolite was completely dissolved and 1 ml of CH_2Cl_2 with o-Cl-Toluene as an internal standard (IS) was added to extract the coke species. Although the HF and CH_2CL_2 phases separated quite readily, the Teflon tube with content was left for 30 minutes. The organic phase was then transferred to a glass vial and analysed using a Agilent Technologies 7890 A GC connected to a combined Agilent Technologies 5975 C inert XL MSD and FID.

The compounds were identified by comparison to the mass spectral library NIST98.

6.3 Calibration

26.0 mg of naphthalene, 26.1 mg of hexamethylbenzene, 26.5 mg of pentamethylbenzene and 25.1 mg of durene were added to 100 ml of CH_2Cl_2 with IS. This solution was diluted twice (1/10 x2), providing a concentration range expected to cover the amount of hydrocarbons extracted from the spent catalysts. The three solutions were analysed using a similar GC-setup as described in section 6.2.6.

7. Catalytic tests

The following paragraphs will cover the reactor system with emphasis on setup, the reactor, test conditions and product analysis.

7.1.1 The reactor system

The reactor system used for the catalytic tests in this thesis was designed by Rønning [75]. A flowchart of the system is presented in figure 7.1. Line 1 and 2 are connected to helium and employed to feed carrier gas that can be led to saturation evaporators with the desired reactants in liquid states. In this work line 2 was disconnected and only line 1 with ^{12}C methanol was in use. The carrier gas bubbles through the reactant and gets saturated in accordance to the temperature of the reactant and the flow of helium passing through it. A water bath surrounding the evaporator keeps the temperature constant and Porter P-150 ball flow meters were used to control the carrier gas flow.

Pressure build-ups in the line can be detected with the connected manometer, which is also useful during leak tests of both the reactor and the complete system. Line 3 and 4 are connected to pure helium and oxygen, respectively. The oxygen line was used for *in situ* calcination and pre-treatment of the zeolite catalysts. To ensure correct gas flow during both pre-treatment and reactions, it was measured with an external flow meter. The catalytic reactions were conducted in a U-shaped, fixed bed glass reactor with an internal diameter of 15 mm. A thermocouple was placed in the catalyst bed to monitor the reaction temperature.
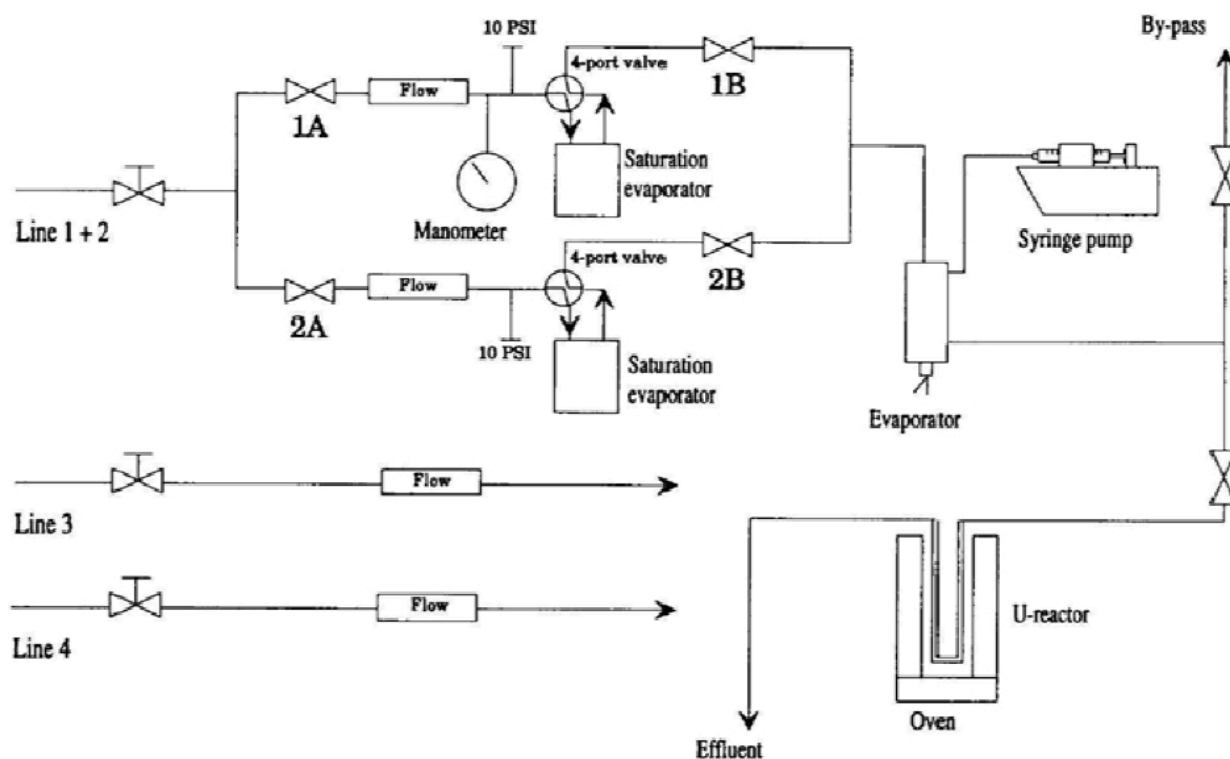
Figure 7.1: Flowchart of the reactor system used in this thesis [75].

7.1.2 Test conditions and operation

To obtain the desired size of catalyst particles, the catalyst powders were pressed to wafers, gently crushed and sieved to particles ranging from 250 – 420 µm in size. This was done to avoid pressure build-ups over the catalyst bed, to ensure test reproducibility and to keep the catalytic material in place. In order to have sufficient amounts of spent catalyst for further studies, 100 mg of catalyst was used.

Prior to each test, the catalyst was pre-treated *in situ* at 500 °C in a flow of pure oxygen for 1 hour. The flow was then changed to pure helium and the temperature was decreased to 400 °C (reaction temperature). While the temperature was stabilizing at 400 °C, the helium flow in line 1 (for feeding methanol) was set to 17.30 ml/min and the water bath temperature was adjusted to 20 °C. When taking the catalyst mass of 100 mg into consideration, this corresponds to a methanol weight hourly space velocity (WHSV) of 2.00 h^{-1}. After stabilization of the

43

temperature, the feed was changed to methanol-saturated helium and the reaction was started while monitoring the TOS with a stopwatch.

The catalyst lifetime obviously varies depending on the catalyst used, and after ensuring reproducibility of the tests, a number of experiments with varying TOS were conducted. The different experiments were thermally quenched at individually desired TOS and in this way, series of gradually deactivated catalysts were obtained.

7.1.3 Product analysis

The product analysis was performed with an online Agilent 6890 A GC connected to a FID. The GC has a Supelco SPB-5 capillary column with dimensions 60 m × 0.53 mm × 3 μm.

Depending on the catalyst used in the experiments, the GC temperature program was varied slightly. The temperature was increased from 45 – 260 °C with a rate of 25 °C/min and with a 5 minute holding time at 45 °C for all samples. The final hold time was increased for large pore zeolites where larger hydrocarbons in the effluent were present.

8. Results and discussion

This chapter contains results and discussion on catalyst characterization, conversion properties and the main section on deactivation in the end. As this thesis involves no synthesis of new materials the focus has been shifted from product formation to the qualitative and quantitative study on coke formation.

8.1 Catalyst characterization

In the following subchapter, the physical characteristics of the different catalysts are given with elaborations. Except for the H-ZSM-5, where no FTIR measurement was done, all the catalysts were examined using all techniques.

8.1.1 XRD

X-ray diffractograms for the five different catalyst samples are shown in figure 8.1. They confirm that the samples are highly crystalline and of the expected phases. The broadening of the peaks for the two beta zeolites is well known and arises because of their special disordered structure. As mentioned in section 2.4.3, the beta zeolite consists of an intergrowth of three similar, but distinct structures. The intergrowth of these polymorphs give similar reflections, but at slightly different angles, leading to wider peaks. From the micrographs of the corresponding zeolites (figure 8.3, top panel), it also seems like the two beta zeolites consists of very small crystals, a property that additionally may lead to peak broadening [76].

In the diffractograms to the two beta zeolites there is also observed an intensity difference at reflections ~8 and ~22.6°. For zeolites, the low-angle reflection intensities are sensitive to the presence of non-framework species [54, 77]. In the case for H-BEA, with a specified Si/Al ratio from the manufacturer of 12.5 (supported by EDS), FTIR spectroscopy shows a lack of Brønsted acid sites (see below), and it is therefore likely that much of the Al content is not located in framework positions for this material. With this in mind, it is conceivable that Al located

45

elsewhere affects the observed intensities. This could have been confirmed or disproved by the use of ^{27}Al-NMR.
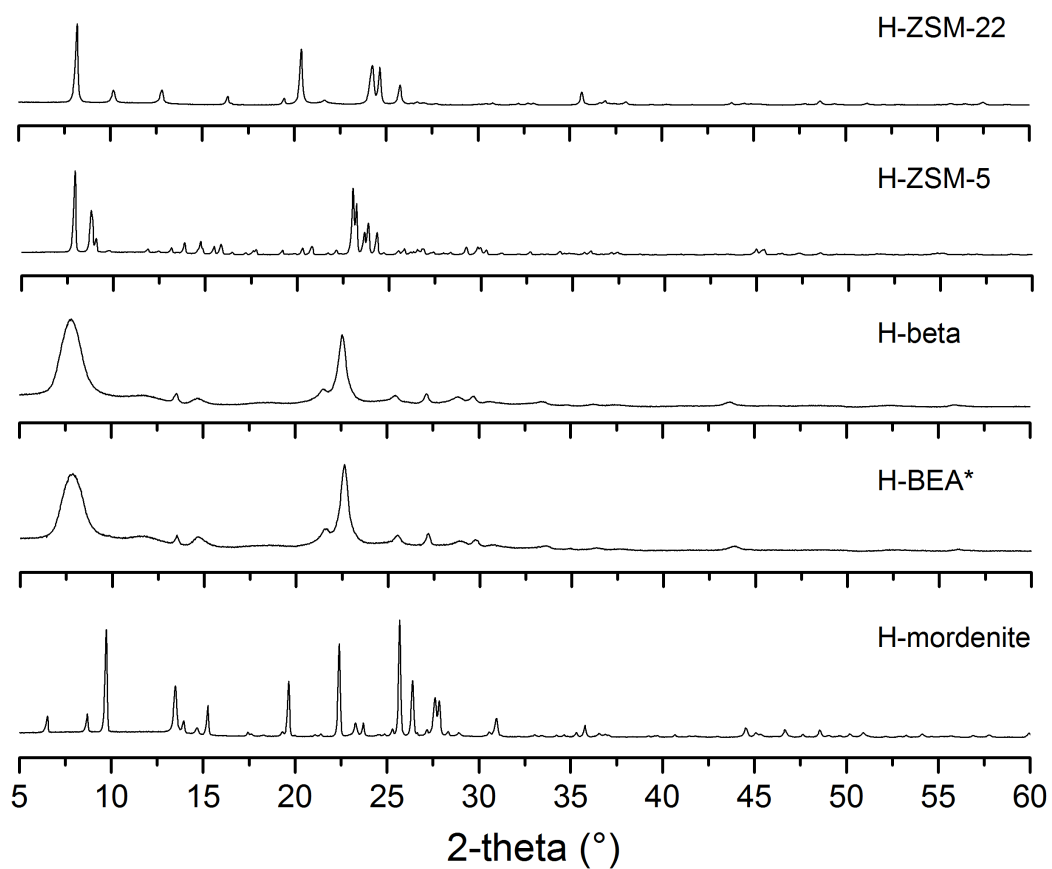

Figure 8.1: Powder X-ray diffractograms of the different catalysts.

8.1.2 SEM

The size distributions of the catalyst particles were investigated with SEM and representative micrographs of the different samples are given in figure 8.2 and 8.3.

From figure 8.2 it can be observed that H-ZSM-22 (left panel) and H-ZSM-5 (right panel) possess needle shaped crystals with a major size distribution around 3-4 and 2-3 µm respectively. The crystal sizes for H-ZSM-22 appear to be highly uniform, while for H-ZSM-5 larger variations are observed.
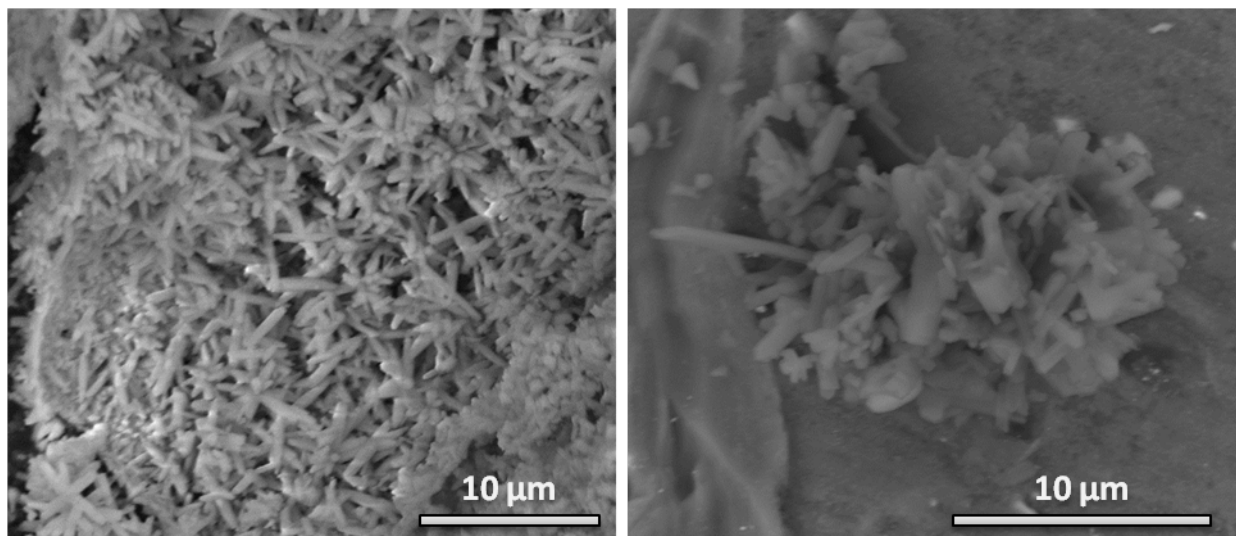
Figure 8.2: SEM micrographs of H-ZSM-22 (left panel) and H-ZSM-5 (right panel)

The beta zeolites and the H-mordenite were not easily characterized, and the beta zeolites in particular were not amenable to SEM. It looks like the crystals for H-beta (top left panel) and H-BEA (top right panel) are smaller compared to H-ZSM-22 and H-ZSM-5, but it is hard to say with certainty. It could have been desirable to use transmission electron microscopy (TEM) to determine the particle size further, but this has not been given priority.

The H-mordenite (bottom panel) distinguishes itself quite clearly from the needle shaped crystals observed for H-ZSM-22 and H-ZSM-5, and appears more oval. The size of the crystals is approximately 3 µm, but from the overview image it might also look like the formation of agglomerates is a case for this zeolite.
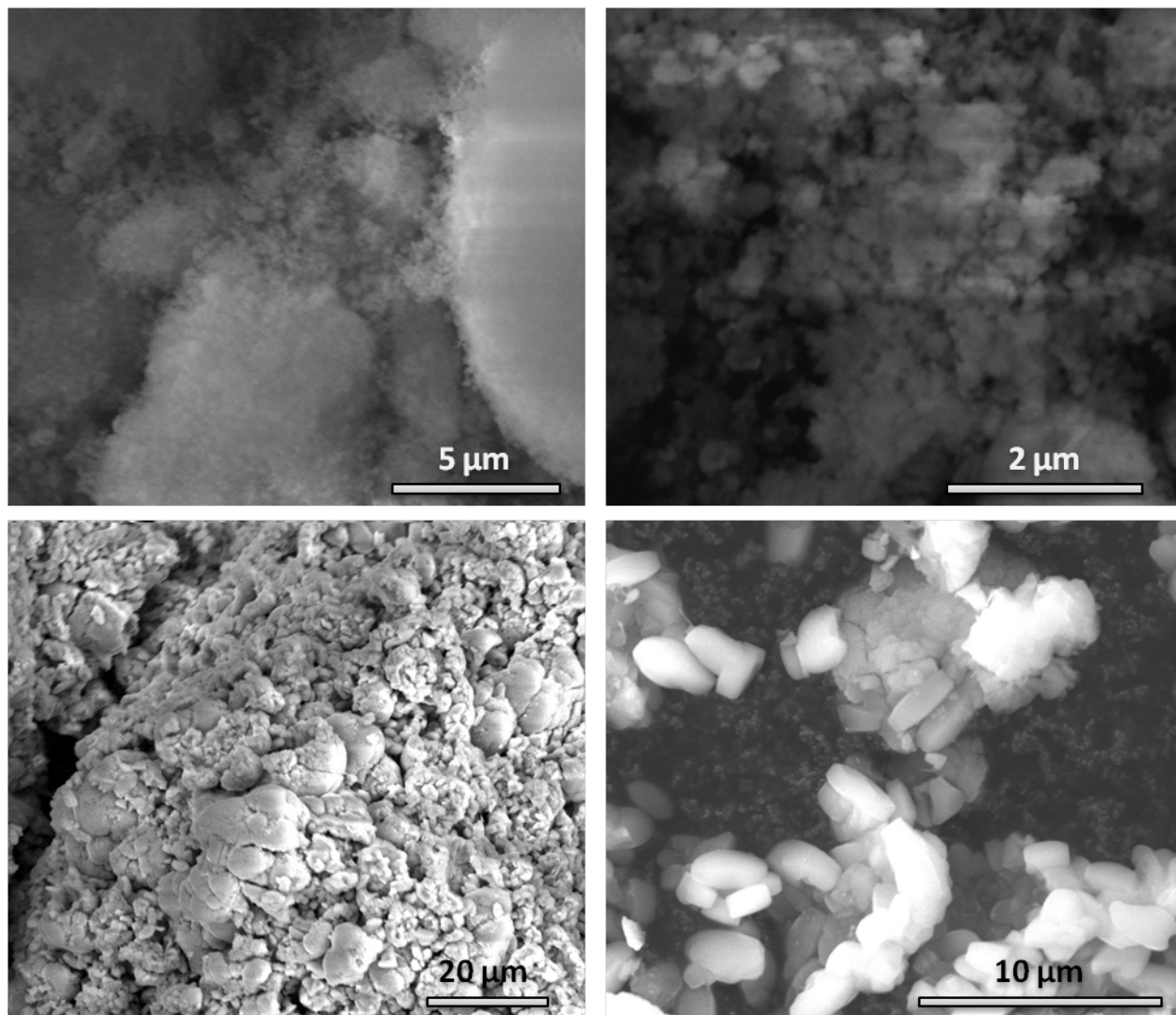
Figure 8.3: SEM micrographs of H-beta (top left panel), H-BEA (top right panel) and H-mordenite (bottom panel).

During the SEM investigations, an EDS analysis was also conducted to estimate the elemental composition of the different samples. The obtained Si/Al ratios are given in table 8.1.

Table 8.1: Silicon to aluminium ratio for the different catalysts obtained by EDS analysis.

Catalyst	Si/Al ratio
H-ZSM-22	32.1
H-ZSM-5	13.7
H-beta	15.4
H-BEA	12.4
H-mordenite	8.8

The results are quite consistent for the zeolites with a lower Si/Al ratio, but deviate for H-ZSM-22 and H-beta having lower Al contents. These results are based on a one-point analysis only, which can give a possible explanation for the deviation for the zeolites with lower Al content. It should be noted that this method is a bit unreliable with respect to zeolites, and the results can very much be affected by signal overlap of Si and Al signals.

8.1.3 Sorption measurements and TGA

Table 8.2 summarizes the determined surface area, micropore volume and water loss (from TGA) of the different catalysts. Without further discussion, it seems like the relative water content increases with pore size. BET surface areas in these regions have previously been reported in literature for the respective materials [47, 54, 78].

Table 8.2: Textural properties and water weight loss for the different catalysts.

Catalyst	BET surface area (m²/g)	Langmuir surface area (m²/g)	Micropore volume[a] (cm³/g)	Weight loss[b] (wt%)
H-ZSM-22	202	219	0.072	3.0
H-ZSM-5	406	460	0.168	8.4
H-beta	701	736	0.189	10.7
H-BEA	503	504	0.139	11.6
H-mordenite	507	537	0.194	13.2

[a] t-plot method
[b] TGA

The related N_2 adsorption/desorption isotherms are illustrated in figure 8.4. H-ZSM-5 and H-mordenite display typical isotherms for microporous solids and possess well-defined saturation limits that correspond to complete filling of the intracrystalline pore system. In the case of H-ZSM-22, a flat and wide hysteresis loop is observed, which is usually ascribed to materials with slit-shaped pores [71].

In the beta zeolites, no notable hysteresis is visible, but the amount adsorbed does not approach a well-defined saturation limit as the relative pressure increases. It is also evident that H-beta exhibits a significantly higher adsorption capacity compared to H-BEA. The absence of a clear saturation limit may possibly be ascribed to the formation of multilayers in these materials, but the relatively large difference in adsorption capacity between the two is harder to explain. A possible explanation can be seen in connection with Al in non-framework positions

for H-BEA (described above), as extra framework species may block the access to the intracystalline pore system for this material.
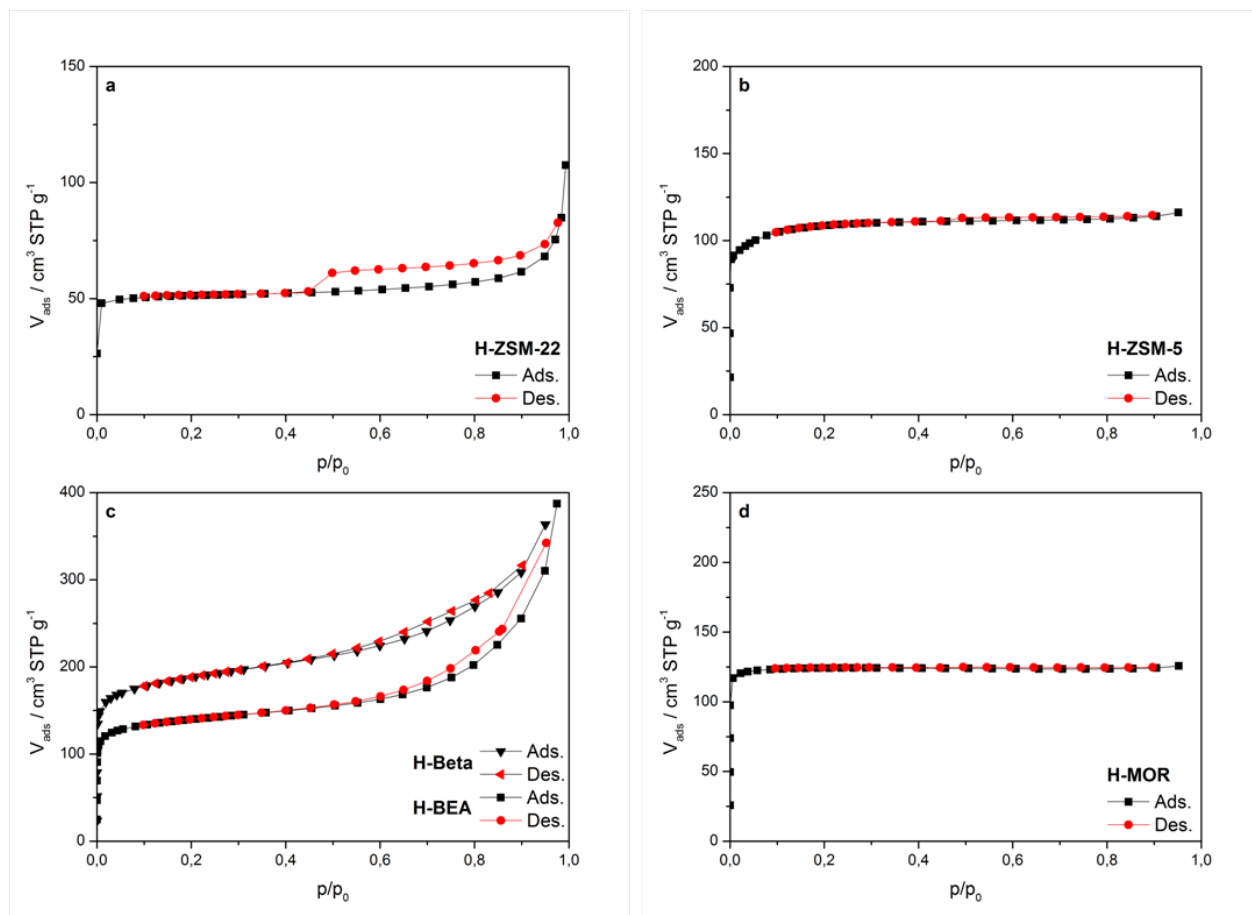

Figure 8.4: BET adsorption/desorption isotherms for the different catalyst, a: H-ZSM-22 b: H-ZSM-5 c: H-beta and H-BEA d: H-mordenite.

8.1.4 FTIR Spectroscopy

FTIR measurements were performed for identification and to investigate the acidic property of the different zeolites. The figures 8.5-8.8 report series of FTIR spectra collected for H-ZSM-22, H-beta, H-BEA and H-mordenite, respectively. The spectra are separated into two regions; the v(OH) region is given in the left panel and the v(CO) region is given in the right. In the measurements, CO desorption were followed and the spectra in cyan represent samples saturated with CO, while the spectra in magenta represent complete, or almost complete, desorption of CO. The light grey spectra in between are spectra recorded at decreasing CO pressures.
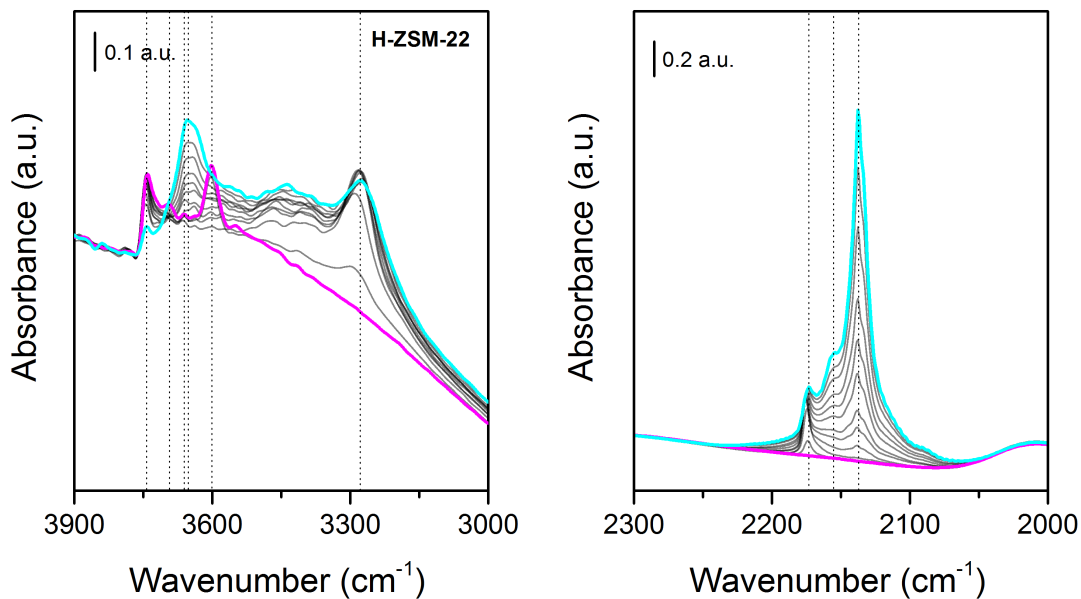
Figure 8.5: FTIR spectra of H-ZSM-22 in the v(OH) (left panel) and the v(CO) (right panel) region collected at desorption of CO at -196 °C. The spectrum in cyan represents complete saturation, while the spectrum in magenta represents complete desorption of CO.
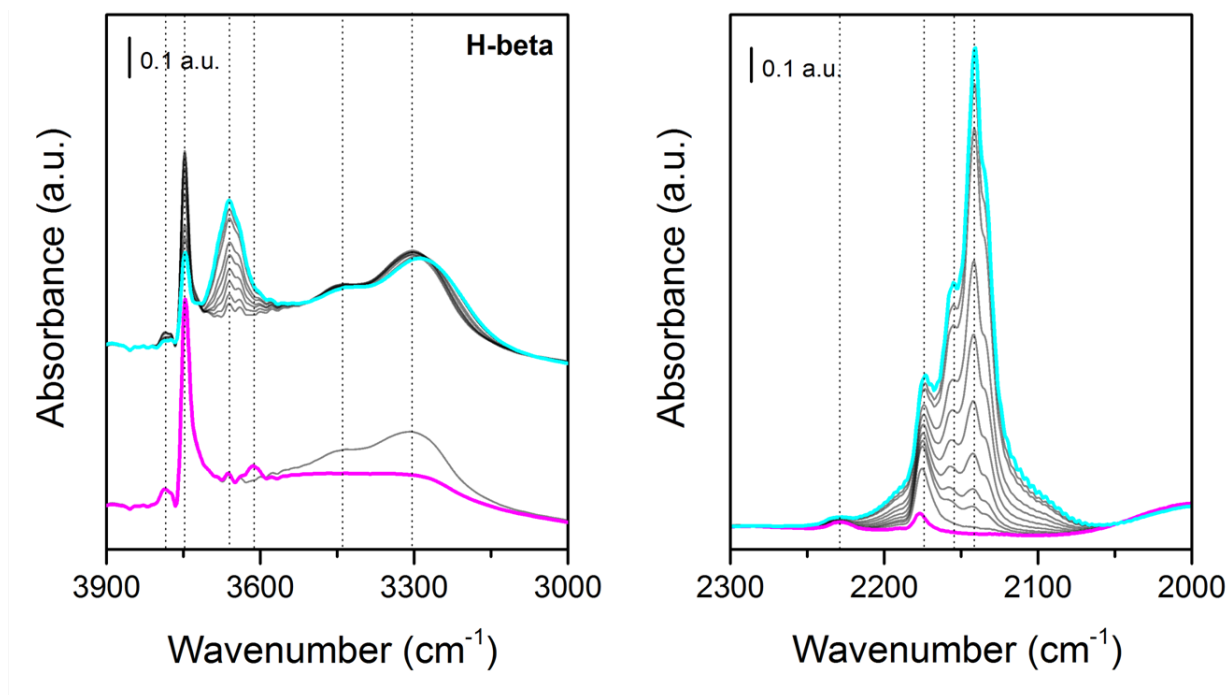
Figure 8.6: FTIR spectra of H-beta in the v(OH) (left panel) and the v(CO) (right panel) region collected at desorption of CO at -196 °C. The spectrum in cyan represents complete saturation, while the spectrum in magenta represents almost complete desorption of CO.
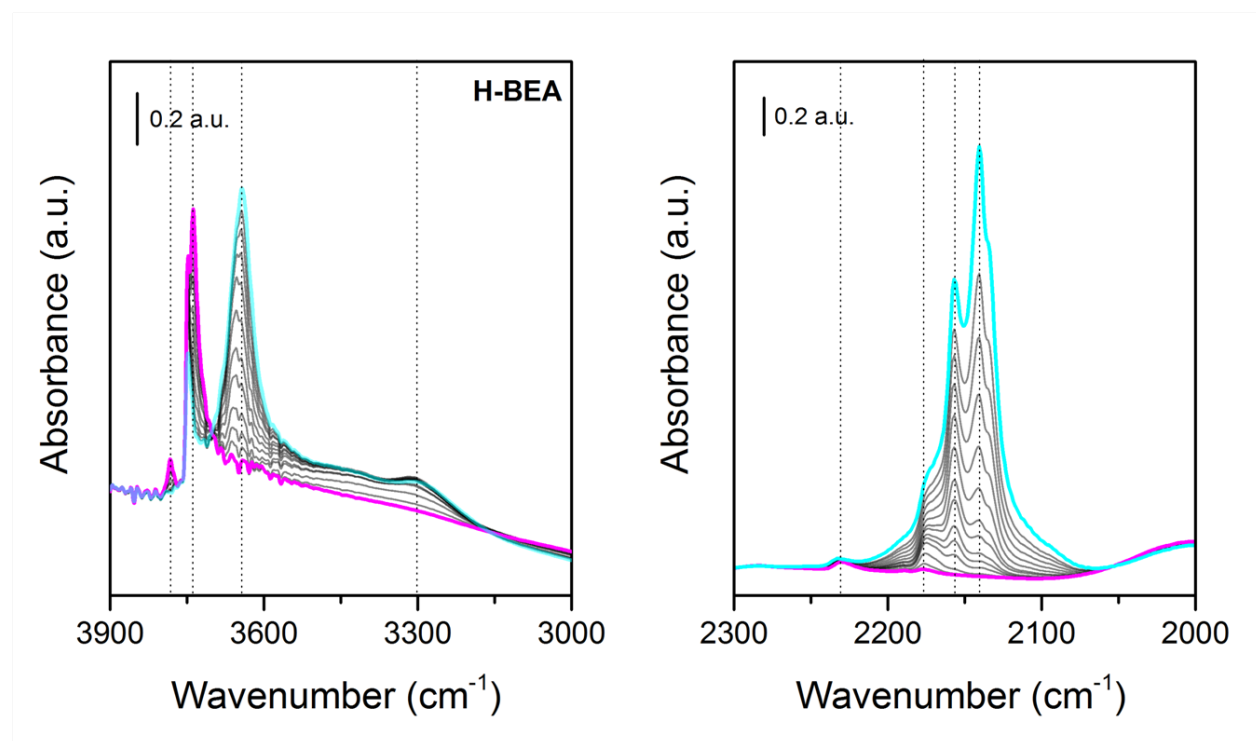
Figure 8.7: FTIR spectra of H-BEA in the v(OH) (left panel) and the v(CO) (right panel) region collected at desorption of CO at -196 °C. The spectrum in cyan represents complete saturation, while the spectrum in magenta represents almost complete desorption of CO.

53
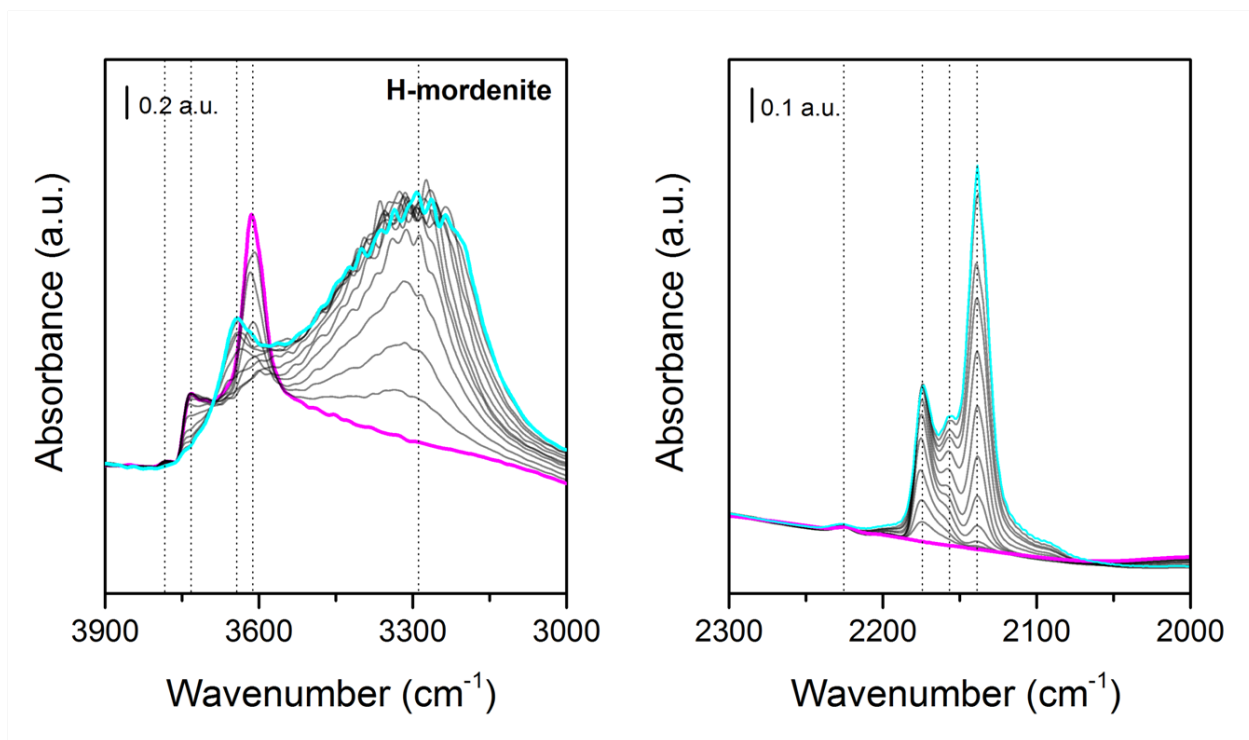
Figure 8.8: FTIR spectra of H-mordenite in the *ν*(OH) (left panel) and the *ν*(CO) (right panel) region, collected at desorption of CO at -196 °C. The spectrum in cyan represents complete saturation, while the spectrum in magenta represents almost complete desorption of CO.

Although there are some differences, the spectra of the different zeolites obviously possess similarities. For convenience, both similar and individual bands in the spectra will in the following be assigned in one. At complete desorption (magenta) several bands are present. With decreasing frequency:

(i)   Band at ~3782 cm^{-1}. To some extent, it may look like there is absorption at this frequency for all samples, but the band is particularly evident for the two beta zeolites. This indicates the presence of extra-framework Al-OH groups.

(ii)   Band at ~3747 cm^{-1}. This peak is observed for all samples and represents isolated Si-OH groups (silanols) on the external surface of the zeolites. A low frequency tail accompanying this main band is also clearly visible for H-ZSM-22, which indicates the presence of internal silanol defects.

(iii)   Weak absorption band around 3660-3680 cm^{-1}. This not so prominent band is associated with partially hydrolyzed extra-framework Al species and is present for H-ZSM-22 and H-beta.

(iv)   Band at ~3610 cm^{-1}. This feature is the most interesting with respect to zeolite catalysts and represents strongly acidic Si-OH-Al Brønsted sites. These sites are clearly visible for H-ZSM-22, H-beta and H-mordenite, but remarkably, no peak is observed for the H-BEA sample.

To summarize, the two families of OH groups expected in zeolites, terminating silanols and Brønsted acid sites, can be clearly distinguished in the spectra for all samples except for H-BEA, which seemingly lack Brønsted acid sites (see below). Additionally:

- Extra-framework Al-OH groups are present for H-beta and H-BEA
- Internal silanols are present in H-ZSM-22
- Partially hydrolyzed extra-framework Al is present for H-ZSM-22 and H-beta

The fact that that no peak corresponding to Brønsted acid sites is observed in the H-BEA sample could be due to poor sample preparation or large particle size (pronounced scattering), but might of course also indicate few, or a complete lack of these sites. This catalyst (identical material) has earlier been studied with FTIR and also here no band corresponding to Brønsted acid sites was observed [79]. From this it is therefore reasonable to assume that the catalyst lacks these sites. However, after CO adsorption, which induces shifts on the original vibrations (see next paragraph), a small band corresponding to the Brønsted acid sites can be observed. The catalyst also proved to be active in the conversion of methanol to hydrocarbons (section 8.2) and it is therefore clear that the material contain some sites, yet significantly fewer than what the given Si/Al ratio suggests.

The acidic strength of the species observed cannot be assessed by direct measurements of the vibrational frequency of the unperturbed OH groups, but by the shift in frequency caused by the interaction with CO (or other basic molecules). When adsorbing a base, the observed shift of the v(OH) band will be proportional to the Brønsted acidic strength of these species [46, 74]. When CO is adsorbed (in this case desorption is followed), the original bands are gradually consumed and give rise to new bands associated with OH···CO interactions. The formation of such OH···CO adducts is schematically illustrated at a Brønsted acid site in figure 8.9.
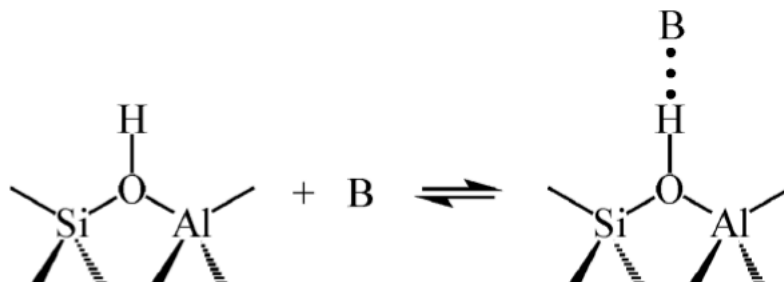
Figure 8.9: Schematic illustration of the formation of a OH···B adduct at a Brønsted acid site when a base (B) is adsorbed in zeolites [74].

The course from no, or small amounts of CO adsorbed, to complete saturation, is as previously mentioned displayed by the light grey spectra in the figures 8.5-8.8 above. While the original v(OH) bands gradually decrease, the vibrations of the OH···CO adducts grow in a similar manner at lower frequencies. The silanol and Brønsted bands at ~3747 and ~3610 cm^{-1} are shifted to broader bands at around 3600-3640 cm^{-1} and ~3270 cm^{-1}, respectively. More precise frequencies and the value of the frequency shifts for silanols and Brønsted acid sites for all investigated samples are given in table 8.3.

Table 8.3: Band frequencies with induced shifts for the Si-OH groups (left) and the Si-OH-Al groups (right) for the different catalysts after adsorption of CO.

Catalyst	Si-OH				Si-OH-Al		
	v(OH) (cm^{-1})	v(OH···CO) (cm^{-1})	Δv(OH) (cm^{-1})	Δv(OH) (cm^{-1})	v(OH···CO) (cm^{-1})	Δv(OH) (cm^{-1})
H-ZSM-22	3744	3654	-90	3601	3276	-325
H-beta	3750	3660	-90	3615	3295	-320
H-BEA	3741	3643	-98	-	3294	-
H-mordenite	3738	3648	-90	3616	3291	-325

An important feature, as can be seen from the frequency shifts for the Brønsted acid sites, shows that the acid strength is very similar for all materials. From the table it can also observed that the induced shifts are much stronger for the Brønsted acid sites compared to the silanols, which simply reflects their difference in acid strength.

A comment should also be made on the bands in the v(CO) region. For all zeolites three distinct bands are present at approximately 2138, 2160 and 2175 cm^{-1}. These bands can be ascribed to liquid like CO, CO adsorbed on Si-OH sites or partially extra-framework Al-OH and CO adsorbed on strongly acidic Si-OH-Al Brønsted sites, respectively. For the beta zeolites and the H-mordenite, a band at ~2230 cm^{-1} is also observed, which can be explained by extra framework Al of Lewis acidic character. The band corresponding to CO adsorbed on Si-OH-Al sites in the H-BEA zeolite is clearly different compared with the other samples and appears more like a shoulder to the bigger silanol band. This observation is in accordance with the previous explanations for this material.

8.2 Catalyst conversion properties

Although the main purpose of this thesis is to analyse coke formation in the MTH process, it is nevertheless of interest to show the conversion properties of the materials investigated. In addition to showing how well suited a catalyst is for a certain process, conversion versus TOS curves can be helpful when describing deactivation behavior. This section will therefore serve to provide an insight in the differences in catalyst lifetime and product formation for the different catalysts employed.

8.2.1 Catalyst lifetime

The catalytic tests in the MTH conversion were conducted at identical conditions for all catalysts (see chapter 7), but the materials showed major differences in stability. The deactivation profiles for each catalyst, given as loss in methanol conversion with TOS, are presented in figure 8.10.
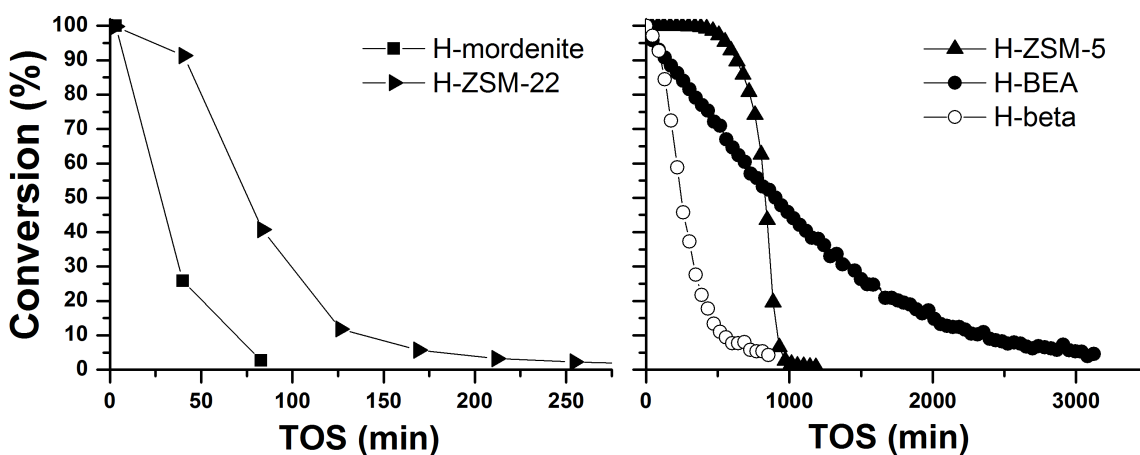
Figure 8.10: Catalyst lifetime for the different zeolites at a reaction temperature of 400 °C and a WHSV = 2.00 h^{-1}, given as loss in methanol conversion with TOS.

Direct comparisons between catalyst lifetime and deactivation for different topologies can be complicated by differences in other parameters which are known to influence catalyst deactivation, such as crystal size, acid strength and acid site density [30]. Although the examination of the catalyst's salient features in the previous section clarifies some differences, the catalysts undoubtedly fall into two groups of conversion capacities. On one hand, the one-dimensional zeolites H-ZSM-22 and H-mordenite lose activity quickly, while on the other, the three-dimensional H-ZSM-5 and beta zeolites are able to convert methanol over a longer period of time.

The unique properties of the H-ZSM-5 in the MTH process is illustrated by its ability to maintain a high conversion for several hours; in clear contrast to the other catalysts investigated. For this material, the conversion versus TOS curve takes an S form, with a period of full conversion for several hours followed by rather rapid, then diminishing, deactivation. According to Olsbye *et al*. is this typical of a situation in which the reactions, also those leading to deactivating species, occur in a narrow zone of the reactor bed [30].

The two beta zeolites, which have larger pores compared to H-ZSM-5, also possess a relatively long lifetime, but the conversion decreases immediately. Although H-beta is unable to maintain a high conversion level, the conversion versus TOS curve takes a resembling form as for H-ZSM-5. H-BEA on the other hand, loses activity more gradually and lacks a clear breakthrough with rapid deactivation. The fact that H-beta deactivates more rapidly compared to H-BEA is in accordance with their respective acid site density, as H-BEA possesses fewer active sites (see section 8.1.4). A more rapid catalyst deactivation with a higher acid site density has previously been reported as a general trend by Stöcker [29], and Guisnet *et al.* has in more recent times explained this connection more thoroughly [30, 80]: "The higher the density of the acid sites, thus the closer these sites are to each other, the larger the number of successive chemical steps undergone by reactant molecules along the diffusion path within the zeolite crystallites and the more favorable the condensation reactions, hence the faster coking rate."

It has previously been specified that it is the same hydrocarbon compounds that are built up and retained in large pore beta and mordenite zeolites [47], but from figure 8.10 it is evident

that H-mordenite in this case deactivates much more rapidly. Under the reaction conditions used in this work, the catalyst is completely deactivated in just over 75 minutes, which is even faster than for H-ZSM-22. H-mordenite is a large pore zeolite with a one-dimensional channel system (contains side pockets), and the catalyst employed in this work has in fact the highest Al content and the largest micropore volume of all samples investigated. Caution should be used when comparing different zeolite topologies, but it is nevertheless clear that coke species are formed readily over this material. For H-ZSM-22, a rapid deactivation was expected, as low feed rates and temperatures above 350 °C have previously been reported to be essential to even get an appreciable conversion over this material [66]. This was also confirmed.

8.2.2 Selectivity and yield

This section has not been given much emphasis, but it is of interest to investigate if and how the product distribution changes with ongoing deactivation in the different catalysts. Figure 8.11 - 8.15 show product selectivities (left panel) and product yield (right panel) for all catalysts investigated at a reaction temperature of 400 °C and a WHSV = 2.00 h^{-1}.
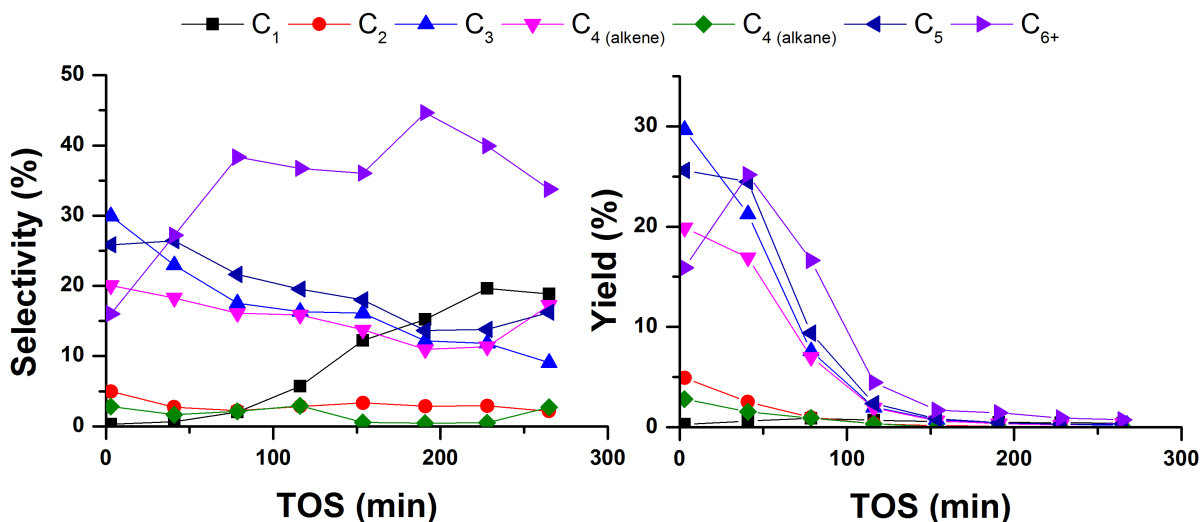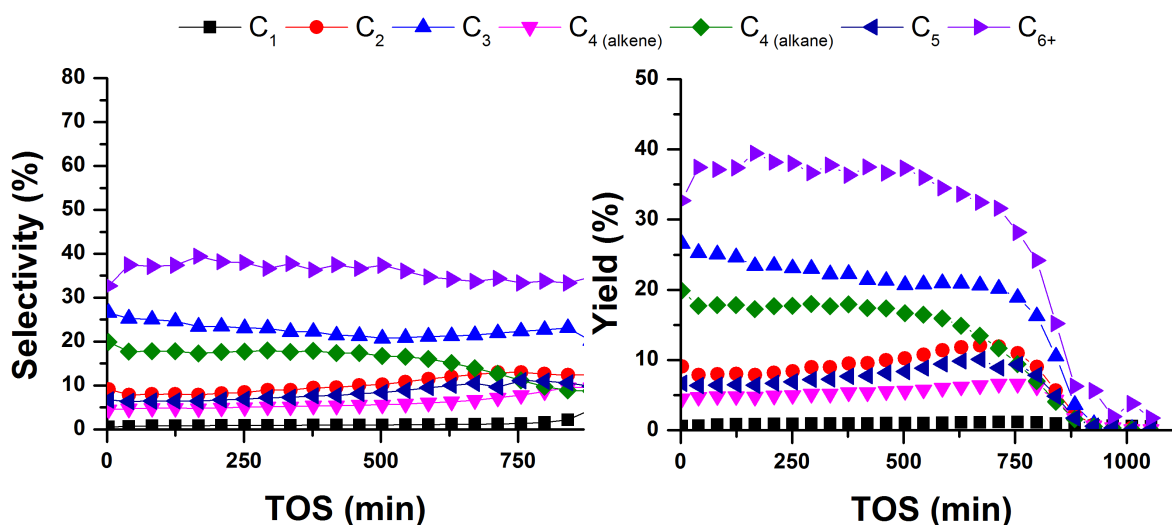

Figure 8.11: Product selectivity (left panel) and product yield (right panel) at 400 °C and WHSV = 2.00 h^{-1} over H-ZSM-22.

60

Initially, for H-ZSM-22, a wide range of hydrocarbons is formed, with selectivity to C_3 - C_{6+} compounds, but with minimal amounts of alkanes in the C_4 fraction. Very little ethane/ethane is formed over this catalyst. This is consistent with earlier observations where the methylation/cracking cycle is dominant, and the aromatic based hydrocarbon pool mechanism is suppressed over this topology [55]. With progressive deactivation of the catalyst, the selectivity to C_{6+} and methane increases, while there is a small decrease in selectivity towards $C_3 - C_5$.

Figure 8.12: Product selectivity (left panel) and product yield (right panel) at 400 °C and WHSV = 2.00 h^{-1} over H-ZSM-5.

At full conversion for H-ZSM-5, the product formation is dominated by C_{6+} hydrocarbons, but also significant amounts of propane/propene and C_4 alkanes are produced. After 500 minutes of TOS, the catalyst gradually starts to deactivate and the selectivity to C_4 alkanes decreases slightly, while the selectivity towards C_2, C_4 alkenes and C_5 hydrocarbons increase in a similar manner. Despite of this, it is fair to say that the product distribution remains fairly unchanged throughout the lifetime of the catalyst, a feature that has previously been reported for this material [81].
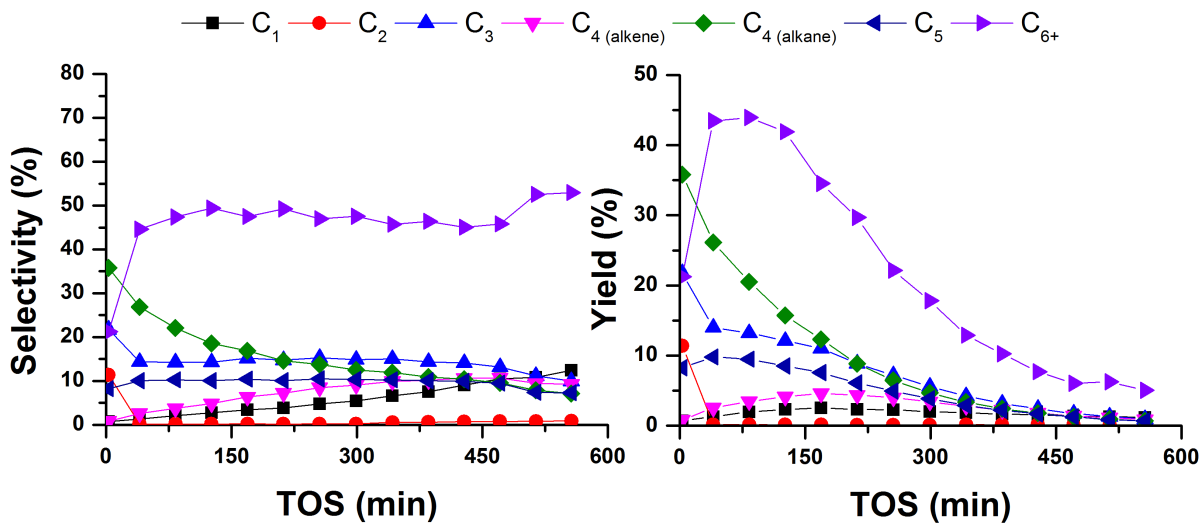
Figure 8.13: Product selectivity (left panel) and product yield (right panel) at 400 °C and WHSV = 2.00 h⁻¹ over H-beta.
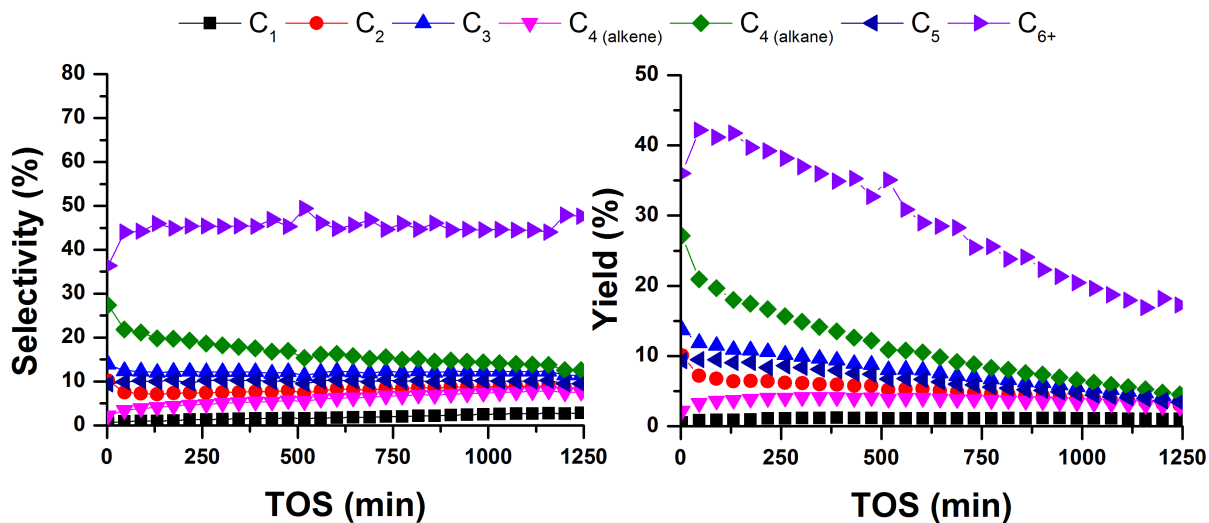

Figure 8.14: Product selectivity (top panel) and product yield (bottom panel) at 400 °C and WHSV = 2.00 h⁻¹ over H-BEA.

Also for the beta zeolites, the primary products are C_{6+} hydrocarbons. Initially, the selectivity towards these compounds is a bit lower, but it quickly stabilizes around 45 %. Other noticeable products include hydrocarbons of C_3, C_4 alkanes and C_5. The C_4 alkane fraction decreases with increasing TOS for both zeolites.
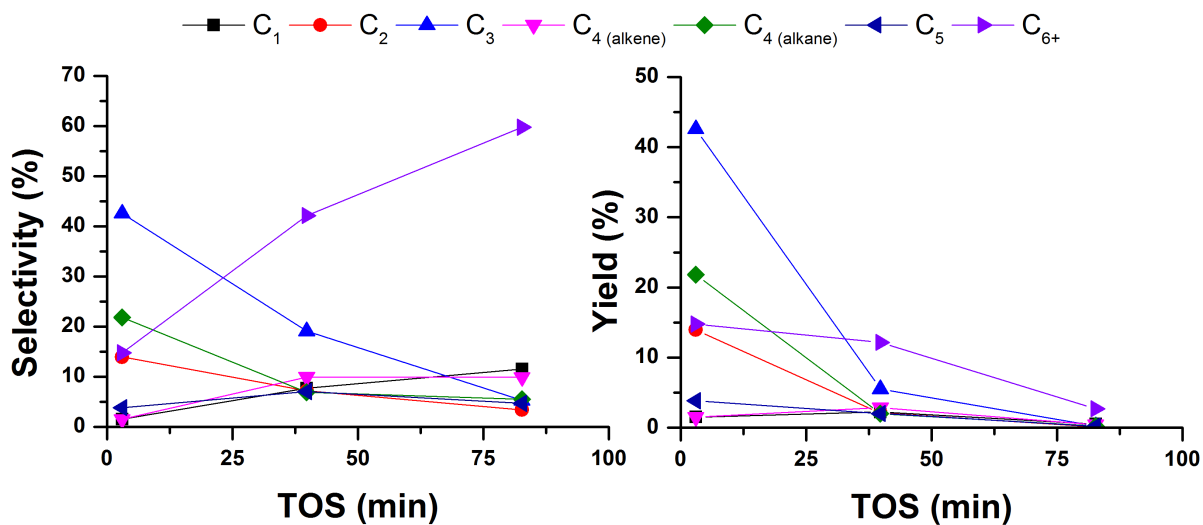
Figure 8.15: Product selectivity (left panel) and product yield (right panel) at 400 °C and WHSV = 2.00 h^{-1} over H-mordenite.

H-mordenite deactivated as mentioned rapidly, but at almost full conversion (TOS = 3 minutes), the product distribution is dominated by the formation of propane/propene. Also minor amounts of C_2, C_4 alkanes and C_{6+} hydrocarbons were observed in the effluent. The C_{6+} fraction increased with TOS, but as this is at a low conversion level (< 30 %), it should not be given much emphasis.

8.3 Qualitative analysis of retained material

Based on the deactivation profiles for the respective catalysts, the MTH reactions were thermally quenched after a certain TOS in order to be able to cover the entire course of deactivation. In the following, GC-MS total ion chromatograms of the gradually deactivated catalysts are presented and discussed.

8.3.1 H-ZSM-22

Figure 8.16 displays the total ion chromatograms of the hydrocarbon extracts from gradually deactivated H-ZSM-22 catalysts from MTH conversions at 400 °C and WHSV = 2 h^{-1}.
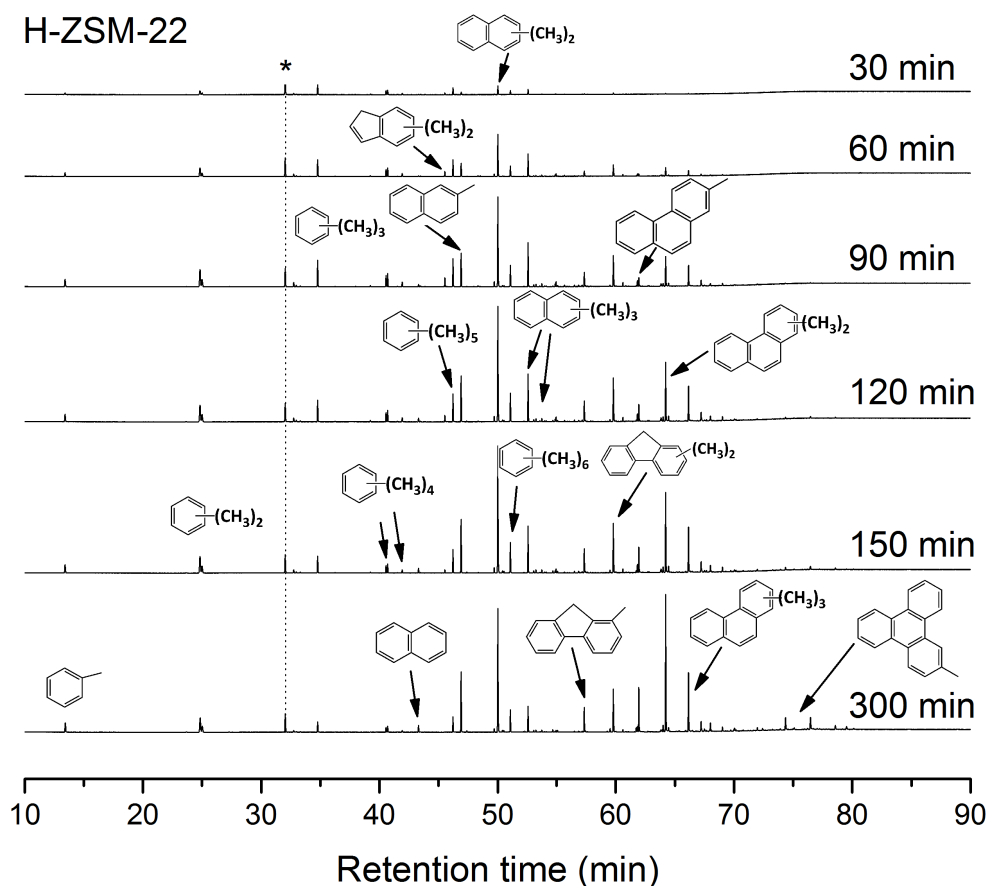
Figure 8.16: GC/MS total ion chromatograms of gradually deactivated H-ZSM-22. Reactions are carried out at 400 °C, WHSV = 2 h^{-1} and thermally quenched at the indicated TOS. All peaks are normalized relative to the internal standard peak, indicated by * in the chromatograms.

After 30 minutes of conversion only small amounts of methylbenzenes and bicyclic arenes are detected. This changes with time, and at a TOS of 60 minutes (conversion ≈ 70 %), also tricyclic arenes are observed.

While it seems like the amounts of methylated benzenes remain relatively unchanged with increasing TOS and deactivation, a higher concentration of the heavier hydrocarbons are observed. Dimethylnaphthalene and dimethylphenanthrene in particular are getting more and more abundant. Seeing that the concentration of these compounds increases with time, it is likely that their diffusivity is severely reduced in the material. Previously, selectivity to retention of slim hydrocarbons with small diameters has been reported for this material at similar conditions [54]. This is in accordance with the observed results and may probably be ascribed to the narrow pore channels in the zeolite. Surprisingly, also aromatics containing four fused benzene rings, which are too big to fit in the pore channels, were detected at a high degree of deactivation. With boiling points around 400 °C for such compounds, it is unlikely that these species are located at the external surface of the catalyst. Although this is only a hypothesis, it is conceivable that they in some way are formed and trapped at the pore mouths of the zeolite, with the inner channels most likely being completely filled with other lower polycyclic coke species.

8.3.2 H-ZSM-5

A similar material to the H-ZSM-5 used in this work has previously been investigated in a comparative study by Bleken *et al.* [78]. After methanol conversion at a reaction temperature of 350 °C and a WHSV = 9 h^{-1}, a clear cut-off after hexamethylbenzenes in the retained material was observed. These observations match Bjørgen *et al.*'s previously described findings [44] (see section 3.3.3), and it was therefore expected that only methylbenzenes would be found as retained material for the investigated catalyst.

The total ion chromatograms of the hydrocarbon extracts from the gradually deactivated H-ZSM-5 catalyst from MTH conversion at 400 °C and WHSV = 2 h^{-1} are displayed in Figure 8.17.
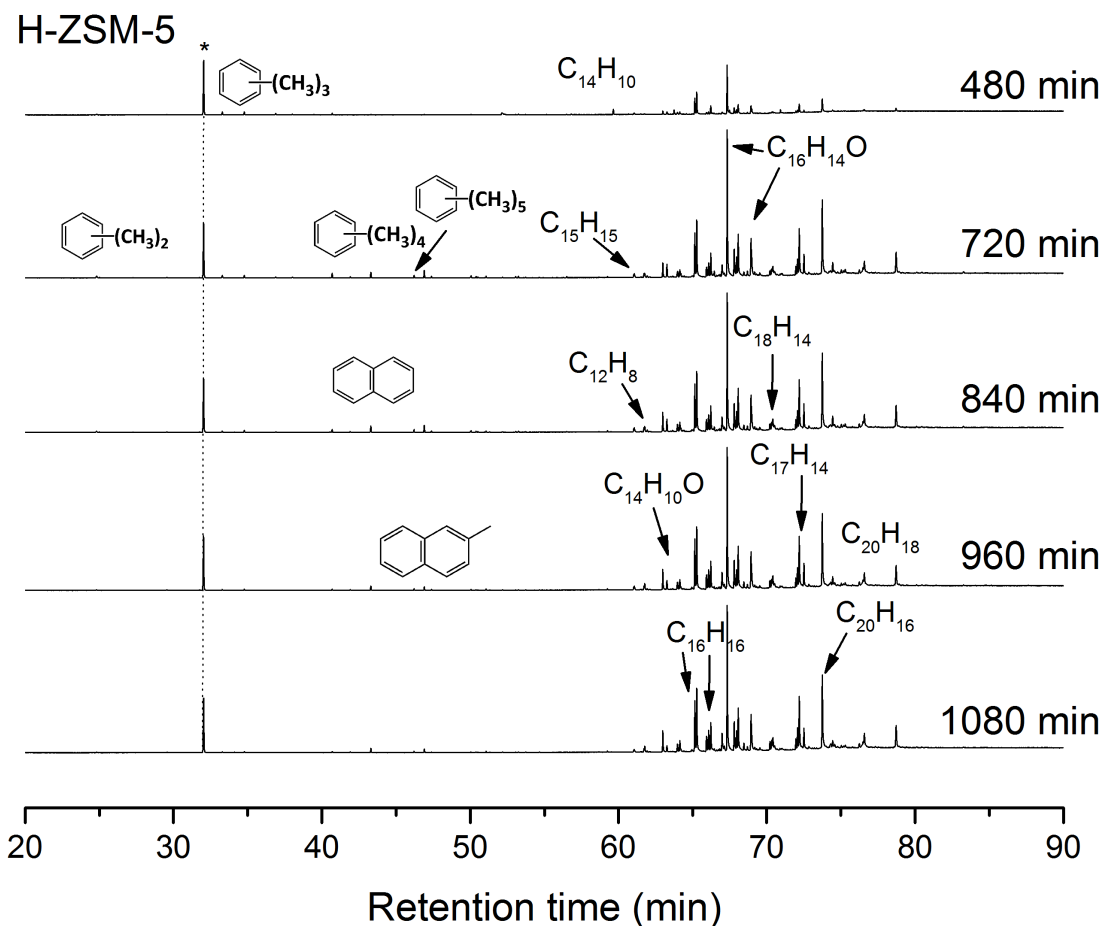
Figure 8.17: GC/MS total ion chromatograms of gradually deactivated H-ZSM-5. Reactions are carried out at 400 °C, WHSV = 2 h^{-1} and thermally quenched at the indicated TOS. All peaks are normalized relative to the internal standard peak, indicated by * in the chromatograms.

In addition to the expected methylated benzenes (hydrocarbon pool species), considerable amounts of more complex, polycyclic arenes of up to four fused benzene rings were detected. These results are clearly contradictory to Bleken and Bjørgen *et al.'s* earlier findings, and raise some doubt around the former assumption on the importance of external versus internal coke formation in H-ZSM-5. It must be mentioned that the conditions in the mentioned studies were a bit different, and especially lower reaction temperatures might play a key role in this matter. The influence of temperature is supported by earlier described findings by Lee *et al.* [63], where

66

polycyclic aromatics were observed after methanol conversion at 500 °C for a similar catalyst, but with lower Al content. The observed results are surprising and not satisfactory understood, and further studies are therefore required.

After methanol breakthrough (TOS > 480 minutes), the chromatograms further show that the distribution of the complex coke species retained does not change significantly with a higher degree of deactivation. On the other hand does the concentration of methylbenzenes, which are key hydrocarbon pool components, gradually decrease before vanishing completely.

The oxygenated hydrocarbons observed were first believed to originate from oxidation during quenching of the reactions, but as these were observed for all samples, this is less likely. As it is not entirely clear what kind of oxygenates that are formed, it has not been investigated further.

8.3.3 Beta Zeolites

The total ion chromatograms of the hydrocarbon extracts from gradually deactivated H-beta and H-BEA catalysts from MTH conversion at 400 °C and WHSV = 2 h^{-1}, are displayed in figure 8.18 and figure 8.19, respectively.

Although a difference in catalyst lifetime for the two beta zeolites has previously been illustrated, there were, because of their identical topology, expected major similarities in retained hydrocarbons for the two. This was also true, and the higher methylated benzenes from tetramethylbenzene to hexamethylbenzenes were observed as the only significant compounds for both catalysts. These compounds are reported to be the most active hydrocarbon pool species for the large pore beta zeolite [46], and the observation of these was therefore no surprise.

More surprisingly, no larger hydrocarbons were detected in any noticeable amounts (only small traces of polycyclic arenes) with on-going deactivation. This indicates that large hydrocarbons (not soluble in CH_2Cl_2) and other heavy coke species are formed readily over this material.
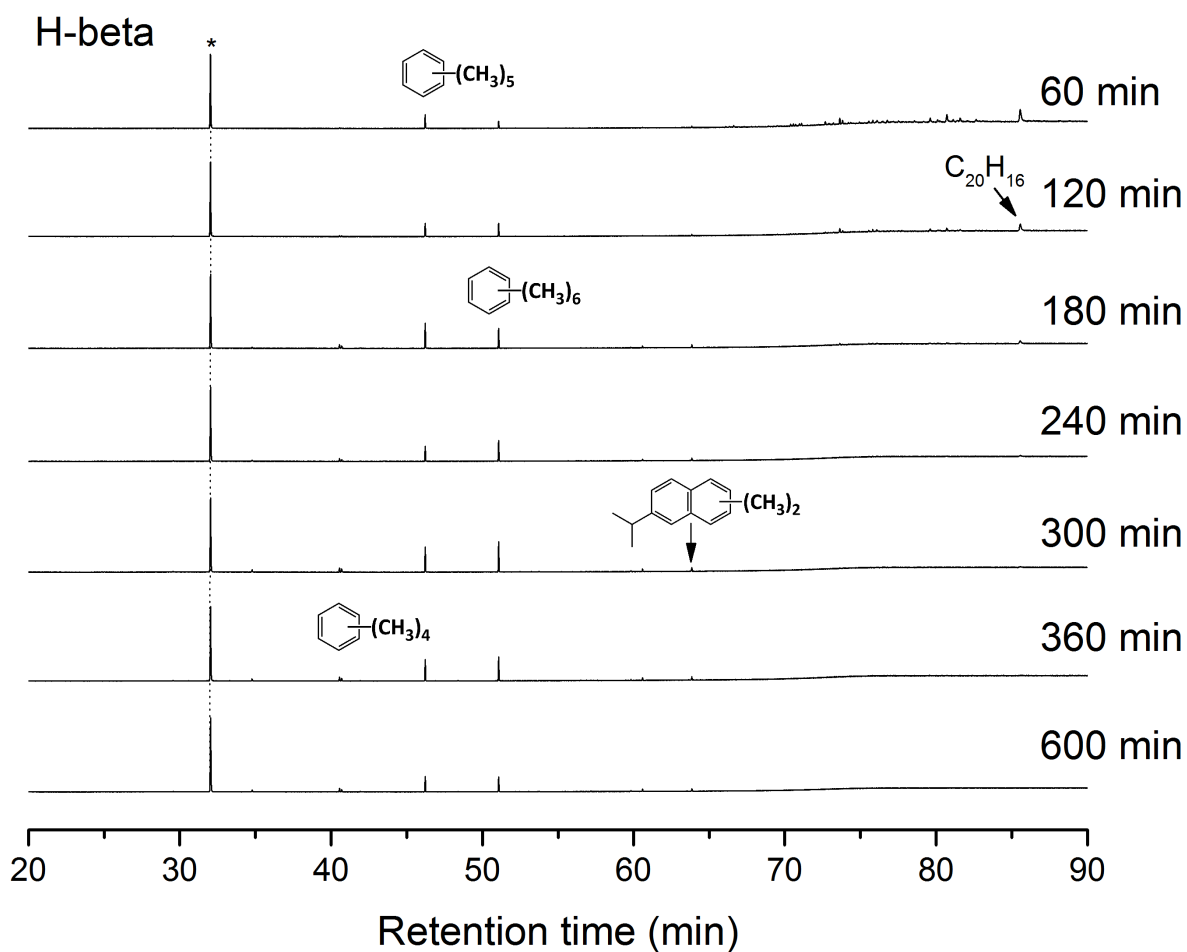
Figure 8.18: GC/MS total ion chromatograms of gradually deactivated H-beta. Reactions are carried out at 400 °C, WHSV = 2 h^{-1} and thermally quenched at the indicated TOS. All peaks are normalized relative to the internal standard peak, indicated by * in the chromatograms.
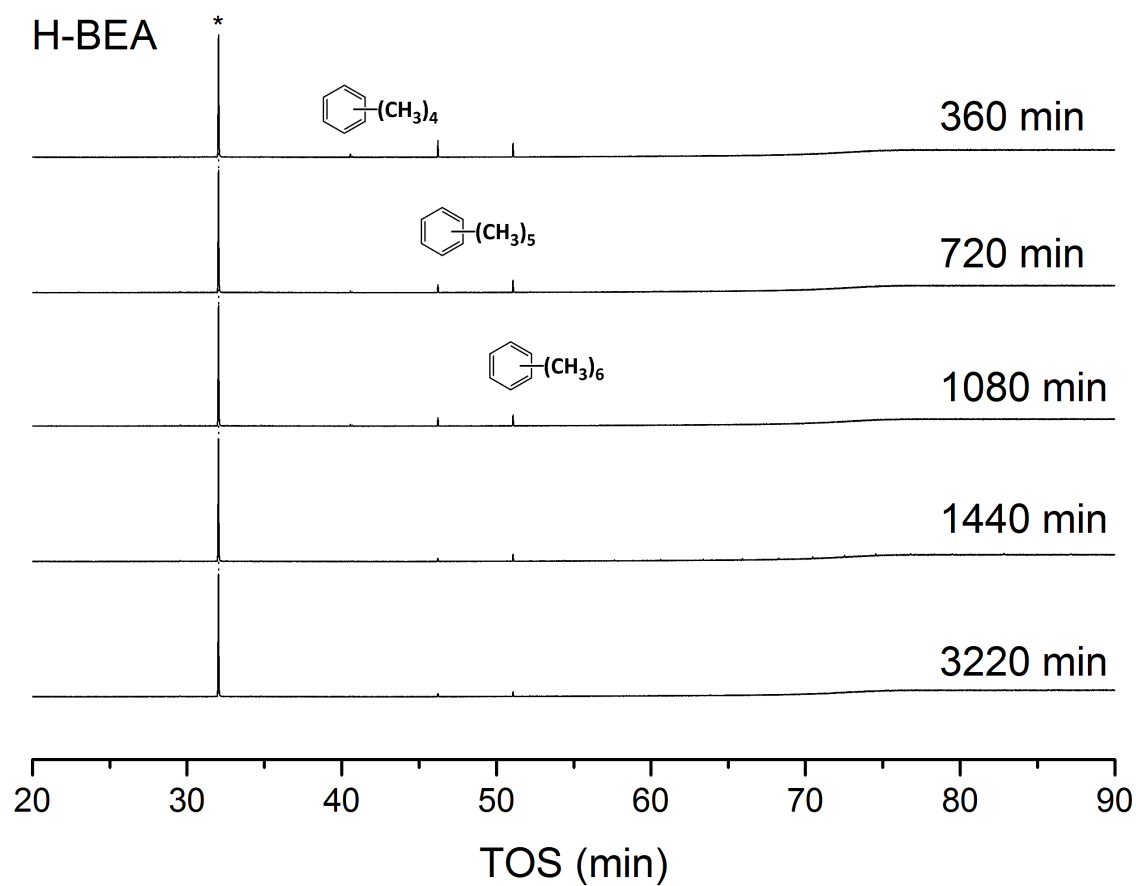
Figure 8.19: GC/MS total ion chromatograms of gradually deactivated H-BEA. Reactions are carried out at 400 °C, WHSV = 2 h^{-1} and thermally quenched at the indicated TOS. All peaks are normalized relative to the internal standard peak, indicated by * in the chromatograms.

8.3.4 H-Mordenite

Figure 8.20 displays the total ion chromatograms of the hydrocarbon extracts from gradually deactivated H-mordenite catalysts from MTH conversion at 400 °C and WHSV = 2 h^{-1}.
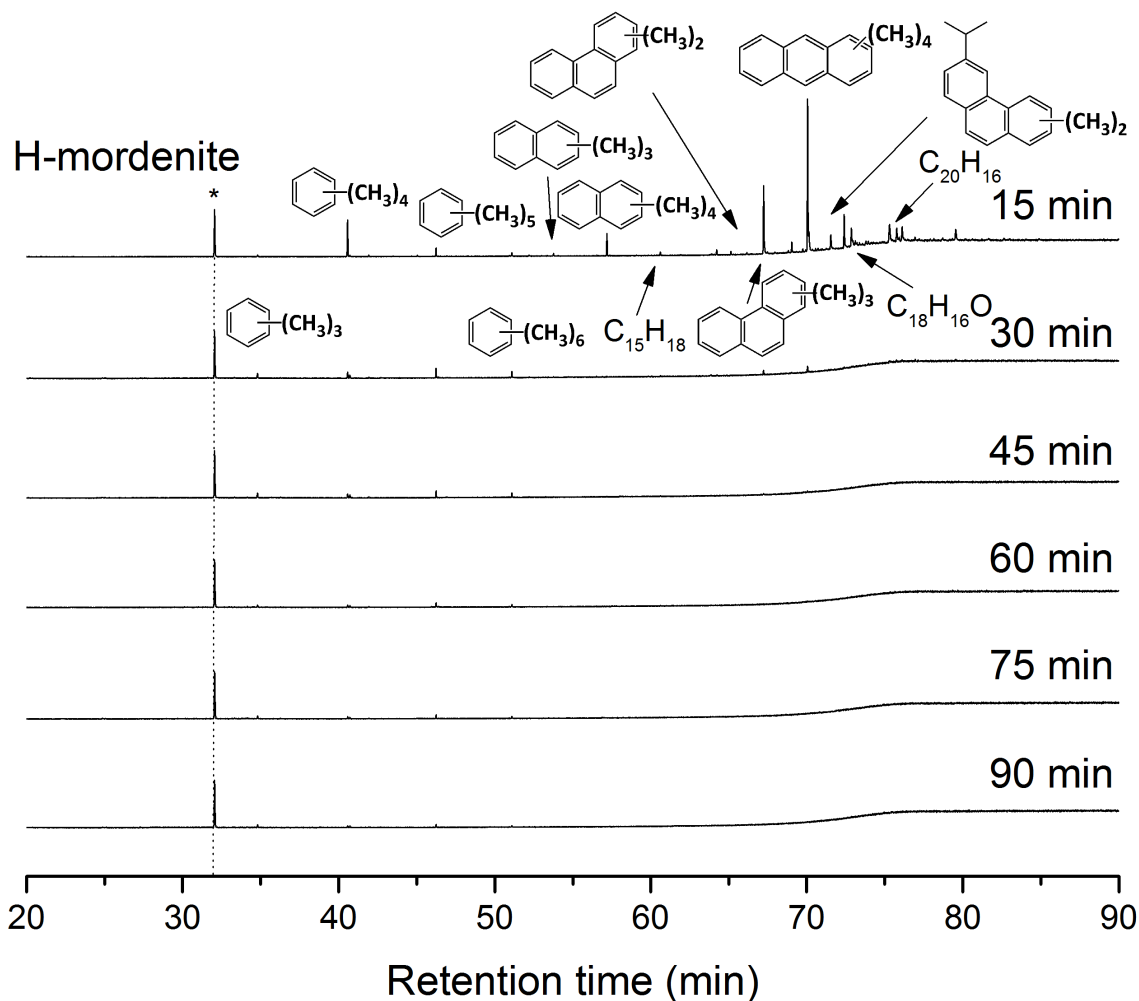

Figure 8.20: GC/MS total ion chromatograms of gradually deactivated H-mordenite. Reactions are carried out at 400 °C, WHSV = 2 h^{-1} and thermally quenched at the indicated TOS. All peaks are normalized relative to the internal standard peak, indicated by * in the chromatograms.

H-mordenite possessed the shortest lifetime of all investigated samples, and after just 15 minutes of TOS methylated polycyclic arenes with varying degree of methylations are observed as the most abundant species. Any arene containing two or more rings may be considered as deactivating species in the MTH reaction [30], and the fast formation of these compounds, together with a rapid deactivation, illustrate the ineptness of the catalyst in this process. Already after 15 minutes of TOS, there is a clear decrease in the observed amount of hydrocarbons, and as for the beta zeolites, this indicates formation of even heavier coke species.

8.4 Quantification of coke and retained material by BET, TGA & GC-FID calibration

The gradually deactivated catalysts were investigated with BET and TGA in order to investigate changes in adsorption capacity and to determine the total amount of oxdiable retained material for each sample. Combined data from TGA and the GC-FID calibration was used to determine the relative amounts of soluble coke from the dissolution/extraction procedure. The data will only be presented and described – a short summary of the combined results follows in the next subchapter.

8.4.1 H-ZSM-22

Table 8.4 and 8.5 lists the textural properties and the relative amounts of oxidable and soluble coke for the gradually deactivated H-ZSM-22 catalysts.

For H-ZSM-22 a clear trend is seen with respect to the textural properties from fresh to completely deactivated catalysts. Initially, both the surface area and the micropore volume are severely reduced and with increasing TOS (and deactivation) these features decrease even further, though at a lower rate.

The amount of oxidable material increases with TOS, which is natural as the catalyst becomes progressively more deactivated. There are no large alterations in the temperature of oxidation,

but it follows more or less a similar trend, with increased temperatures needed to combust material from more deactivated samples.

From the relative amount of soluble coke listed in the table, it follows that a large part of the retained material in H-ZSM-22 are analysable with the dissolution/extraction technique. The soluble part decreases from 60 % to around 35 % after TOS longer than 30 minutes, but remains at an almost unchanged level until complete deactivation.

Table 8.4: Textural properties of fresh and gradually deactivated samples of H-ZSM-22.

TOS of H-ZSM-22 (min)	BET surface area (m²/g)	Langmuir surface area (m²/g)	Micropore volume[a] (cm³/g)
Fresh	202	219	0.072
30	87	106	0.028
60	59	72	0.015
90	37	45	0.007
120	35	43	0.006
150	29	34	0.003
300	22	27	-

[a]t-plot method

Table 8.5: Quantification of coke from TGA and GC-FID calibration of gradually deactivated samples of H-ZSM-22.

TOS of H-ZSM-22 (min)	Amount of oxidable coke[a] (wt%)	Temperature of oxidation[b] (°C)	Rel. amount of soluble coke[c] (%)
30	0.3	390	60
60	1.1	390	36
90	2.1	390	36
120	2.3	400	38
150	2.3	410	40
300	2.8	420	33

[a]TGA
[b]appx. from inspection
[c]dissolution/extraction

8.4.2 H-ZSM-5

The textural properties and the relative amounts of oxidable and soluble coke for the gradually deactivated H-ZSM-5 catalysts are listed in table 8.6 and 8.7.

Although it is slightly reduced, H-ZSM-5 maintains a large share of the surface area and micropore volume up to a TOS of 480 minutes. This is also reflected by the fact that, at this time, the catalyst still operates at full, or nearly full, conversion. From TOS > 480 minutes both properties are drastically reduced. This also applies to the coke content in the different samples. The catalyst from the thermally quenched reaction at a TOS of 480 minutes contains relatively small amounts of coke, compared to the samples from longer reaction times, where coke content increases. Clearly for H-ZSM-5, also the temperatures required for oxidation of coke are substantially higher for more deactivated samples.

The relative amount of soluble coke is quite low for this catalyst, and the analysable fraction decreases slightly with TOS.

Table 8.6: Textural properties of fresh and gradually deactivated samples of H-ZSM-5.

TOS of H-ZSM-5 (min)	BET surface area (m²/g)	Langmuir surface area (m²/g)	Micropore volume[a] (cm³/g)
Fresh	406	460	0.17
480	335	380	0.14
720	38	44	0.02
840	10	11	0.01
960	9	11	-
1080	7	7	-

[a]t-plot method

73

Table 8.7: Quantification of coke from TGA and GC-FID calibration of gradually deactivated samples of H-ZSM-5.

TOS of H-ZSM-5 (min)	Amount of oxidable coke[a] (wt%)	Temperature of oxidation[b] (°C)	Rel. amount of soluble coke[c] (%)
480	2.4	390	7.6
720	7.5	405	6.5
840	7.8	425	6.1
960	8.2	430	5.8
1080	8.4	450	5.7

[a]TGA
[b]appx. from inspection
[c]dissolution/extraction

8.4.3 Beta Zeolites

The textural properties for the gradually deactivated H-beta and H-BEA catalysts are given in table 8.8 and 8.9 below. The relative amounts of oxidable and soluble coke for the equivalent samples of deactivated H-beta (top panel) and H-BEA (bottom panel) are given in table 8.10.

For both beta zeolites clear trends in textural properties with progressive deactivation are observed. H-beta experiences a drastic reduction in both surface area and micropore volume from fresh to the least deactivated sample (TOS = 60 minutes). With further deactivation, the reduction is maintained, though at a diminishing rate. Although the micropore volume is severely reduced at increasing deactivation, H-beta maintains a considerable portion of its surface area.

Much of the above mentioned also applies to the H-BEA material, but there are some differences. The surface area for this material is not reduced as strongly (relatively) from fresh to the partially deactivated sample (TOS = 360 minutes), and larger parts of the micropore volume are also maintained for a longer TOS.

Table 8.8: Textural properties of fresh and gradually deactivated samples of H-beta.

TOS of H-beta (min)	BET surface area (m^2/g)	Langmuir surface area (m^2/g)	Micropore volume[a] (cm^3/g)
Fresh	701	736	0.19
60	425	493	0.09
120	338	406	0.06
180	275	337	0.04
240	250	312	0.03
300	222	286	0.01
360	214	269	0.01
600	187	224	-

[a] t-plot method

Table 8.9: Textural properties of fresh and gradually deactivated samples of H-BEA.

TOS of H-BEA (min)	BET surface area (m^2/g)	Langmuir surface area (m^2/g)	Micropore volume[a] (cm^3/g)
Fresh	503	504	0.14
360	429	485	0.10
720	395	437	0.09
1080	378	428	0.08
1440	357	369	0.07
3220	288	318	0.05

[a] t-plot method

The catalysts show similar features when it comes to the accumulation of coke. As expected, the coke content increases with TOS for both materials. Larger amounts are formed and retained in H-beta, with a coke content that increases from around 6 to 14 wt% with increasing TOS. Roughly half as much is detected in H-BEA, even at much longer TOSs.

The temperatures required for oxidation of the retained hydrocarbons are in the same range for both catalysts, and increases with time and build up of coke. From table 8.10 it is evident that

the relative amount of soluble coke is very low for both catalysts, at the respective TOS. The amounts, nevertheless seem to decrease with increasing TOS.

Table 8.10: Quantification of coke from TGA and GC-FID calibration of gradually deactivated samples of H-beta (top panel) and H-BEA (bottom panel).

TOS of H-beta (min)	Amount of oxidable coke[a] (wt%)	Temperature of oxidation[b] (°C)	Rel. amount of soluble coke[c] (%)
60	6.4	350	2.0
120	8.3	365	0.5
180	10.3	365	0.4
240	11.1	365	0.2
300	11.9	370	0.3
360	12.5	380	0.2
600	14.1	385	0.2

TOS of H-BEA (min)	Amount of oxidable coke[a] (wt%)	Temperature of oxidation[b] (°C)	Rel. amount of soluble coke[c] (%)
360	3.2	365	0.3
720	4.2	370	0.2
1080	5.3	370	0.1
1440	6.0	385	0.2
3220	8.7	390	-

[a]TGA
[b]appx. from inspection
[c]dissolution/extraction

8.4.4 H-mordenite

Table 8.11 and 8.12 lists the textural properties and the relative amounts of oxidable and soluble coke for the gradually deactivated H-mordenite catalysts.

The rapid deactivation of this material is reflected in the listed data, where it is evident that the surface area and micropore volume are dramatically reduced after just 15 minutes of TOS. With extended TOS, the features are reduced further and the material loses its microporous properties. Considerable amounts of coke are formed at early stages, and the coke content increases from 5.6 to around 9.6 wt% for the severely deactivated samples.

The approximate temperature of oxidation increases from around 280 to 370 °C with progressive deactivation, and also for this catalyst, low concentrations of coke compounds are amenable to the dissolution/extraction procedure.

Table 8.11: Textural properties of fresh and gradually deactivated samples of H-mordenite.

TOS of H-mor (min)	BET surface area (m²/g)	Langmuir surface area (m²/g)	Micropore volume[a] (cm³/g)
Fresh	507	537	0.19
15	100	112	0.04
30	5	5	-
45	5	5	-
60	4	4	-
75	4	4	-
90	4	5	-

[a]t-plot method

Table 8.12: Quantification of coke from TGA and GC-FID calibration of gradually deactivated samples of H-mordenite.

TOS of H-mor (min)	Amount of oxidable coke[a] (wt%)	Temperature of oxidation[b] (°C)	Rel. amount of soluble coke[c] (%)
15	5.6	280	4.1
30	9.6	325	0.5
45	9.7	340	0.3
60	9.8	350	0.2
75	9.9	365	0.1
90	9.8	370	0.1

[a]TGA
[b]appx. from inspection
[c]dissolution/extraction

8.5 Summarization

This section will serve to summarize, compare and clarify the obtained results from the comparative investigations done over the different catalysts.

Of all investigated catalysts, the highest relative amount of soluble coke was observed for H-ZSM-22. Much of the retained material was amenable to the dissolution/extraction procedure for this catalyst and with increasing deactivation more bi and tricyclic arenes were observed. At the reaction conditions used, it seems like there is a critical point with respect to deactivation for this zeolite somewhere around 30 minutes of TOS. After this point, the mentioned polycyclic arenes are observed in more abundance, and it is likely that these species occupy the narrow 10-ring channels in the material and block access to the acid sites in the zeolite. This is also supported by the fact that the micropore volume decreases significantly with increasing time of reaction. H-ZSM-22 also showed the least build up of retained material as determined by TGA, which together with the accumulation of bi and tricyclic arenes in the pores, give good explanations for the high relative amount of soluble coke observed.

Also for H-ZSM-5 large polycyclic arenes were observed, and this is more surprisingly given the previous descriptions of deactivation in this material. Although not reflected in the listed relative amounts of soluble coke (because of large increase in total amount of coke), these species were detected in significant amounts during the course of deactivation. Furthermore for this material, is the change in observed features for the catalysts thermally quenched at TOS = 480 and TOS = 720 minutes, respectively, of particular interest. At 480 minutes is H-ZSM-5 still operating at almost full conversion, and only minor differences are observed in the textural properties of the catalyst when compared to a completely fresh sample. For the catalyst quenched after 720 minutes, the situation is completely different, and the BET surface area and micropore volume have been reduced from 335 to 38 m^2/g and from 0.14 to 0.02 cm^3/g, respectively. This illustrates the rapid deactivation process in this material, going from full conversion to a deactivated catalyst in a short period of time. The total coke content also increases significantly at the time, without any serious changes in the relative amount of soluble coke. This indicates the importance of external coke formation in this zeolite, but the presence of polycyclic arenes, located in the channel system, are nevertheless interesting and should be given further attention and studies.

H-beta and H-BEA stood out compared to both H-ZSM-22 and H-ZSM-5 with respect to the retained species observed in the hydrocarbon extracts, as no significant amounts of polycyclic arenes or other large hydrocarbon compounds were detected. H-BEA in particular, showed a different course of deactivation. Instead of a rapid loss of activity after methanol breakthrough, a more gradual deactivation was obsereved. This is also in accordance with the change in textural properties of the material with increasing TOS. Also here, a gradual reduction in surface area and micropore volume is the case.

8.6 Uncertainties in measurements

With respect to the GC-FID calibrations there are some uncertainties involved. The biggest are believed to be the automatic dosage of solvent, which might give variations of plus minus 10 %

9. Conclusions and further work

The deactivation by coke formation is studied over the medium and large pore zeolites H-ZSM-22, H-ZSM-5, H-Beta (two) and H-mordenite at a reaction temperature of 400 °C and WHSV = 2.00 h^{-1}. Gradually deactivated zeolites have been investigated with gas adsorption measurements, thermogravimetry and coke analysis by dissolution and extraction with subsequent chromatography. Large differences in catalyst lifetime was observed with rapid deactivation of H-mordenite and H-ZSM-22, compared to H-beta and the archetype H-ZSM-5. A broad distribution of polycyclic arenes was observed as retained coke species in gradually deactivated samples of both H-ZSM-22 and H-ZSM-5. This is in contrast to earlier observations done for H-ZSM-5, and might shed some light on the assumption of coking exclusively on the external surface of this catalyst at normal reaction temperatures.

GS-MS/FID analyses have been applied in a quantitative manner, but only H-ZSM-22 showed high relative amount of soluble coke, with a maximum of 60 % after 30 minutes time on stream. Only small amounts were detected for the large pore H-mordenite and beta zeolites and, it is believed that deactivation is caused by coking from larger graphitic species for these materials.

Further work should include:

- Altering of reaction conditions
- Spectroscopy to investigate heavier compounds
- Multiple calibrations to ensure reproducibility of the GC-FID quantifications

Appendix 1

Calculations

Methanol conversion, product selectivity and product yield was calculated from the integrated peak areas obtained from GC-FID signals. For methanol and DME response factors of 0.766 and 0.598 was used, respectively.

$$Conversion = \frac{\sum Area\ (all\ compounds) - Area(methanol) - Area(DME)}{\sum Area\ (all\ compounds)} \cdot 100$$

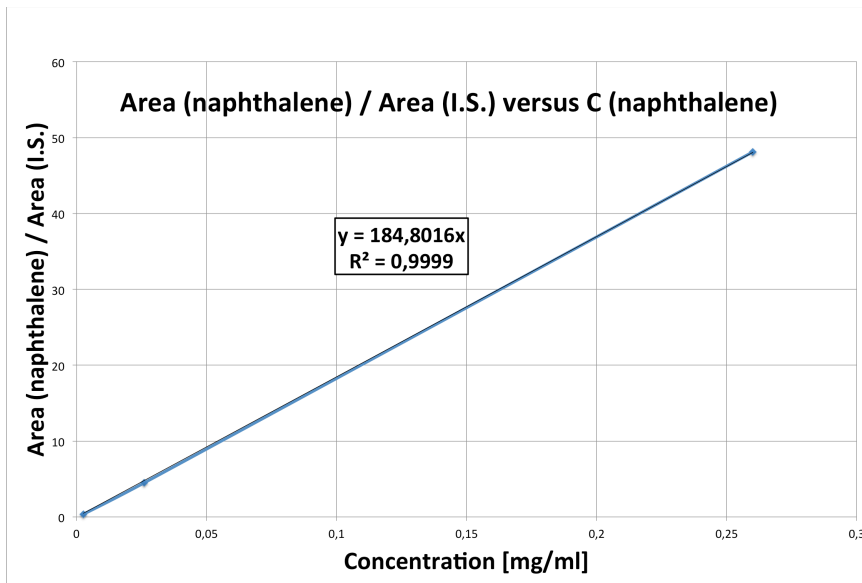$$Selectivity\ (i) = \frac{\sum Area\ (i)}{\sum Area\ (all\ compounds)} \cdot 100$$

$$Yield\ (i) = \frac{Conversion \cdot Selectivity(i)}{100}$$

Appendix 2

Calibration

Three calibration mixtures of naphthalene, hexamethylbenzene, pentamethylbenzene and durene were made to quantify detected hydrocarbons GC-MS/FID analyses.

Area (durene) / Area (I.S.) versus C (durene)

$y = 188,6863x$
$R^2 = 0,9999$

Area (pentaMB) / Area (I.S.) versus C (pentaMB)

$y = 192,7722x$
$R^2 = 1,0000$

Area (hexaMB) / Area (I.S.) versus C (hexaMB)

$y = 212{,}5029x$
$R^2 = 1{,}0000$

Area (naphthalene) / Area (I.S.) versus C (naphthalene)

$y = 184{,}8016x$
$R^2 = 0{,}9999$
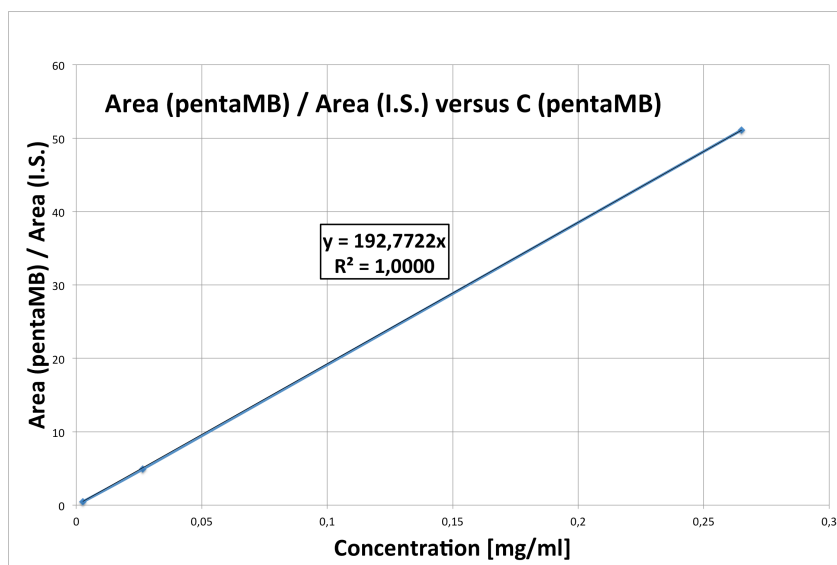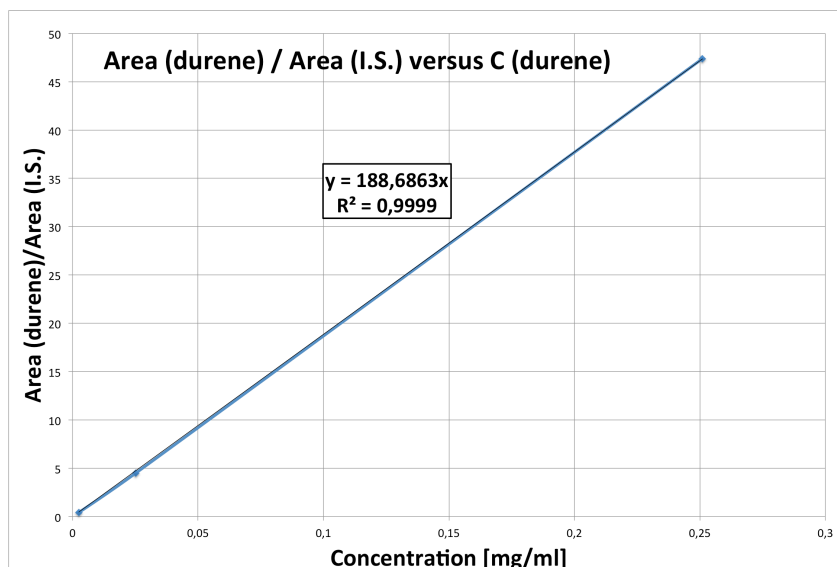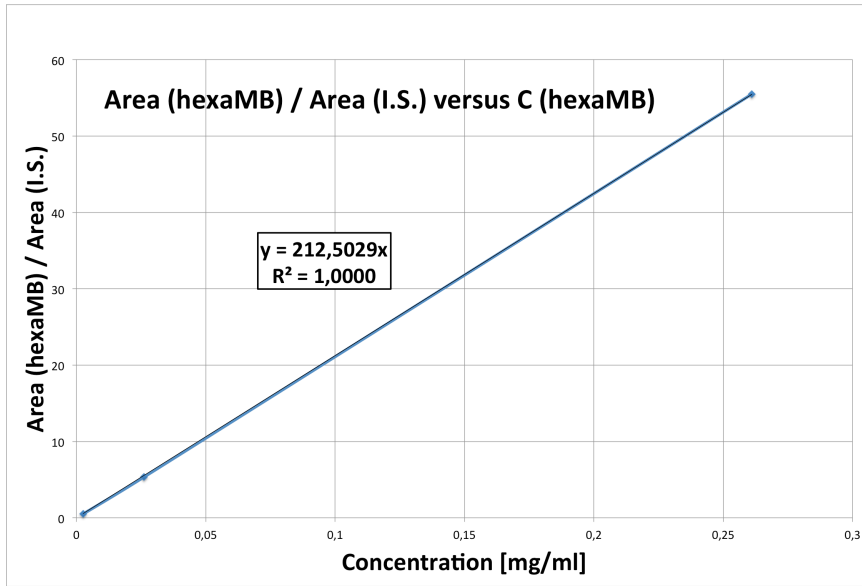
Appendix 3

Conversion

Conversion versus TOS curves for the investigated compounds. The reactions were thermally quenched at after the listed TOS, in order to cover the entire course of deactivation.

H-ZSM-22

H-ZSM-5

H-beta
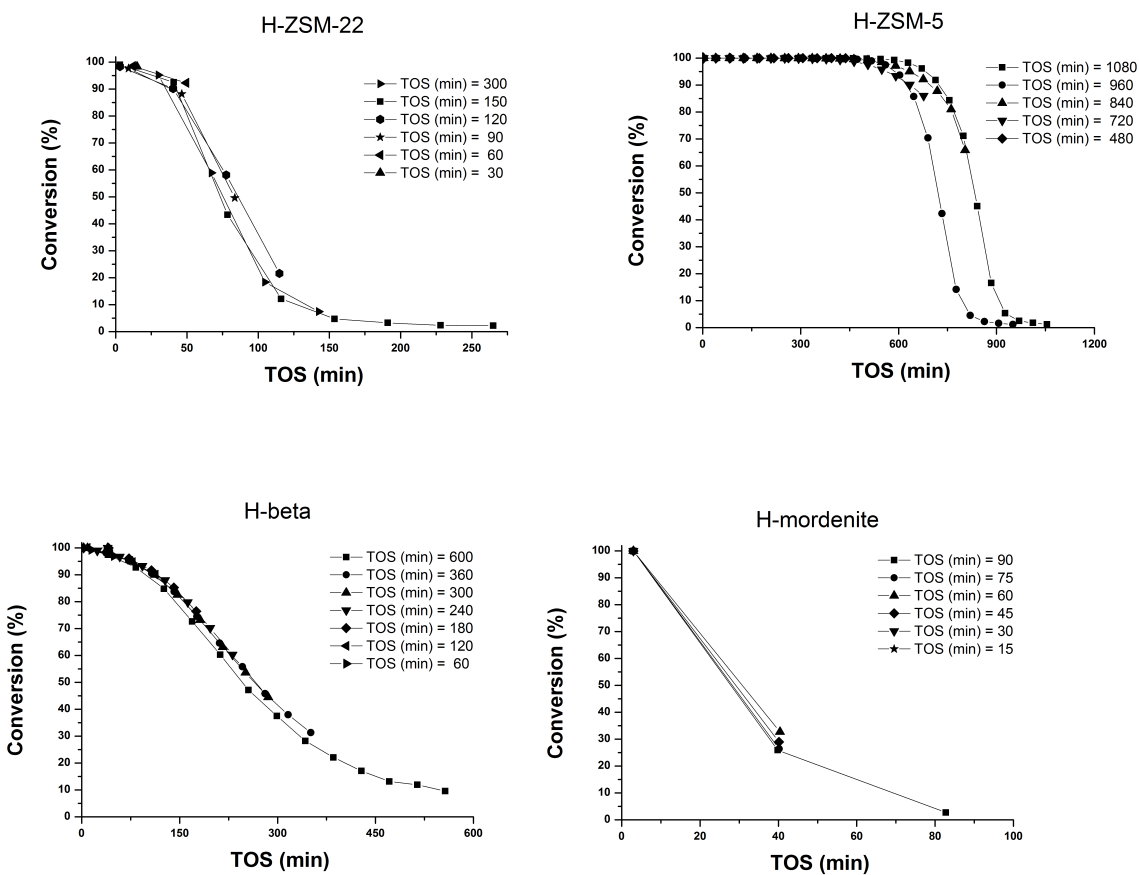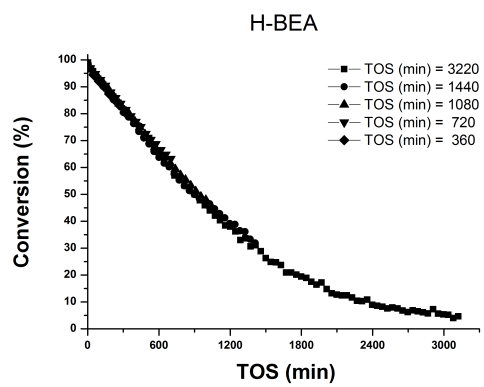
H-mordenite

H-BEA

Appendix 5

TGA

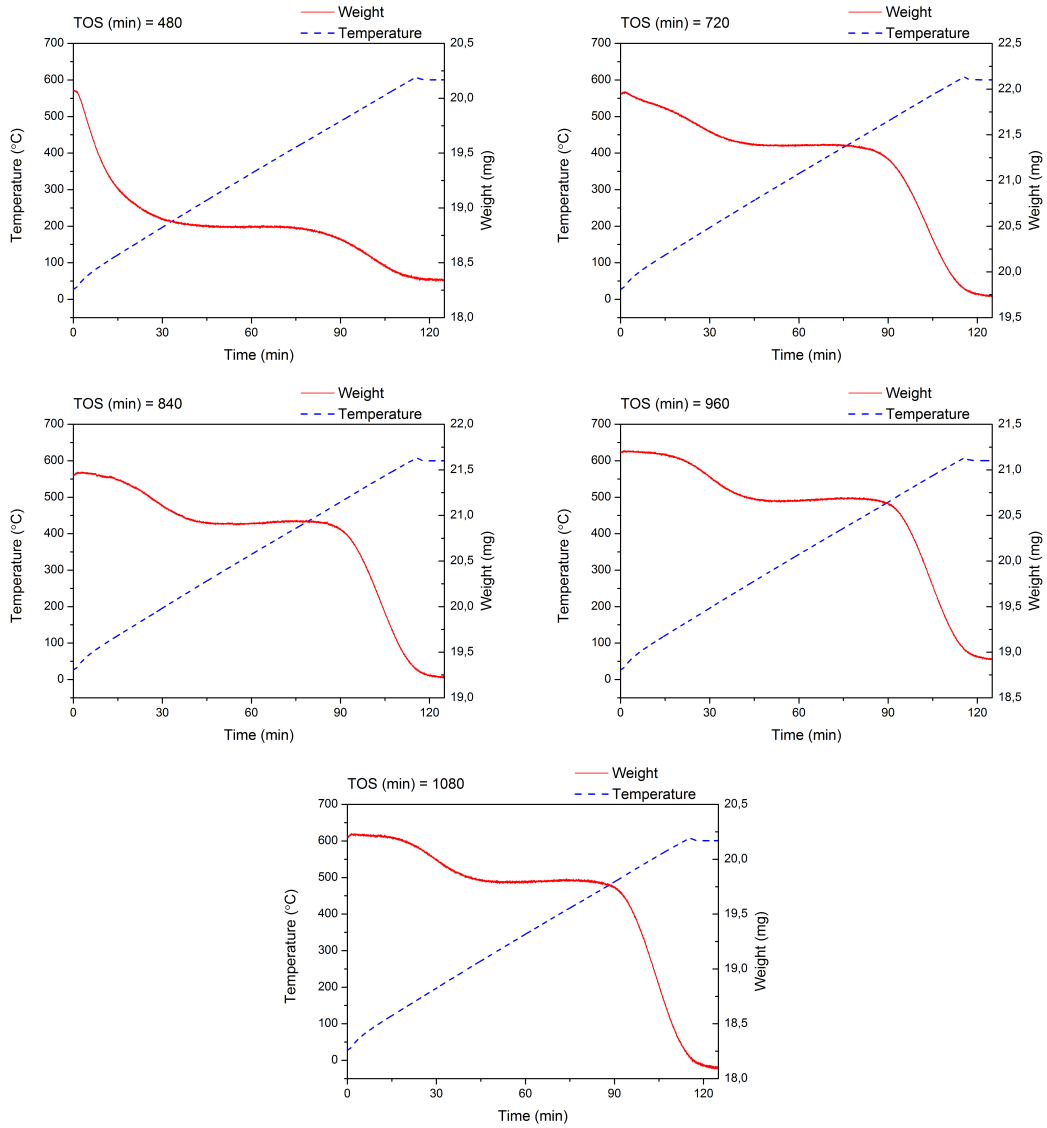TGA plots for all investigated samples are given below. The total amount of coke was calculated from
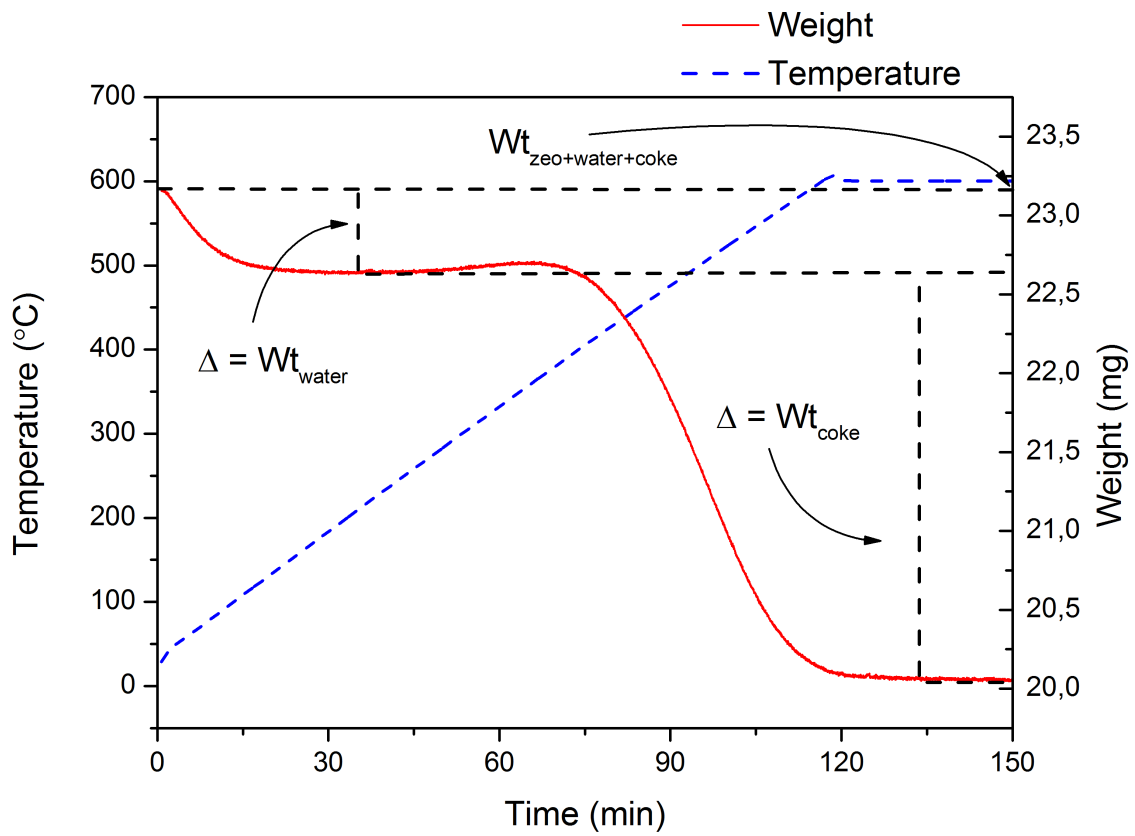
H-ZSM-22:
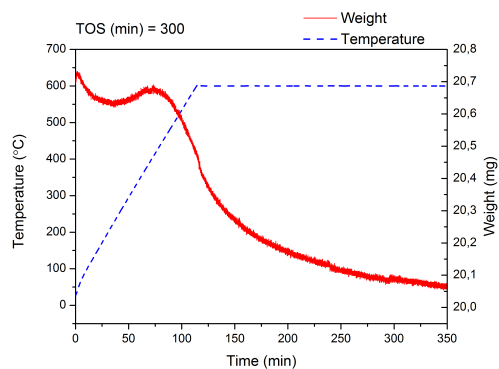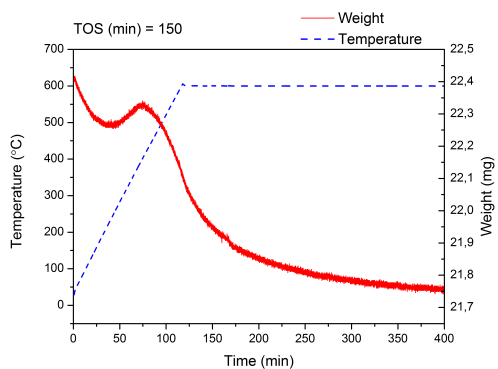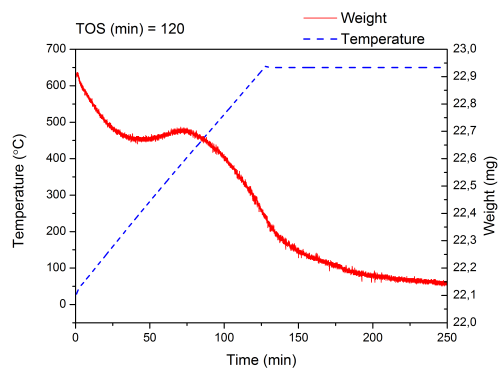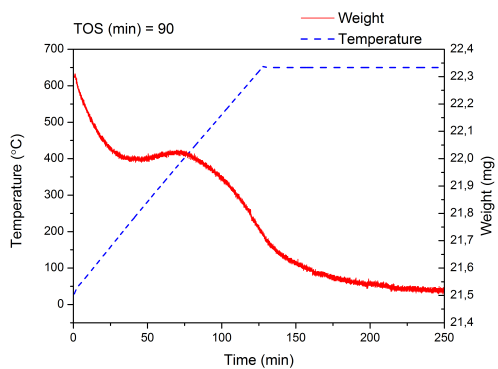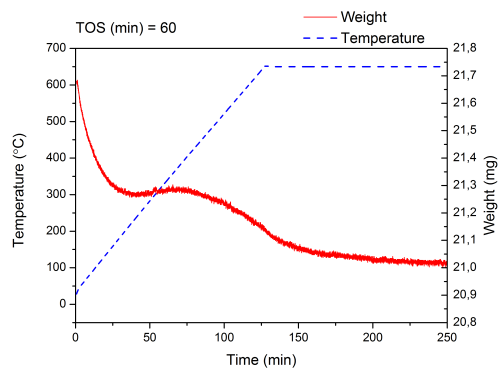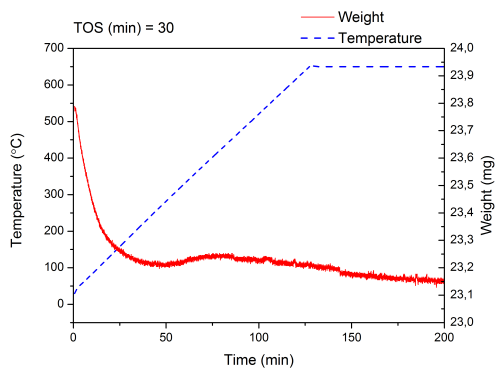
H-ZSM-5
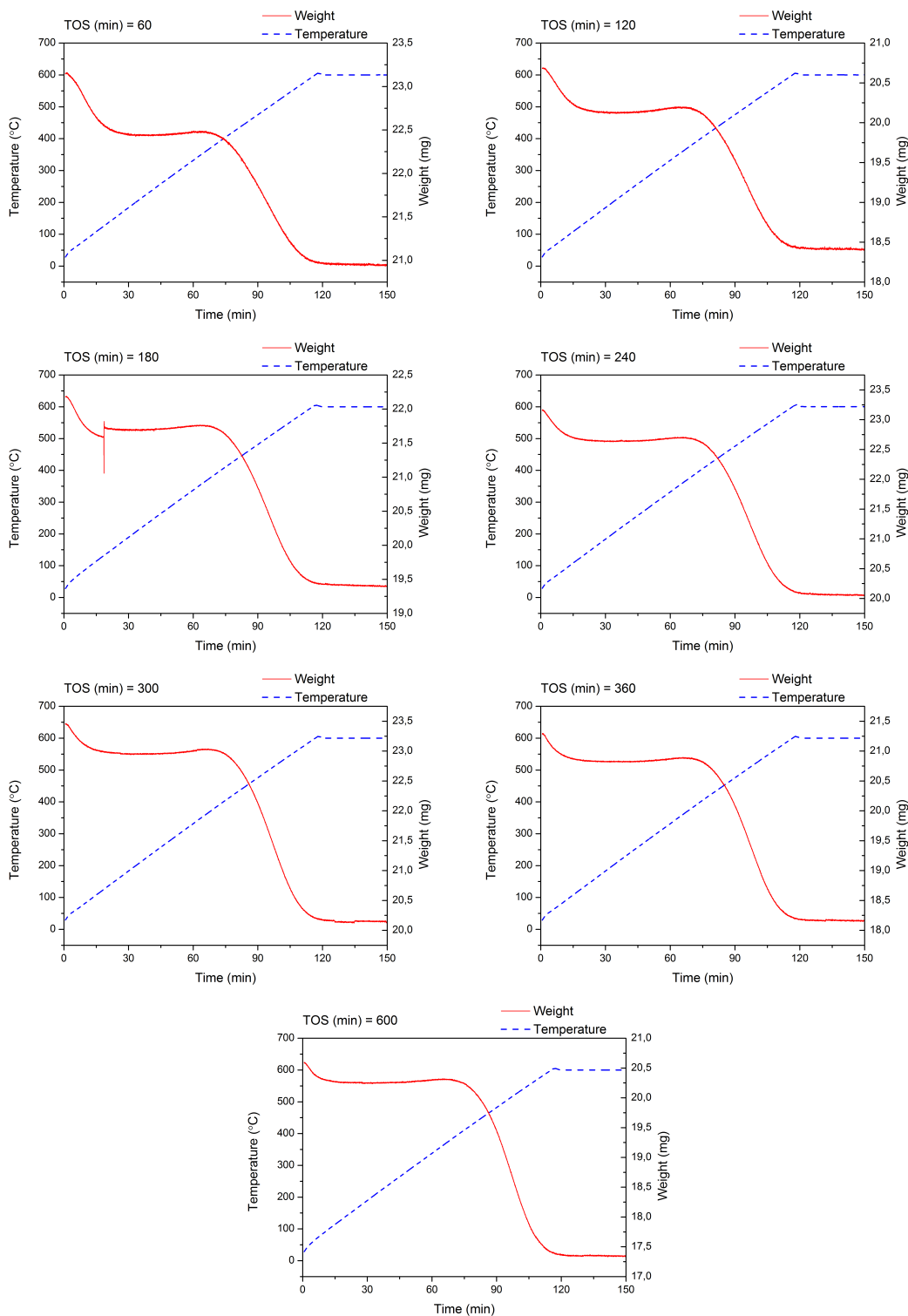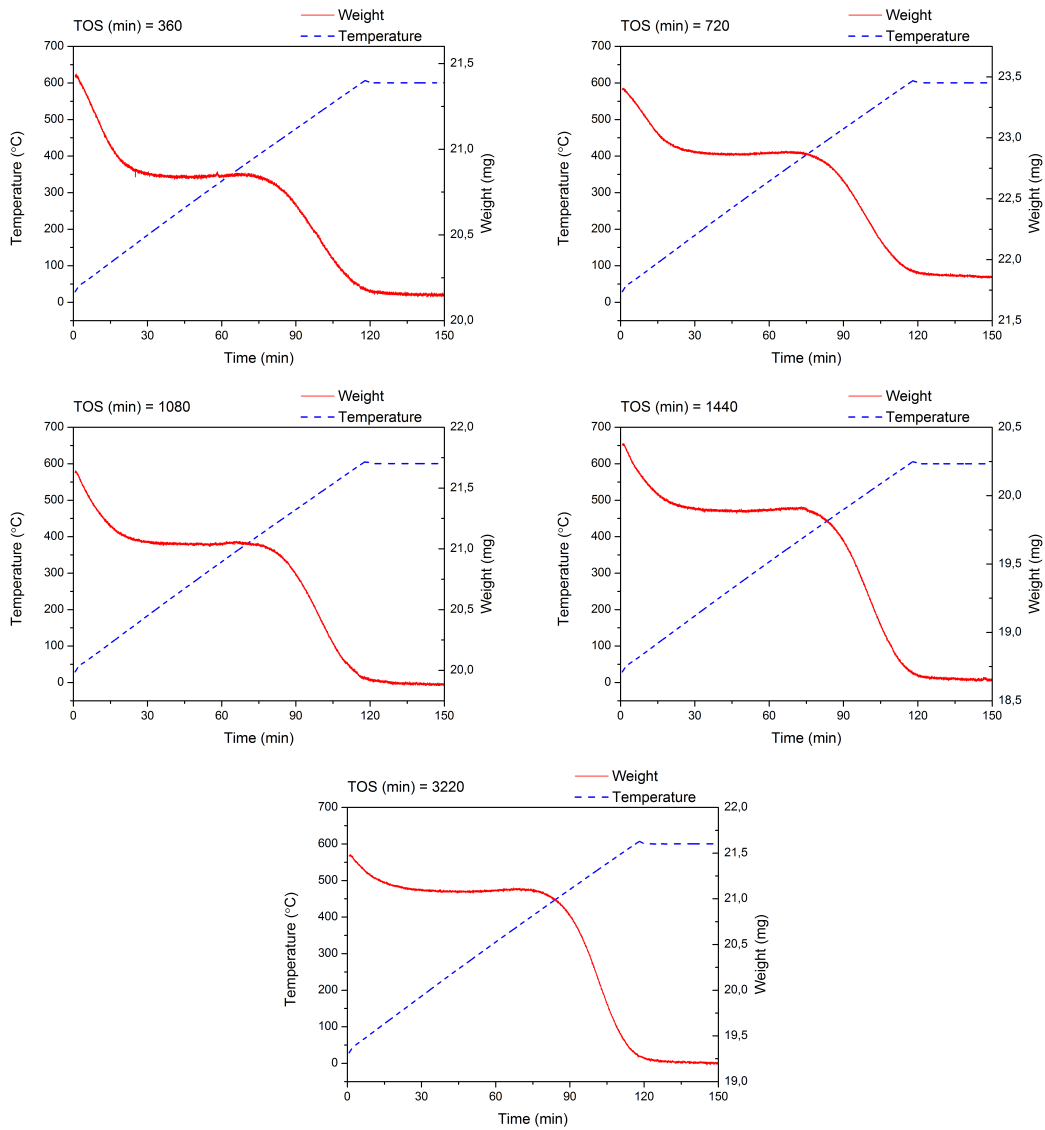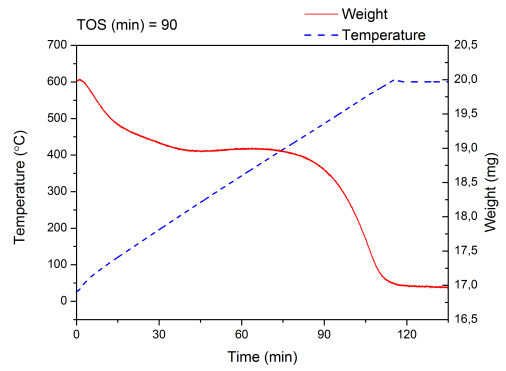
H-beta

H-BEA

H-mordenite
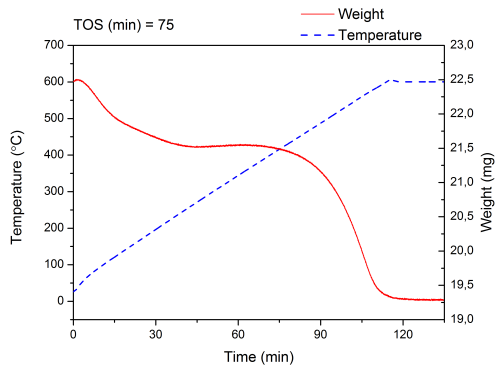
10. References

[1] J.W.N. I. Chorkendordd, Concepts of Modern Catalysis and Kinetics, WILEY-VCH, Weinheim, 2003.

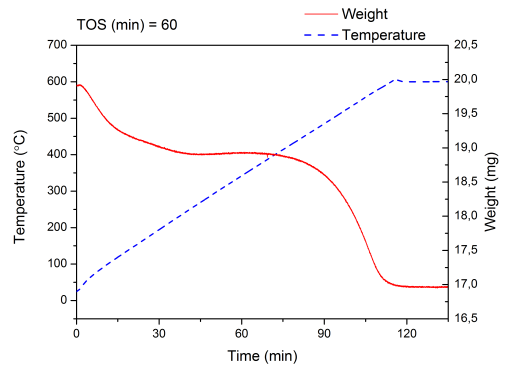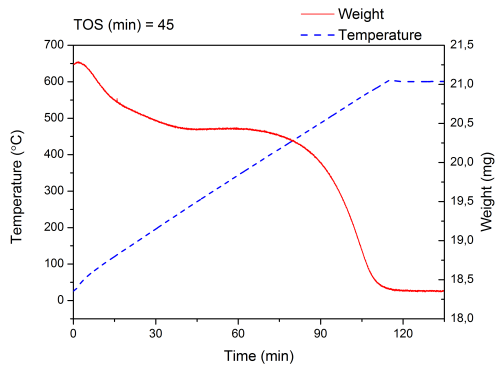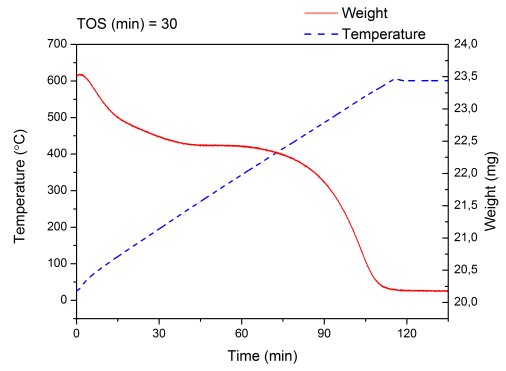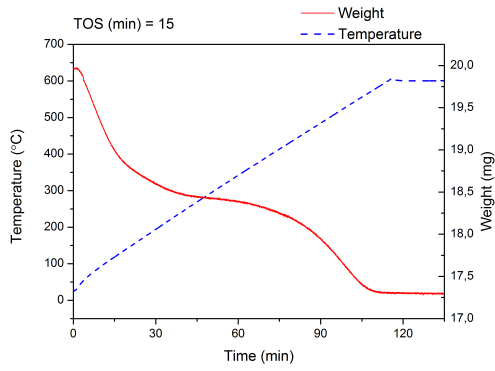[2] H.S.T. G. M. Schwab, R. Spence, Catalysis - From the Standpoint of Chemical Kinetics, D. van Nostrand Company, 1937.

[3] S.S.a.M. Bjørgen, Selective Catalysts for Petrochemical Industry, in: S.B. Adriano Zecchina, Elena Groppo (Ed.) Selective Nanocatalysts and Nanoscience: Concepts for Heterogeneous and Homogeneous Catalysis, Wiley, Weinheim, 2011, pp. 240, 241-253.

[4] A.F. Cronstedt, Ron och beskriting om en obekant bärg ant, som kallas zeolites, Akad. Handl. Stockholm, (1756) 120–130.

[5] H.v.B. Jiri Cejka, Avelino Corma, Ferdi Schüth (Eds.), Introduction to Zeolite Science and Practice, 3rd ed., Elsevier, 2007.

[6] R.W.B. Edith M. Flanigen , Stephen T. Wilson, Zeolites in Industrial Separation and Catalysis, WILEY, 2010.

[7] F.A. Mumpton, Natural Zeolites: A New Industrial Mineral Commodity, in: L.B.S.a.F.A. Mumpton (Ed.) Natural Zeolites: Occurrence, Properties, Use, Pergamon Press, U.K., 1978, pp. 3-4.

[8] E.M. Flanigen, Introduction to Zeolite Science and Practice, 2nd ed., ELSEVIER, 2001.

[9] M.L. Walter Loewenstein, The distribution of aluminum in the tetrahedra of silicates and aluminates, American Mineralogist, 39 (1954) 92.

[10] J. Weitkamp, Zeolites and Catalysis, Solid State Ionics, (2000) 176.

[11] L.B.M. Ch. Baerlocher, D.H. Olson, Atlas of Zeolite Framework Types, 6 ed., Elsevier, Amsterdam, 2007.

[12] P.A.W.a.M. Lozinska, Structural Chemistry and Properties of Zeolties, in: C.M.a.J. Pérez-Pariente (Ed.) Zeolites and Ordered Porous Solids: Fundamentals and Applications, Universitat Politécnica de Valéncia, Spain, 2011, pp. 6-7.

[13] S. International Zeolite Association, IZA 3D Structure generator, in, 2013.

[14] IUPAC Compendium of Chemical Terminology, Version 2.3.2, 2012.

[15] M.G.a.J.P. Gilson, Zeolites for Cleaner Technologies, Imperial College Press, 2002.

[16] S. Teketel, Studies of the Methanol-to-hydrocarbon (MTH) reaction over new 8- and 10-ring acidic zeolites, in: Chemistry, Oslo, 2009, pp. 125 (124).

[17] W.O. Haag, Zeolites and Related Microporous Materials: State of the Art 1994, Elsevier, Amsterdam, 1994.

[18] B.S.T.L.M. Maesen, Towards a molecular understanding of shape selectivity, Nature, (2008) 671-678.

[19] International Zeolite Association, Structure, in.

[20] J.L.S. G. T. Kokotailo, F. G. Dwyer, E. W. Valyocsik, The framework topology of ZSM-22: A high silica zeolite, Zeolites, 5 (1985) 349-351.

[21] G.K.C. T.F. Degnan, P.H. Schipper, History of ZSM-5 fluid catalytic cracking additive development at Mobil, Microporous and Mesoporous Materials, 35-36 (2000) 245-252.

[22] MENA3100, Scanning Electron Microscopy, in, 2010.

[23] G.T.K. R. L. Wadlinger, E. J. Rosinski, U. S. Patent 3,308,069, in, 1967.

[24] R.B.L. J.B. Higgins, J.L. Schlenker, A.C. Rohrmana, J.D. Wooda, G.T. Kerr, W.J. Rohrbaugha, The framework topology of zeolite beta, Zeolites, 8 (1988) 446-452.

[25] L.B. Sand, Synthesis of large-port and small port mordenites, Molecular Sieves, Society of Chemical Industry, (1968) 71-77.

[26] International Zeolite Association, in, http://www.iza-online.org/natural/Datasheets/Mordenite/mordenite.html.

[27] Enerdata, Sluggish growth of World energy demand in 2011, in, 2012.

[28] A.G. George A. Olah, G. K. Surya Prakash, Beyond Oil and Gas: The Methanol Economy, 2 ed., Wiley, Weinheim, 2009.

[29] M. Stöcker, Methanol-to-hydrocarbons: catalytic materials and their behavior, Microporous and Mesoporous Materials, 29 (1999) 3-48.

[30] S.S. Unni Olsbye, Morten Bjørgen, Pablo Beato, Ton V.W. Janssens, Finn Joensen, Silvia Bordiga, Karl Petter Lillerud, Methanol to hydrocarbons - gasoline or olefins – how zeolite cavity and pore size control product selectivity, (2012) 2.

[31] http://www.chemicals-technology.com/projects/tjeldbergoddenethpro, in.

[32] D.M.M. W. Song, H. Fu, J.O. Ehresmann, J.F. Haw, An Oft-Studied Reaction That May Never Have Been: Direct Catalytic Conversion of Methanol or Dimethyl Ether to Hydrocarbons on the Solid Acids HZSM-5 or HSAPO-34, Journal of the American Chemical Society, (2002) 3844-3845.

[33] S.K. I. M. Dahl, On the reaction mechanism for propene formation in the MTO reaction over SAPO-34, Catalysis Letters, 20 (1993) 329-336.

[34] S.K. I. M. Dahl, On the Reaction Mechanism for Hydrocarbon Formation from Methanol over SAPO-34: I. Isotopic Labeling Studies of the Co-Reaction of Ethene and Methanol Journal of Catalysis, 149 (1994) 458-463.

[35] S.K. I. M. Dahl, On the Reaction Mechanism for Hydrocarbon Formation from Methanol over SAPO-34: 2. Isotopic Labeling Studies of the Co-reaction of Propene and Methanol, Journal of Catalysis, 161 (1996) 304-309.

[36] J.A.W. T. Mole, D. Seddon, Aromatic co-catalysis of methanol conversion over zeolite catalysts, Journal of Catalysis, 82 (1983) 261-266.

[37] P.O.R. Ø. Mikkelsen, S. Kolboe, Use of isotopic labeling for mechanistic studies of the methanol-to-hydrocarbons reaction. Methylation of toluene with methanol over H-ZSM-5, H-mordenite and H-beta, Microporous and Mesoporous Materials, 40 (2000) 95-113.

[38] S.K. B. Arstad, Methanol-to-hydrocarbons reaction over SAPO-34. Molecules confined in the catalyst cavities at short time on stream, Catalysis Letters, 71 (2001) 209-212.

[39] H.F. W. Song, J. F. Haw, Supramolecular Origins of Product Selectivity for Methanol-to-Olefin Catalysis on HSAPO-34, Journal of the American Chemical Society, 123 (2001) 4749-4754.

[40] W.S. H. Fu, J. Haw, Polycyclic Aromatics Formation in HSAPO-34 During Methanol-to-Olefin Catalysis: Ex Situ Characterization After Cryogenic Grinding, Catalysis Letters, 76 (2001) 89-94.

[41] M.A.W. A. Sassi, H. J. Ahn, P. Prasad, J. B. Nicholas, J. F. Haw, Methylbenzene Chemistry on Zeolite HBeta: Multiple Insights into Methanol-to-Olefin Catalysis, The Journal of Physical Chemistry B, 106 (2002) 2294-2303.

[42] U.O. M. Bjørgen, S. Kolboe, Coke precursor formation and zeolite deactivation: mechanistic insights from hexamethylbenzene conversion, Journal of Catalysis, 215 (2003) 30-44.

[43] U.O. M. Bjørgen, S. Svelle, S. Kolboe, Conversion of Methanol to Hydrocarbons: The Reactions of the Heptamethylbenzenium Cation over Zeolite H-Beta, Catalysis Letters, 93 (2004) 37-40.

[44] S.S. M. Bjørgen, F. Joensen, J. Nerlov, S. Kolboe, F. Bonino, L. Palumbo, S. Bordiga, U. Olsbye,, Conversion of methanol to hydrocarbons over zeolite H-ZSM-5: On the origin of the olefinic species, Journal of Catalysis, 249 (2007) 195-207.

[45] Unni Olsbye, Morten Bjørgen, Stian Svelle, Karl-Petter Lillerud, Stein Kolboe, Mechanistic insight into the methanol-to-hydrocarbons reaction, Catalysis Today, 106 (2005) 108-111.

[46] U.O. Stian Svelle, Finn Joensen, Morten Bjørgen, Conversion of Methanol to Alkenes over Medium- and Large-Pore Acidic Zeolites: Steric Manipulation of the Reaction Intermediates Governs the Ethene/Propene Product Selectivity, The Journal of Physical Chemistry, 111 (2007) 17981-17984.

[47] S.A. Morten Bjørgen, Unni Olsbye, Sandrine Benard, Stein Kolboe, Stian Svelle, Methanol to hydrocarbons over large cavity zeolites: Toward a unified description of catalyst deactivation and the reaction mechanism, Journal of Catalysis, 275 (2010) 170-180.

[48] C.J.E. R. F. Sullivan, G. E. Langlois, R. P. Sieg, A New Reaction That Occurs in the Hydrocracking of Certain Aromatic Hydrocarbons, Journal of the American Chemical Society, 83 (1960) 1156-1160.

[49] G.B. T. Mole, D. Seddon, Conversion of methanol to hydrocarbons over ZSM-5 zeolite: An examination of the role of aromatic hydrocarbons using 13carbon- and deuterium-labeled feeds, Journal of Catalysis, 84 (1983) 435-445.

[50] A.H. David Lesthaeghe, Michel Waroquier, Guy B. Marin, Veronique Van Speybroeck, Theoretical Insights on Methylbenzene Side-Chain Growth in ZSM-5 Zeolites for Methanol-to-Olefin Conversion, Chemistry a European Journal, 15 (2009) 10803-10808.

[51] F.J. S. Svelle, J. Nerlov, U. Olsbye, K. P. Lillerud, S. Kolboe, M. Bjørgen, Conversion of Methanol into Hydrocarbons over Zeolite H-ZSM-5: Ethene Formation Is Mechanistically Separated from the Formation of Higher Alkenes, Journal of American Chemical Society, 128 (2006) 14770-14771.

[52] R.B.L. R. M. Dessau, On the mechanism of methanol conversion to hydrocarbons over HZSM-5, Journal of Catalysis, 78 (1982) 136-141.

[53] R.M. Dessau, On the H-ZSM-5 catalyzed formation of ethylene from methanol or higher olefins, Journal of Catalysis, 99 (1986) 111-116.

[54] S.S. S. Teketel, K. P. Lillerud, U. Olsbye, Shape-Selective Conversion of Methanol to Hydrocarbons Over 10-Ring Unidirectional-Channel Acidic H-ZSM-22, ChemCatChem, 1 (2009) 78-81.

[55] U.O. S. Teketel, K. P. Lillerud, P. Beato, S. Svelle, Selectivity control through fundamental mechanistic insight in the conversion of methanol to hydrocarbons over zeolites, Microporous and Mesoporous Materials, 136 (2010) 33-41.

[56] H.G. Karge, Coke Formation on Zeolites, Studies in Surface Science and Catalysis, 58 (1991) 531-570.

[57] F.R.R. M. Guisnet, Deactivation and Regeneration of Zeolite Catalysis, Imperial College Press, London, 2011.

[58] G.F. Froment, Kinetic Modeling of Hydrocarbon Processing and the Effect of Catalyst Deactivation by Coke Formation, Catalysis Reviews: Science and Engineering, 50 (2008) 1-18.

[59] R.F.H. David M. Bibby, Gavin D. McLellan, Coke formation in high-silica zeolites, Applied Catalysis A, 93 (1992) 1-34.

[60] H. Schulz, "Coking" of zeolites during methanol conversion: Basic reactions of the MTO-, MTP- and MTG processes, Catalysis Today, 154 (2010) 183-194.

[61] F.B. Luisa Palumbo, Pablo Beato, Morten Bjørgen, | Adriano Zecchina, Silvia Bordiga, Conversion of Methanol to Hydrocarbons: Spectroscopic Characterization of Carbonaceous

Species Formed over H-ZSM-5, Journal of Physical Chemistry, 112 (2008) 9710-9716.

[62] S.S. Katia Barbera, Silvia Bordiga, Jørgen Skibsted,, P.B.a.T.V.W.J. Henrik Fordsmand, Role of internal coke for deactivation of ZSM-5 catalysts after low temperature removal of coke with NO2, Catalysis Science Technology, 2 (2012) 1196-1206.

[63] M.-Y.K. Ki-Yong Lee, Son-Ki Ihm, Deactivation by coke deposition on the HZSM-5 catalysts in the methanol-to-hydrocarbon conversion, Journal of Physics and Chemistry of Solids, 73 (2012) 1542-1545.

[64] F.B. Katia Barbera, Silvia Bordiga, Ton V. W. Janssens, Pablo Beato, Structure-deactivation relationship for ZSM-5 catalysts governed by framework defects, Journal of Catalysis, 280 (2011) 196-205.

[65] U.O. Morten Bjørgen, Dirk Petersen, Stein Kolboe, The methanol-to-hydrocarbons reaction: insight into the reaction mechanism from [^{12}C]benzene and [^{13}C]methanol coreactions over zeolite H-beta, Journal of Catalysis, 221 (2004) 1-10.

[66] W.S. Shewangizaw Teketel, Sandrine Benard, Unni Olsbye, Karl Petter Lillerud, Pablo Beato, and Stian Svelle, Shape Selectivity in the Conversion of Methanol to Hydrocarbons: The Catalytic Performance of One-Dimensional 10-Ring Zeolites: ZSM-22, ZSM-23, ZSM-48, and EU-1, ACS Catalysis 2(2012) 26-37.

[67] Y.W. Jinzhe Li, Yue Qi, Peng Tian, Bing Li, Yanli He, Fuxiang Chang, Xinde Sun, Zhongmin Liu, Conversion of methanol over H-ZSM-22: The reaction mechanism and deactivation, Catalysis Today, 164 (2011) 288-292.

[68] W.D.K. David Brandon, Microstructural Characterization of Materials, 2nd ed., John Wiley & Sons Ltd, Chichester, 2008.

[69] D. Jürgens, in.

[70] J. USA, Invitation to the SEM world, in, 2006.

[71] J.R.K.S. F. Rouquerol, Adsorption by Powders & Porous Solids, Academic Press, London, 1999.

[72] K. Kaneko, Determination of pore size and pore size distribution 1. Adsorbents and catalysts, Journal of Membrane Science, 96 (1994) 59-89.

[73] G.M.L. Donald L. Pavia, George S. Kriz, Introduction to Spectroscopy, 3 ed., The Wadsworth Group, 2001.

[74] G.S.a.S.B. Adriano Zecchina, Probing the acid sites in confined spaces of microporous materials by vibrational spectroscopy, Physical Chemistry Chemical Physics, 7 (2005) 1627-1642.

[75] P.O. Rønning, in: Chemistry, University of Oslo, 1998.

[76] A.W. Burton, Powder Diffraction in Zeolite Science, in: E.G.D. Arthur W. Chester (Ed.) Zeolite Characterization and Catalysis, 2010, pp. 1-64.

[77] B.M.L. B. Christian, Studies in Surface Science and Catalysis, 85 (1994) 391-428.

[78] W.S. Francesca Bleken, Katia Barbera, Marina Kustova, Silvia Bordiga, Pablo Beato, Karl Petter Lillerud, Stian Svellea, Unni Olsbye, Conversion of methanol over 10-ring zeolites with differing volumes at channel intersections: Comparison of TNU-9, IM-5, ZSM-11 and ZSM-5, Physical Chemistry Chemical Physics, 13 (2011) 2539-2549.

[79] S. Forselv, An In-situ FTIR Study of the Methanol to Hydrocarbons Reaction Over Zeolite Catalysts, in, NTNU, 2011.

[80] L.C. Michel Guisnet, Fernando Ramôa Ribeiro, Prevention of zeolite deactivation by coking, Journal of Molecular Catalysis A: Chemical, 305 (2009) 69-83.

[81] T.V.W.J. Francesca L. Bleken, Stian Svelle, Unni Olsbye, Product yield in methanol conversion over ZSM-5 is predominantly independent of coke content, Microporous and Mesoporous Materials, 164 (2012) 190-198.